Laser communication concept for space weather forecasting CubeSat fleet mission

Olli Törmänen

School of Electrical Engineering

Thesis submitted for examination for the degree of Master of Science in Technology.

Espoo 17.5.2016

Thesis supervisor:

Prof. Esa Kallio

Thesis advisors:

D.Sc. Christian Möstl

D.Sc. (Tech.) Jari J. Hänninen

Aalto University
School of Electrical
Engineering

AALTO UNIVERSITY
SCHOOL OF ELECTRICAL ENGINEERING

ABSTRACT OF THE
MASTER'S THESIS

Author: Olli Törmänen

Title: Laser communication concept for space weather forecasting CubeSat fleet mission

Date: 17.5.2016 Language: English Number of pages: 9+81

Department of Radio Science and Technology

Professorship: Space Technology

Supervisor: Prof. Esa Kallio

Advisors: D.Sc. Christian Möstl, D.Sc. (Tech.) Jari J. Hänninen

The most damaging geomagnetic storms are produced by solar coronal mass ejections (CMEs). They represent a great threat to mankind's technological systems, since the prediction lead time of storms is too short today. The geoeffectiveness of the ejections can only be predicted by in situ magnetic field measurements in space. The HelioRing mission, proposed by the Space Research Institute of the Austrian Academy of Sciences, has the goal of providing magnetic field properties of Earth-directed CMEs using a CubeSat fleet in a heliocentric orbit for increasing the lead time of geomagnetic storms on Earth.

As this is the first study of the mission, one of the goals of this thesis was to define the objectives and requirements of the mission. The primary goal of the thesis was to investigate how the CubeSat fleet communicates with the Earth in the mission. It was found that the traditional radio frequency (RF) communication method would have two major disadvantages. Firstly, this method would require the construction of large ground stations, which would increase the total mission cost significantly. Secondly, forecasting would not be successful for about 3 % of the mission lifetime due to increased background noise from the Sun. Laser communication was chosen to overcome the two RF communication problems. The main idea of the concept is to deliver data by laser crosslink communication to an additional CubeSat (RelayCube) that orbits in a Sun-synchronous orbit. RelayCube would transmit all data to the ground stations using RF communication. The objectives of the thesis were successfully achieved. The results show that the laser communication concept is feasible and fulfils the mission requirements. It permits low-cost amateur RF ground stations and enables continuous space weather forecasting. However, further studies are needed, e.g., to achieve the required laser pointing accuracy and for the development of the high peak power transmitter.

Keywords: space weather, coronal mass ejections, CubeSat, satellite, laser communication, laser, link budget

AALTO-YLIOPISTO
SÄHKÖTEKNIIKAN KORKEAKOULU

DIPLOMITYÖN
TIIVISTELMÄ

Tekijä: Olli Törmänen

Työn nimi: Avaruussään ennustamiseen suunnitellun CubeSat-luotainohjelman laserkommunikaatiojärjestelmä

Päivämäärä: 17.5.2016 Kieli: Englanti Sivumäärä: 9+81

Radiotieteen ja -tekniikan laitos

Professuuri: Avaruustekniikka

Työn valvoja: Prof. Esa Kallio

Työn ohjaajat: TkT Christian Möstl, TkT Jari J. Hänninen

Auringon koronan massapurkaukset eli CME:t muodostavat suuren uhan ihmiskunnan teknologisille järjestelmille, koska varoitusaika massapurkauksia vastaan on liian lyhyt ennen kuin ne saavuttavat Maan. Purkausten vaikutukset Maassa voidaan ennustaa vain avaruudessa tehtävistä purkauksien magneettikentän mittauksista. HelioRing-luotainohjelman, jota on ehdottanut Itävallan tiedeakatemian avaruustutkimusinstituutti (Space Research Institute of Austrian Academy of Sciences), tavoitteena on välittää Maata kohti suuntautuneen CME:n magneettikentän ominaisuudet ja täten pidentää varoitusaikaa. Tavoitteena on myös käyttää mittauksiin CubeSat-piensatelliittiryhmää aurinkokeskisellä kiertoradalla.
Koska kyseessä oli HelioRingin ensimmäinen tutkimus, yhtenä työn tavoitteena oli määrittää luotainohjelman tavoitteet ja vaatimukset. Tärkein päämäärä oli selvittää se, miten HelioRingin CubeSat-ryhmä kommunikoisi maa-asemien kanssa. Tässä työssä osoitettiin, että radiotaajuisella kommunikaatiotavalla olisi kaksi merkittävää heikkoutta. Ensimmäiseksi se vaatisi niin suuret maa-asemat, että HelioRingin kokonaiskustannukset kasvaisivat huomattavasti. Toiseksi avaruussään ennustaminen ei olisi mahdollista noin 3 % luotainohjelman eliniästä Auringon aikaansaaman taustakohinan vuoksi silloin kun lähin CubeSat kulkee Auringon ja Maan välissä. Laserkommunikaatio valittiin pääkommunikaatiotavaksi, koska se ratkaisisi RF-kommunikaation ongelmat. Pääperiaatteena on välittää data laserilla CubeSatilta toiselle ja edelleen Maata kiertävälle ns. linkki-CubeSatille, joka lähettää kaikkien CubeSatien datan radiotaajuuksilla maa-asemille.
Työn tavoitteet saavutettiin onnistuneesti. Tulokset osoittavat, että laserkommunikaatiosuunnitelma on mahdollista toteuttaa ja että se täyttää luotainohjelmalle asetetut vaatimukset. Se mahdollistaisi edulliset maa-asemat ja jatkuvan avaruussään ennustamisen. Suunnitelman yksityiskohdat, esimerkiksi vaadittava laserin suuntaustarkkuus ja laserlähetin, edellyttävät kuitenkin vielä lisätutkimuksia.

Avainsanat: avaruussää, koronan massapurkaukset, CubeSat, satelliitti, laserkommunikaatio, laser, linkkibudjetti

Preface

This thesis has mostly been written at the Space Research Institute of the Austrian Academy of Sciences during July 2015 - January 2016. First and foremost, I would like to thank Dr. Werner Magnes and Dr. Christian Möstl from the Space Research Institute for their expert guidance and making the writing of this thesis possible.

I would also like to express my deep gratitude to my supervisor, Prof. Esa Kallio, for helpful guidance, and numerous useful comments and remarks during the writing process. I also thank my advisors Dr. Christian Möstl and Dr. Jari Hänninen for their useful comments and opinions. Also, I would like to say many thanks to the Space Research Institute staff for their support, especially to David Fischer and Manuel Kubicka.

I owe many thanks to the Erasmus+ Programme for awarding me with the Erasmus Grant for the traineeship in Austria.

I would like to express special thanks to Prof. Walter Leeb from the Vienna University of Technology, Dr. Fabio Di Teodoro, Prof. Erich Leitgeb from the Graz University of Technology, and Dr. Georg Kirchner.

Finally, I thank to my family for their endless support and love.

Otaniemi, 17.5.2016

Olli Törmänen

Contents

Symbols and abbreviations

Symbols

λ	carrier wavelength
$\Delta\lambda_{\mathrm{nf}}$	narrowband noise filter bandwidth
η_{code}	coding efficiency
η_{det}	photon detection efficiency of a detector
η_{pr}	pointing efficiency of a receiver
η_{pt}	pointing efficiency of a transmitter
η_{r}	receiver efficiency
η_{t}	transmitter efficiency
ω_{CS}	orbital angular frequency of a HelioRing CubeSat
ω_{E}	orbital angular frequency of the Earth
$A(\lambda)$	planet spectral albedo
B_{z}	strength of the z component of the magnetic field of a CME or the solar wind
c	speed of light in vacuum $\approx 3 \times 10^8$ m/s
C/N_0	signal-to-noise-power-density ratio
D_{r}	aperture diameter of a receiver
D_{t}	aperture diameter of a transmitter
E_{b}/N_0	bit energy to noise power density
f	carrier frequency
G_{r}	receiver gain
$G_{\mathrm{r}}/T_{\mathrm{sys}}$	figure of merit of a receiving system
G_{t}	transmitter gain
h	Planck's constant
H_λ	Sun spectral irradiance at 1 AU
Hz	hertz
k	number of bits encoded onto one of PPM slots
k_{B}	Boltzmann constant ($\approx 1.3806 \times 10^{-23}$ J/K)
$L(\lambda)$	background irradiance
L_{A}	atmospheric loss
L_{L}	total loss due to the attenuation by transmission lines
$\mathrm{L_{Li}}$	laser link on the left side of the Sun seen from the Earth
L_{N}	projected length of a 3° sunlit sector at 0.72 AU
$\mathrm{L_{Ri}}$	laser link on the right side of the Sun seen from the Earth
L_{s}	free-space loss
M	PPM alphabet size
n_{b}	number of detected background noise photons per slot width
n_{s}	number of detected signal photons per PPM word
N	newton
N_{dc}	dark count rate, i.e, noise photons per second produced by a detector
P_{peak}	peak transmit power

P_r	received power
P_t	average (root mean square) transmit power
R	range between two CubeSats
R_AU	planet-Sun distance in AU
R_b	data rate
R_ECC	error correction coding rate
R_p	radius of a planet or a diameter of a footprint of a laser beam on a planet
R_RF	range between a CubeSat and a ground station in the RF concept
rad	radian
T	tesla
t	time
T_d	guard time
T_p	pulse width
T_s	slot width
T_sys	system temperature
T_w	word time
W	watt
Z_pr	planet-receiver distance

Abbreviations and acronyms

ACE	Advanced Composition Explorer
ADACS	attitude determination and control system
AU	astronomical unit ($\approx 149.6 \times 10^6$ km)
BER	bit error rate
CARETAKER	Coronal Mass Ejection Analysis Reporting to Earth To Allow Keeping Everything Running
CINEMA	CubeSat for Ions, Neutrals, Electrons, & MAgnetic fields
CME	coronal mass ejection
CS	CubeSat at 0.72 AU
CSD	Canisterized Satellite Dispenser
DSCOVR	Deep Space Climate Observatory
DSN	Deep Space Network
EO	electro-optic
ESA	European Space Agency
FM	fiber-coupled phase modulator
GM-APD	Geiger-mode avalanche photon detector
GEO	Geostationary orbit
GTO	Geostationary Transfer Orbit
H/K	housekeeping
IKAROS	Interplanetary Kite-craft Accelerated by Radiation Of the Sun
In-FEEP	Indium Field Emission Electric Propulsion
ITU	International Telecommunications Union
IWF	Space Research Institute (Institut für Weltraumforschung)
L1	Lagrange point 1

lasercom	laser communication
LEO	low Earth orbit
MAGIC	MAGnetometer from Imperial College
MarCO	Mars Cube One
MESSENGER	MErcury Surface, Space ENvironment, GEochemistry, and Ranging
MO	master oscillator
MOPA	master oscillator/power amplifier
OCSD	Optical Communications and Sensor Demonstration
P-POD	Poly Picosatellite Orbital Deployer
PCF	photonic crystal fiber
PM	polarization maintaining
PPM	Pulse-Position modulation
PRF	pulse repetition frequency
RF	radio frequency
SCPPM	serially concentrated Pulse-Position modulation
SER	symbol error rate
SLS	Space Launch System
SNR	signal-to-noise ratio
SOA	semiconductor optical amplifier
SOHO	Solar and Heliospheric Observatory
SPE	Sun-probe-Earth angle
RSPPM	Reed Salomon Pulse-Position modulation
SILEX	Semiconductor-laser Intersatellite Link EXperiment
STEREO	Solar Terrestrial Relations Observatory
sub-L1	artificial Lagrange point
U	unit
UHF	ultra high frequency
Yb	ytterbium

1 Introduction

The Sun is the prime factor for the dynamics of the Solar System. It emits plasma, the dynamics and phenomena by which is called space weather. The term ”space weather” comprises conditions on the Sun and in the interplanetary medium as well as on the Earth and in near-Earth space. One must not underestimate the Sun's ability to influence space weather conditions and thereby to impact significantly on the human community. Although many people's primary idea of space weather is the spectacular aurora borealis, space weather actually poses a serious global threat. Extreme space weather conditions have the potential to produce powerful geomagnetic storms that can result in worldwide damages to electric power grids. The conditions also can cause significant hazards resulting in telecommunications and subsystem failures in satellites. [1]

The reasons for such extreme conditions originate from the Sun mainly as coronal mass ejections (CMEs) [1]. These events are currently not predictable and they can occur in the direction of the Earth at any time. An example of the Sun's potential power was witnessed in 1859, when the state of technology was yet in its infancy. A massive CME struck the Earth's magnetosphere, resulting in telegraph disruptions all over the world and some fires in telegraph stations [2]. Nowadays, this event is known as the Carrington Event. Since then, several smaller CMEs have caused hazards after the Carrington Event. A CME in 1989 led to power grid failures and six million people in Canada suffered from lack of electricity for nine hours [2]. This event was much weaker than the Carrington Event. If a Carrington-scale CME were to hit the Earth today, it would affect us more destructively as mankind is more reliant on technology systems now than in the 19th century. Also, technology is more widespread and susceptible today, due to more complex and minituarized systems [2].

Although the occurence of CMEs is unpredictable, they have a well-known velocity when they encounter the Earth (up to approximately 2300 km/s) [3, p. 58], [4]. Therefore, by measuring the characteristics of an incoming CME sunward, one can forecast whether the incoming CME is harmful to mankind or not [2, 5]. The forecasts are based on several parameters of a CME. The direction and strength of the magnetic field of the plasma carried by an incoming CME are significant factors that indicate how harmful the CME could potentially be. If the direction is southward (relative to the Earth's geographic poles), the CME has the potential to produce powerful geomagnetic storms that can damage power grids. The speed of a CME is also one of the crucial parameters for estimating the consequences on the Earth. [3, p. 40, 55]

The state of the Sun is continuously monitored from the Earth by several scientific and governmental organizations for the forecasting of possible extreme CMEs. Observations are made in near real-time as solar flares are visible on the Earth after about eight minutes, when the light from the flares has reached the Earth. However, the speed and direction of a CME are difficult to be estimated accurately, and therefore, the predicted arriving time of the CME can vary by several hours [6]. Another problem is determining whether the incoming CME will be able to cause hazards on

the Earth or not. This depends mainly on the direction of the magnetic field of the CME's plasma, which is impossible to predict accurately by remote observations [2].

In addition to ground-based observations, monitoring is also done in space. At the moment, the only spacecraft that can provide real-time solar wind observations for space weather forecasting on the Earth is the Advanced Composition Explorer (ACE) satellite [2]. It observes the Sun and measures the solar wind properties at the Lagrange point 1 (L1), i.e., at 0.99 Astronomical units (AU). This L1 point is 1.5 million kilometers sunwards from the Earth. Thus, ACE is able to forewarn of impending geomagnetic storms and other hazards. However, the prediction lead time is only tens of minutes for fast-travelling CMEs. For example, if a massive CME, travelling as fast as 2300 km/s, is observed by ACE, the lead time is only about 10 minutes. This is too short a time to prepare mitigating actions for power grids and satellites in order to prevent catastrophic consequences [7].

This fact has raised interest in the research community for increasing the prediction lead time, and thus, several new space missions have been proposed [8]. Most of them aim to place their satellite at a sub-L1 point (sunward of the classical L1 point). Of the proposed missions, the closest to the Sun is Sunjammer, which is designed to reside at 0.98 AU [8]. However, using the above example, the lead time would still only be about 20 minutes, which is still far from ideal. Another way to increase the lead time of ACE is to measure space weather conditions in a heliocentric orbit. This necessitates several probes to orbit the Sun, since a single probe would not stay in the Sun-Earth line due to the faster rotation period. This kind of mission has already been (unofficially) proposed, and it is called CARETAKER (at 0.72 AU) [9]. It presents a significant increase in the lead time (about 5 hours, using the above example). However, its major limitation is the large total cost estimate due to six heavy probes (about 800 kg each) and six large ground stations.

Based on CARETAKER, the Space Research Institute (Institut für Weltraumforschung, IWF)[1] of the Austrian Academy of Sciences has an idea about a new kind of mission called HelioRing. The primary objective of this mission is to measure the magnetic field properties of the solar wind with ten CubeSats at around 0.6–0.8 AU in order to increase the prediction lead time of geomagnetic storms on the Earth. Each CubeSat carries a magnetometer which is used to measure the strength and direction of the magnetic field of CMEs. Having just a magnetometer as a space weather instrument permits the use of low-mass spacecraft, such as CubeSats, in the mission. In addition, measuring a CME's magnetic field properties would be the key element to increase the lead time by several hours, as is discussed in the next chapter. This would be a significant achievement for space weather science, and especially for the safety of mankind's vital technological systems.

CubeSats typically have a mass of around 1–10 kg [11]. This is the major difference compared to the CARETAKER mission, and it will lead to considerably more affordable costs in the space segment. Cost savings are mainly due to the faster development process and lighter launch mass of CubeSats. However, the

[1]The Space Research Institute: `http://www.iwf.oeaw.ac.at/en/`
IWF does research in various fields, such as space weather and the Solar system. It also develops space instruments like magnetometers [10]. The institute is located in Graz, Austria.

use of such small spacecraft in deep space[2] will pose new challenges. Hundreds of CubeSats have been launched into space since the first one in 2003 [13, 14]. They have represented new technology demonstrations and scientific research [15]. However, to date, they have been launched no farther than to low Earth orbit (LEO) [16]. Therefore, communication with the Earth from deep space may be considered one of the major challenges. A deep-space spacecraft is typically equipped with high-power transmitters and high-gain antennas, which are not feasible with CubeSats. Mass and size restrictions for CubeSats introduce limitations to the achievable transmit power and antenna gain, which are the two most critical parameters for deep-space communication in the space segment [17]. In addition, in comparison with a LEO, deep space is a more difficult environment due to increased ionizing radiation levels. Also, there is only limited experience of CubeSat propulsion systems, which are probably needed in every deep-space mission.

However, CubeSat subsystems have advanced substantially from the beginning in terms of power, attitude determination and control systems (ADACSs) as well as communication and propulsion systems [18]. This has led to several mission proposals, even into deep space. One of the most advanced proposals is the Mars Cube One (MarCO) mission to Mars scheduled for 2018 [19].

The HelioRing mission also faces the same aforementioned challenges. Two of them are considered the most difficult: communication with the Earth and how to achieve the final orbit for the CubeSats. Radiation is also a challenge but it is not regarded as problematic [15] as the first two, as there is extensive experience in radiation shielding from various deep-space missions. Communication may be the major challenge as there is no experience of CubeSats in deep space. The distance between the orbit and the Earth is from tens to hundreds of millions of kilometres in HelioRing. Each near-future, deep-space CubeSat mission will be supported by large ground station systems, such as the NASA Deep Space Network (DSN) [16]. They consist of large dishes (mainly $\geq$34 m) and modern receivers. It is not practically and economically feasible to communicate continuously with the HelioRing CubeSats using the DSN, since it is heavily used for other missions [20, 9]. Therefore, the construction of a new, more or less similar-scale network of ground stations all over the world would increase the costs dramatically. Thus, there is an interest to look for ways to reduce the size and the complexity of the ground stations for the mission.

One possible choice is to use laser communication in HelioRing. Laser communication is a promising and growing field in space communication, since it enables more efficient communication[3] and a much higher data rate than radio frequency (RF) communication. The use of laser communication also makes it more feasible to communicate from deep space without using large antennas on CubeSats. Among several advantages, deep-space laser communication also faces considerable challenges. Some of these are stringent laser pointing accuracy requirements and the influence of the Earth's atmosphere on communication. [21]

[2]Deep space is defined to begin at a distance of two million kilometers from the Earth by the International Telecommunications Union (ITU) [12].

[3]Mainly due to the much narrower beam directed to the receiver. This leads to a lower average transmit power, which is beneficial for a CubeSat mission.

Laser communication (also inter-satellite) has been demonstrated in many space missions. However, this has not taken place within deep-space distances, but laser beam pointing has been demonstrated to a ground station by the MESSENGER probe from 24 million km from the Earth [21]. Regarding CubeSats, laser communication will be demonstrated for the first time by the Optical Communications and Sensor Demonstration (OCSD) mission [22]. In this mission, a 1.5-unit (U) CubeSat will use a laser to communicate with a ground station from LEO.

1.1 Objectives of the thesis

The main objectives of this thesis are the following:

1. To define the objectives and requirements of the HelioRing mission.
2. To investigate how the CubeSat fleet would communicate with the Earth.
3. To evaluate the performance of the communication concept.

Since the thesis is the first study of the HelioRing mission, the objectives and requirements of the mission shall be defined first. In addition, a brief introduction to the mission is given. The primary objective of the thesis is to design communication between CubeSats and the Earth, which will preliminarily solve one of the mission's major challenges. Inter-CubeSat laser communication between the HelioRing CubeSats is designed in order to use inexpensive ground stations. The thesis suggests that there could be an additional CubeSat orbiting the Earth that would relay data to the ground stations using RF communication. In this way, also the total cost of the mission will stay relatively low, which is inherent for CubeSat missions. This is the main reason why this thesis focuses on using a laser wavelength instead of RF in deep-space communication.

The scope of the thesis is to design the concept and systems at high level rather than to introduce detailed system designs. The critical subsystems, especially for communication, are proposed and presented. The concept includes the design of the communication architecture, the link budgets and the communication schedule. Finally, it is demonstrated that the concept fulfils the requirements of the mission.

The results of the thesis demonstrate the feasibility of communication in the HelioRing mission. Thus, the results are also significant for the feasibility of the whole mission. Also, the results may be useful to other organisations who are interested in designing a small spacecraft mission into deep space where laser communication could be the choice for crosslinks or even for making communication to the Earth feasible.

1.2 Structure of the thesis

The thesis is organized into five chapters, the first of which is this introductory chapter. Chapter 2 gives an introduction to space weather and how it is forecast. In Chapter 3, the overview of the HelioRing mission is presented and the thesis

proposes some system designs for the CubeSats. Chapter 4 comprises the background theory of deep-space laser communication and the design of the laser communication concept for the HelioRing mission. At the end of the same chapter, the concept is briefly evaluated and compared to one possible RF communication concept. Finally, Chapter 5 summarizes the thesis with conclusions and suggestions for future work.

2 Space weather and its forecasting

The previous chapter explained why space weather forecasting is important and why there is a need for increasing the prediction lead time of geomagnetic storms on the Earth. In order to understand how the HelioRing mission would increase the lead time, the origin and characteristics of space weather are discussed in more detail in this chapter. Additionally, how space weather can be forecast by using in-situ measurements is explained in short. At the end of the chapter, current and proposed forecasting missions are briefly introduced.

2.1 Solar wind

The Sun continuously emits plasma in all directions from its corona. This stream is called the solar wind and it consists mainly of electrons and protons, but also heavier particles. The properties of the solar wind vary continuously in terms of speed, density as well as magnetic strength and direction. During normal conditions, the speed is below 450 km/s, which is referred to as low speed. But it can evolve fast, up to around 600–800 km/s, which is known as fast solar wind. The magnitude of the solar wind's magnetic field is in the order of 4–5 nT during low and fast wind speed at 1.0 AU. During a coronal mass ejection, the speed and magnetic strength values can increase rapidly [23]. [3, p. 39]

CMEs are the most massive and hazardous eruptions from the Sun's corona. Although their average speed is in the order of 400 km/s, they can accelerate up to 3000 km/s or faster within a distance of some solar radii from the Sun [3, p. 51]. A fast CME, travelling about 1100 km/s, is shown in Figure 1 which was taken by the Solar and Heliospheric Observatory (SOHO). Superfast CMEs ($\geq$2000 km/s) are relatively rare [3, p. 64]. On the other hand, the interplanetary solar wind will reduce the speed of a CME as it travels farther from the Sun. It has been studied that the maximum speed at 1.0 AU can be around 2000 km/s [3, p. 58]. However, in 2012, a superfast CME having a speed of 2300$\pm$100 km/s at 1.0 AU was measured by NASA's Solar Terrestrial Relations Observatory (STEREO)-A spacecraft [4]. The CME was the fastest ever observed at 1 AU. Luckily, the CME was not directed to the Earth. What made the CME so fast was that there were two consecutive and superfast CMEs in more or less the same direction. The first one cleared the majority of the interplanetary solar wind medium in front. Therefore, the second one did not experience a typical deceleration, and this led to the huge speed recorded at 1.0 AU. These kinds of phenomena are very rare, and therefore, this is a good reason to assume 2300 km/s as the maximum speed for a CME at a distance of 1.0 AU. [4]

The angular widths of CMEs are typically in the range of 24° to 72° [3, p. 51]. Therefore, there can be much variation in the travel direction of a CME, and it can still easily reach the Earth. The daily average CME rates are in the range from 1 (near solar minimum) to about 4 (near solar maximum) [3, p. 51]. The magnitude of the magnetic field is usually between 10–100 nT during a CME at 1.0 AU [3, p. 58].

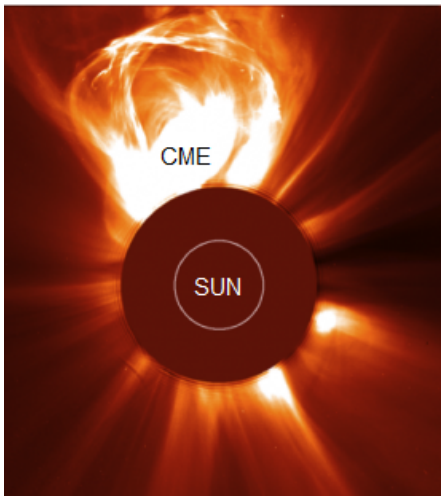

Figure 1: A fast travelling CME seen by SOHO on February 27, 2000. The CME reached a speed of about 1100 km/s. Courtesy: SOHO/LASCO.

2.2 Space weather forecasting

For forecasting geomagnetic storms and other possible effects on the Earth, there are two major parameters that are of interest: the speed and southward[4] component (negative B_z) of the magnetic field of a CME [3, p. 40, 55]. If B_z is southward oriented, the magnetic fields of the CME and Earth reconnect and this allow the transfer of energy of the CME into the magnetosphere resulting in possible geomagnetic storms [24].

Even if an Earth-directed CME had a high speed, it would not cause strong geomagnetic effects as long as the B_z is positive or only slightly negative [25]. But if the B_z component is highly negative, and its duration is pronounced, the speed of the CME and the geomagnetic activity correlate strongly. A faster CME will transfer more energy to the Earth's magnetosphere. The geomagnetic activity is also further amplified by the duration of the high negative B_z value [3, p. 72]. That is, a longer duration results in more energy transfer from the CME's plasma to the magnetosphere and, in turn, more powerful effects on the Earth. A large CME is able to affect the magnetosphere for a long time (several hours) but negative B_z can change considerably during a CME passage [26]. Therefore, it is not only important to forecast the peak value of the negative B_z at the Earth, but also how long the highly negative B_z values last in addition to the CME's speed [3, p. 72].

To observe CMEs and other mass released from the Sun, one uses a coronagraph [3, p. 50–51], such as SOHO. In images captured by a coronagraph, the Sun itself is blocked so that one can see if CMEs are released. From several observation images one can then estimate the speed of these eruptions [3, p. 50–51]. After this, one can estimate when the CME would reach the Earth if it is Earth-directed. Depending on the speed of the CME, the travel time can last from less than 20 hours (for superfast CMEs) up to several days. The problem to date has been to determine

[4]Relative to the Earth's geographic poles.

the accurate arrival time of a CME, and thus, predictions of the arrival time can vary approximately ±12 hours from the real one [6]. But an even larger problem is forecasting whether or not the CME is able to cause strong geomagnetic activity [2]. Although a massive CME is Earth-directed, it may lead to no strong geomagnetic activity or other threats due to an only slightly negative B_z value. The strength and direction of the B_z cannot be determined at the moment by observations from the Earth or from space [2]. In fact, there have been false alarms of large CMEs that seemed hazardous but did not cause strong effects on the Earth [8]. The geoeffective potential of a CME can be accurately known only when it reaches the L1 point, and hence, the ACE satellite. ACE measures the solar wind in detail, including the strength and direction of the magnetic field with a magnetometer [27]. The ACE spacecraft was launched already in 1997 and its operation will cease in the near future due to the depletion of propellant for attitude control [27]. The successor of ACE, the Deep Space Climate Observatory (DSCOVR) has already been launched and it will start operation at the L1 point in 2016 [28].

However, though DSCOVR will replace ACE, the in-situ measurements for continuous space weather forecasting are still made at one point (L1). Also, DSCOVR will be the only spacecraft to measure the solar wind and forewarn of geomagnetic storms in the near future [27]. If the properties (especially magnetic field properties) of an Earth-directed CME would be available well in advance (at least several hours), it could significantly improve the forecasting of the arrival time and B_z strength at the Earth. This necessitates making in-situ measurements of the solar wind farther from the Earth than the L1 point [5].

The direction of the magnetic field of a CME can change while travelling due to interaction with other CMEs or a possible large-scale rotation of the CME [26]. It should be noted that current forecasting models are not able to predict this behaviour but only give some estimations about the speed and arrival time of CMEs [2]. However, there has been promising research into this magnetic problem, and there exist some models that can predict B_z strength at the Earth with relatively good accuracy by using some magnetometer measurements from several space missions as reference [5]. In order to put this model into practice, magnetic field measurements within 1.0 AU would be needed, preferably at around 0.70–0.95 AU. Further investigations are, however, needed for reliable forecasting in addition to the study in [5] as it only consisted of some CME examples.

2.3 Proposed space missions for forecasting

Points farther than the L1 have been of great interest to researchers for gaining in-situ CME measurements more in advance [8]. If a traditional spacecraft was placed closer to the Sun (from L1), it would eventually start to drift out of its stable position on the Sun-Earth line. But if additional earthward thrust is applied at this artificial Lagrange point (sub-L1), one can station-keep there (if the thrust is powerful enough). In this regard, a solar sail technique has been proposed for station-keeping at a sub-L1 point because of its indefinite thrust capability offered by the Sun. The larger the sail, the farther a sub-L1 point from the Earth can be reached, since a

larger sail area produces more thrust. [8]

The most advanced of this kind of proposed concepts is the Sunjammer mission [8]. It is designed to station-keep at a sub-L1 point at 0.98 AU, which would allow doubling the lead time compared to ACE. The spacecraft is capable of measuring the strength and direction of the magnetic field as well as the speed and the density of the solar wind. The major challenge of this mission is the opening of the spacecraft's large solar sail (40 m x 40 m) successfully in space. The spacecraft and its sail are depicted in Figure 2. The attitude is controlled by four triangular vanes, one in each corner. The largest sail (14 m x 14 m) to date has been demonstrated by Interplanetary Kite-craft Accelerated by Radiation Of the Sun (IKAROS) [29]. Therefore, Sunjammer's demonstration would be a difficult but substantial step forward in the field of solar sail technology. Sunjammer was set to launch in March 2015, but the mission was cancelled due to delivery problems of the satellite. The real launch date is unknown. [8]

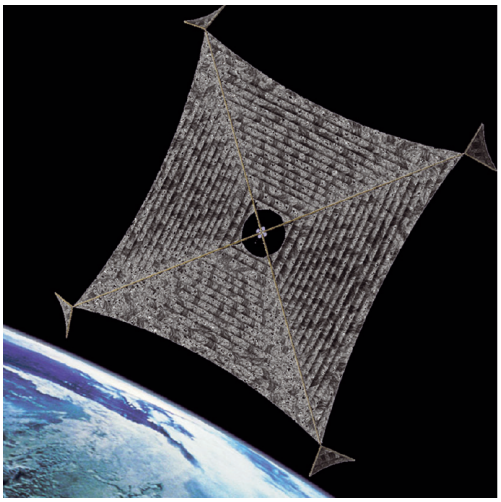

Figure 2: An illustration of the Sunjammer orbiting the Earth. The core (including the main subsystems) of the satellite is in the center surrounded by the solar sail. The spacecraft would fly from Earth orbit to its final sub-L1 point. [8]

In comparison with the Sunjammer, to be able to increase the prediction lead time even more by station-keeping, one would need either a larger sail or a lighter spacecraft [8]. This presents an extremely difficult challenge [8]. Another option to make in-situ measurements is to have a greater number of spacecraft uniformly distributed along a heliocentric orbit. This is the aim of the Coronal Mass Ejection Analysis Reporting to Earth To Allow Keeping Everything Running (CARETAKER) mission concept[5] [9] in which six spacecraft would observe the Sun and measure the solar wind in detail at 0.72 AU. This distance equals the orbital distance of Venus from the Sun. The primary objective is to increase the prediction lead time of

[5]The CARETAKER mission concept was designed by students and researchers in the Alpbach Summer School in 2013. The concept has not been, however, officially proposed to any space agency to date.
Website on the concept: http://www.summerschoolalpbach.at/index.php?file=students.htm

geomagnetic storms on the Earth based on observations of propagation trajectories and in-situ measurements of the properties of CMEs.

All CARETAKER spacecraft would be equipped with a magnetometer as well as a plasma and ion monitor. Two of the six spacecraft would also contain a coronagraph to gain stereo images of the Sun. This enables one to determine the trajectories of CMEs accurately. The three closest spacecraft to the Earth would deliver data to the ground station every 15 minutes. One would use X-band in communication. The spacecraft would contain a 1-m parabolic high-gain antenna, and all six ground stations would consist of 15-m dish antennas. The mission would require the construction of six ground stations that would be more or less uniformly distributed along the longitude axis. Two of the ground stations would communicate continuously with the spacecraft. The orbit of the spacecraft is depicted in Figure 3. It also illustrates the L1 and sub-L1 points in comparison with the orbit of CARETAKER. [9]

The CARETAKER mission would significantly advance space weather forecasting, due to the much closer distance to the Sun in comparison with the L1 and sub-L1 points. Any necessary mitigation actions could be done well before a potentially destructive CME will arrive at the Earth. The major disadvantage of the mission is its large total cost estimate of 1300 million euros. The cost of the ground segment is estimated to be approximately 400 million euros. In comparison, the total cost of the Rosetta mission is about 1400 million euros, which can be considered as an expensive space mission. The detailed CARETAKER concept is further presented in [9]. [9]

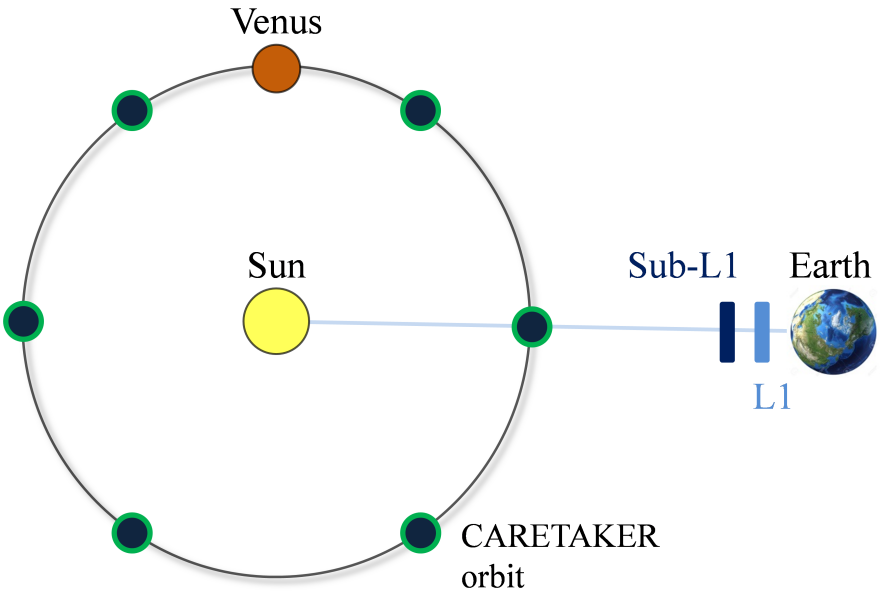

Figure 3: The orbit of the CARETAKER mission (figure not to scale). The six spacecraft are represented as green circles. The L1 and sub-L1 (at 0.98 AU) points are also illustrated.

3 The HelioRing mission overview

The previous chapter discussed space weather and how the properties of CMEs (especially the magnitude of the southward magnetic field direction), are important to be forecast well in advance before they arrive at the Earth. The overview of the HelioRing mission is presented in this chapter in order to show how the mission strives to increase the prediction lead time of geomagnetic storms. The objectives and requirements for the mission are defined first, followed by the mission description.

As already pointed out, there are no previous studies of this mission to date. Thus, this thesis presents the mission for the first time and discusses the mission briefly at a high level. The thesis proposes the configuration and subsystems for the HelioRing CubeSats on a general level. In subsection 3.8, the thesis defines research questions for the communication concept design. These questions are solved in the next chapter. A brief summary of the mission is provided in Table 2 at the end of this chapter.

3.1 Objectives of the mission

Before stating any objectives, it is important at first to present the goal of the HelioRing mission in brief. The mission statement could be phrased as follows:

> *To provide magnetic field properties of Earth-directed coronal mass ejections by using a CubeSat fleet in a heliocentric orbit for increasing the prediction lead time of geomagnetic storms on the Earth.*

It can be assumed that the maximum CME speed is 2300 km/s at the Earth as discussed in subsection 2.1. The CubeSats are intended to be positioned in a heliocentric orbit at around 0.6–0.8 AU, but the exact distance from the Sun has yet to be decided. The following objectives for the mission have been stated:

Primary objectives:

1. To warrant a prediction lead time of at least three hours for the most extreme geomagnetic storms based on in-situ magnetic field measurements.
2. To use only CubeSats as spacecraft in the mission in order to reduce costs.
3. To have a minimum operational lifetime of three years in the final heliocentric orbit for each CubeSat.

Secondary objective:

4. To provide magnetic field properties of the solar wind around the Sun in near real-time for scientific purposes.

Three hours for the minimum prediction lead time was chosen as an objective, since it would permit necessary mitigation actions before a CME arrives at the Earth [7]. This in not a strict objective as, e.g., a minimum lead time of two hours would

also be a significant improvement in space weather forecasting. Though the exact orbital distance is currently unknown, it is reasonable for this thesis to design the communication concept for a single orbital distance. The concept is designed for the orbital distance of 0.72 AU, since it is about in the middle of the anticipated range of 0.6–0.8 AU. It also equals the orbital distance of Venus from the Sun. Venus could be used as a gravity assist during travelling from the Earth to the final orbit.

A CME that has been detected at 0.72 AU requires about five hours or more to reach the Earth. Depending on the communication system, there is a certain delay in delivering measurement data to the ground station. This has been taken into account in Objective 1 and two hours are given for the delivery of the measurement data. The total time (three hours prediction lead time + two hours communication delay) corresponds to the maximum CME speed of about 2300 km/s when it reaches the Earth. If the real orbital distance differs from 0.72 AU, the communication delay may be different.

The minimum operational lifetime of three years was stated as one of the objectives, since it is reasonable to aim at a multiyear space mission for space weather forecasting. The three-year lifetime is estimated to be feasible, but it demands careful design, since numerous CubeSat missions have failed for different reasons during their lifetime [30].

Although only Earth-directed CMEs are relevant for forecasting, it would be beneficial to also deliver also data from all CubeSats aside from this direction. This data would be extremely valuable for scientific use, e.g., in order to advance space weather forecasting with the increased data. It would also allow predicting the space weather phenomena for other planets, such as for Mars during manned missions. It should be noted that the delivery time of offside data is less strict in Objective 4 than in Objective 1, as the most critical measurement data will obviously be from the closest CubeSats to the Earth.

3.2 Requirements of the mission

In order to achieve the objectives, the following seven main requirements for the mission were derived together with a collaborative IWF research group:

1. Spacecraft shall make in-situ 3-axis magnetic field measurements of the solar wind with the angular separation of a maximum of 36° heliospheric longitude between two CubeSats and at an orbital distance range of 0.6–0.8 AU.

2. The magnitude of the magnetic field shall be measured with a resolution of 0.1 nT in the range 0 to 200 nT.

3. The uncertainty of the total magnetic field measurement shall not exceed ± 2 nT below 50 nT and ± 5% above 50 nT.

4. The magnetic field of the solar wind shall be measured with a time resolution of one minute.

5. The uncertainty of the magnetic field direction measurement shall not exceed 10°.

6. The systems and components of the CubeSats shall operate for a minimum of three years in the final heliocentric orbit.

7. Measurement data shall be provided to at least one of the ground stations within two hours once a CME has arrived at the orbital distance of the nearest 36° heliospheric longitude or sector to the Earth.

The closer to the Sun-Earth line a HelioRing CubeSat measures the magnetic field properties of a CME, the more accurate the forecasting of the CME effects on the Earth will be. Furthermore, the more spacecraft reside at the orbit, the closer to the line one of the spacecraft continuously is. Therefore, there is a trade-off between the separation angle of the CubeSats and the mission cost. The orbital separation of 36° heliospheric longitude between two CubeSats is estimated to be sufficient for relatively reliable space weather forecasting. This necessitates having ten CubeSats in the fleet.

A further discussion for Requirements 1 and 2 can be found in subsections 2.1–2.2. There is good reason to suppose that the magnitude of the magnetic field of even the most extreme CMEs does not exceed 200 nT [31, 32]. Requirements 2–5 are consistent with previous missions and observations near to 1 AU, and therefore the required measurement accuracies are in the same order of magnitude as, e.g., for the STEREO spacecraft for solar observation [32]. The values for Requirements 2, 3 and 4 are preliminary at the moment and they give just an order of magnitude of the required performance. However, more exact and realistic values for the accuracies should be studied in greater detail in future work.

The essential requirements for this thesis are Requirements 1, 4, 6 and 7. The primary requirements for the thesis are Requirements 1 and 7 as they have a strong impact on designing the communication concept. Furthermore, the required transmitting data rate for CubeSats is dependent on Requirement 4. The components and systems that are selected for communication are dependent on Requirement 6.

3.3 Mission description

Following the mission requirements, a concept of how these will be achieved is described briefly and at a high level in the following. The ten CubeSats will orbit the Sun in a heliocentric orbit at 0.72 AU, which is depicted in Figure 4. They are uniformly distributed in the orbit, resulting in an orbital separation of 36°.

The orbital separation of Venus and its nearest CubeSat is 18°. Therefore, the distance between them is about 34 million km. Thus, the two CubeSats closest to Venus experience some gravitational force of Venus. These two CubeSats might contain only little more propellant that would be used for restoring the initial orbital separation between the CubeSats. It is beyond the scope of this thesis to show the demonstration of the effect of Venus using calculations. Instead, these can be shown in future work.

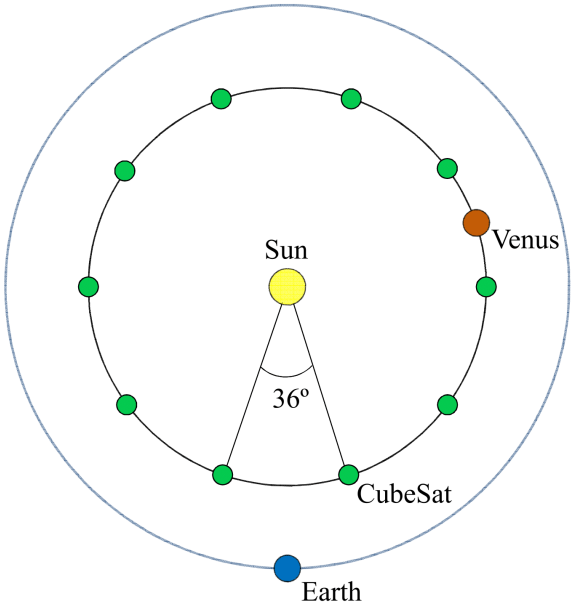

Figure 4: A representation of the heliocentric orbit of the CubeSats (figure not to scale). The ten CubeSats are orbiting the Sun at 0.72 AU, i.e., at the same distance as Venus. The CubeSats are distributed uniformly along the orbit, which leads to the angular separation of 36° heliospheric longitude.

As mentioned above, the primary objective of the mission is to forewarn of Earth-directed CMEs and provide data on their magnetic properties in near real-time. Thus, if a CME had the potential to produce strong geomagnetic storms, it would be known several hours beforehand, due to measurement data provided for future forecasting algorithms. This is the major advantage of the HelioRing mission and it would have a significantly positive effect on the safety of the global technological systems.

If a CME was released from the Sun, it would reach 0.72 AU at some point, where at least one CubeSat would detect the CME and would make measurements of its magnetic field. And if the CME was Earth-directed, the CubeSat closest to the Earth would eventually communicate with the ground station. Furthermore, the ground station would deliver information of the future geomagnetic activity to the relevant organizations (e.g., electricity distribution companies) who would perform mitigation actions. The above process is illustrated in Figure 5. This is the most important phase during the mission. However, the CubeSats would make measurements independently of CMEs and provide the measurement data of the solar wind regularly to the Earth.

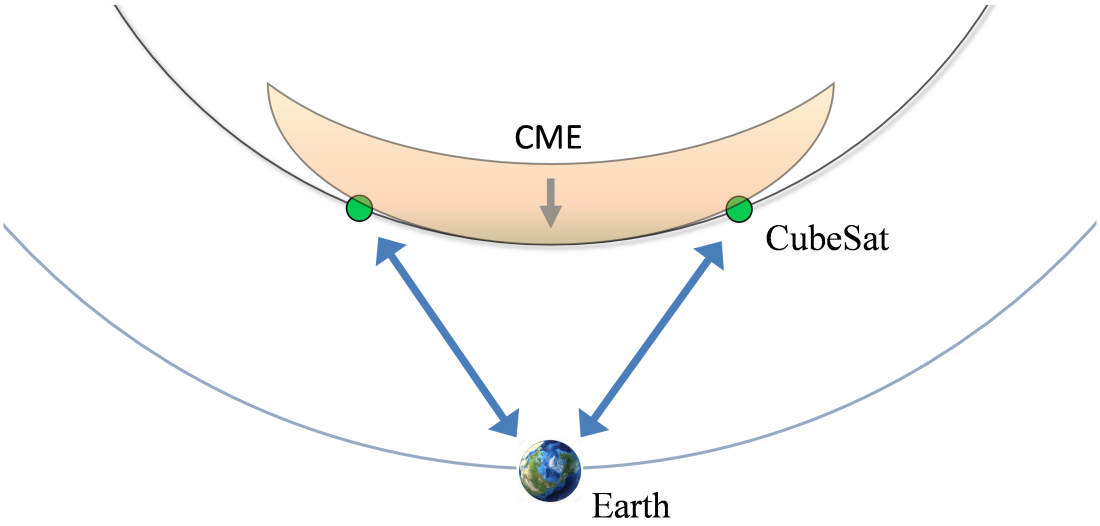

Figure 5: An illustration of the most important communication process for the mission (figure not to scale). The two closest CubeSats to the Earth transmit measurement data of CMEs to the ground station. In this case, a CME has reached 0.72 AU, and its magnetic properties would be transmitted within a certain time period to the ground station.

3.4 Spacecraft: CubeSat

The main reason to use CubeSats as spacecraft is that they are remarkably more inexpensive to design, build and launch compared to conventional spacecraft. Therefore, several universities and organizations have been able to design their own satellites and keep the total cost of their missions low. [15]

The first mention of a CubeSat dates back to the year 1999, when Bob Twiggs from Stanford University and Jordi Puig-Suari from California Polytechnic University introduced the platform [14]. In the same year, the CubeSat standard was developed by California Polytechnic State University and Stanford University [14]. At that time, the standard defined the limits for the dimensions and mass of a CubeSat [14]. The dimensions shall be 10 cm $\times$ 10 cm $\times$ 10 cm, which corresponds to 1 unit (U). The mass shall not exceed 1.33 kg. The standard defines also regulations for, e.g., electrical power, materials and communication (see [33] for further CubeSat standard definitions). A CubeSat that has been designed according to the standard can be ejected from the launcher by the Poly Picosatellite Orbital Deployer (P-POD) [15]. Also other deployer systems exist [15]. The P-POD is an adapter that is integrated into the launcher and, at a certain moment in space, the CubeSat will be jettisoned to its desired orbit.

Since 1999, the standard has been updated several times and larger CubeSat form factors have been introduced. In addition to 1U, the form factors of 2U, 3U, 6U, 12U and even 27U have been standardized and they are multiples of the 1U form factor [34]. The most used form factors have been 1U and 3U [30, 35], the examples of which are shown in Figure 6. They have been designed mostly for purposes of

education, technology demonstration, or scientific research [15]. So far, about 300 CubeSats have been launched into space [13] and many more are under development.

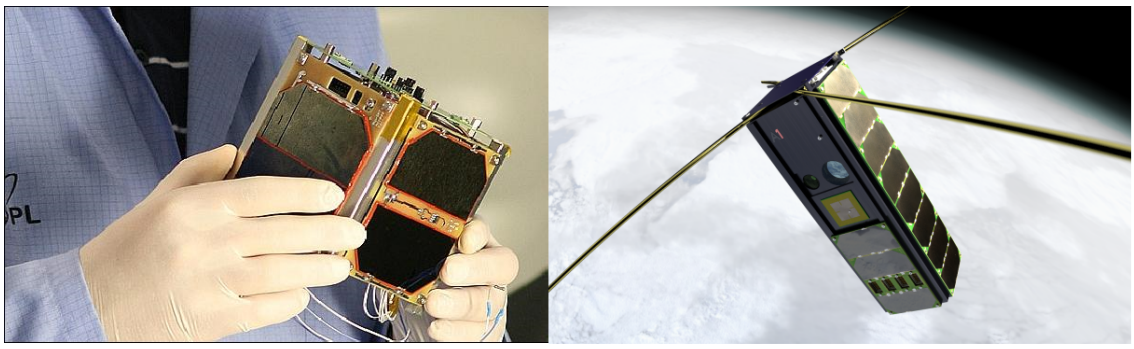

(a) PW-Sat CubeSat (b) Aalto-1 CubeSat

Figure 6: Two typical forms of CubeSats. The flight model of the Polish 1U PW-sat (launched in Feb. 2012) is on the left (a) [36]. The 3U configuration is illustrated on the right (b), where the Finnish Aalto-1 CubeSat (due to be launched in mid-2016) is orbiting the Earth [Courtesy: Pekka Laurila].

The form factors larger than 3U are widely of interest, since they allow more volume and mass and, thus, more performance for such missions where CubeSats could be able to travel farther in space and do operations that could be challenging or even impossible with CubeSats of smaller form factors. In addition, CubeSat subsystems have advanced and matured significantly since the early years, which enables one to design new kinds of missions. [34]

These new missions are mainly based on the 6U form factor, and there are several ambitious concepts to the Moon [37], L1 point [38], Mars [19], and even to Jupiter [39]. 6U has the size of 12 cm $\times$ 24 cm $\times$ 36 cm and shall have a mass of no more than 12 kg [34]. This form of a CubeSat is jettisoned from a Canisterized Satellite Dispenser (CSD) instead of P-POD or from another deployer [34]. Probably the most well-known and advanced 6U CubeSat mission is currently the MarCO mission [19], in which two identical 6U CubeSats will be launched to Mars. Both CubeSats will be ejected from the launcher in near-Earth space and they will fly independently to Mars. They will be able to do correction manoeuvres for their trajectories after the separation. Therefore, the MarCO mission to Mars probably represents a real deep-space mission with CubeSats for the first time in 2018. The CubeSats will not orbit Mars, but they will perform a flyby and will only relay to the Earth information of the landing of the InSight lander. The 6U MarCO CubeSat is illustrated in Figure 7.

The MarCO CubeSats have one of the state-of-the-art antenna concepts for CubeSats as they will be equipped with a high-gain reflect-array X-band antenna (the yellow plate in Figure 7) [17]. The antenna has a gain of about 28 dB. The more gain the spacecraft's antenna has, the smaller dish is needed on the ground station (see Appendix A). Alternatively, a higher gain enables a higher data rate if needed, by keeping the dish size the same. Even though the MarCO CubeSats have their high-gain antennas, they require one of the DSN stations which has a 70-m

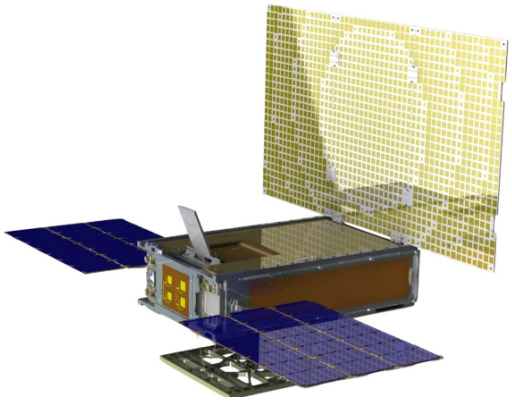

Figure 7: An illustration of the 6U MarCO CubeSat. The yellow plate at the top represents a high-gain reflect-array antenna at X-band. [Courtesy: NASA JPL]

dish in order to achieve a data rate of 8 kbits/s from Mars. This is a low data rate and it is due to the high free-space loss in the link.

There are also several other 6U CubeSats under development. Many of them are due to be launched in 2018 when NASA's Space Launch System (SLS) rocket [40] is scheduled to be launched for the first time. SLS is a new promising rocket for launching, e.g., 6U CubeSats to out of Earth orbit. In 2018, SLS is supposed to launch at least four 6U CubeSats as secondary payload, such as Lunar Flashlight to the Moon, BioSentinel into a heliocentric orbit, and NEA Scout to a near-Earth asteroid [40]. SLS will have the capacity to accommodate up to eleven 6U CubeSats with a single launch and, thus, it enables realistic launch probabilities for this form factor into deep space in the future. Therefore, it could be also the logical choice for the HelioRing mission.

This thesis suggests the 6U form factor for the HelioRing CubeSats, as it is anticipated that all the required subsystems would probably fit into the 6U form factor but probably not into 3U. On the other hand, the 12U form factor would have enough volume to accommodate all subsystems. However, it is uncertain whether there will be launch opportunities for this form factor in the future, despite the standardization of 12U. In addition, the 12U form factor would result in a higher launch cost as the structure has more mass [34].

3.5 Subsystems

A deep-space CubeSat demands many new design approaches compared to CubeSats orbiting in LEO. There is probably a need for a propulsion system and a more powerful communication system as well as a more accurate and more demanding attitude determination and control system (ADACS). These technologies, including the magnetometer payload, are critical for HelioRing and are discussed briefly in the following subsections. [41]

3.5.1 Attitude determination and control systems (ADACSs)

A typical ADACS in LEO is equipped with a magnetometer and perhaps with an Earth sensor, which cannot be utilized in deep space for attitude determination [42]. In addition, magnetotorquers cannot be used for attitude control because of the absence of the Earth's magnetic field. A Sun sensor, however, can be used in deep space for coarse attitude determination and a star sensor for precise determination [30]. For precise attitude control, reaction wheels are typically used, also in CubeSats [30]. To detumble the wheels, magnetotorquers are often used [30]. Again, the magnetotorquers cannot be used in deep space for detumbling, and other systems are needed [42]. Typically, propulsion systems are used for this problem, which is possible for a 6U CubeSat due to the larger volume compared to the smaller form factors [42].

3.5.2 Propulsion systems

There are a few options for how the HelioRing CubeSats could reach their final orbit. Firstly, the CubeSats could be launched inside a carrier. This carrier would fly independently to 0.72 AU, where it would dispense the CubeSats at certain time intervals. Secondly, the CubeSats could travel independently from a Geostationary Transfer Orbit (GTO) to the final orbit [42]. GTO is typically used for geostationary satellites where these satellites use their propulsion system in order to reach geostationary orbit [42]. The first option would require additional launch mass due to the carrier, which would result in a significantly higher launch cost. Costs would also be increased due to additional requirements for integrating the carrier to the launcher. Also, the option would require the development of the carrier.

This thesis recommends the second option, which two main advantages: (1) the option would require only the CubeSats with a propulsion system which would enable travelling from GTO to the final orbit. (2) the option would enable the initial phase of HelioRing to be significantly more affordable due to the lighter launch mass. Nonetheless, it is not straightforward to design this initial phase for several reasons: firstly, no CubeSat has been in deep space to date [16]; secondly, ten CubeSats would probably travel at the same time to the same orbit; finally, only some cold-gas systems for propulsion have been used in CubeSats to date [43]. These systems allow only small trajectory corrections. However, when upcoming deep-space CubeSat missions will become a reality, one will have experience of them, and propulsion systems will have demonstrated their performance and reliability.

There has been research on propulsion systems for CubeSats that are based on either chemical, electrical, or solar sail systems [44, 45]. Solar sail systems have demonstrated their performance for CubeSats, but it is anticipated that this technique would be too difficult for the initial phase. There is only little experience in solar sails [45] and a fleet of ten CubeSats might become too complex to control [42].

Chemical and electrical propulsion systems require propellant to gain thrust. Therefore, it is typically desired to have as little propellant as possible in a spacecraft in order to save volume and mass for other subsystems as well as to save launch mass. Thus, these propulsion systems typically demand a good thrust efficiency, which is

measured by specific impulse [44]. That is, a propulsion system with a higher specific impulse needs less propellant mass to achieve a certain speed. Electrical propulsion systems have a significantly higher specific impulse than chemical propulsion systems [44]. On the other hand, their thrust levels are much weaker compared to chemical propulsion, which leads to a longer time required for reaching a certain speed. [44]

There has been research on electrical propulsion systems for CubeSats that achieve a high specific impulse [44, 46]. They typically require only little system mass and volume. One choice would be Indium Field Emission Electric Propulsion (In-FEEP) electrical propulsion systems [44, 46], which are able to achieve extremely high specific impulse and thrust levels up to 1 mN. Some state-of-the-art In-FEEP systems are described in [46].

The thesis recommends electrical propulsion, e.g., In-FEEP systems for HelioRing, as only those systems might offer a sufficient specific impulse for the CubeSats to fly from an Earth orbit to the final orbit. During the travelling, the CubeSats could exploit Venus as a gravity assist [42] when it is on the other side of the Sun. Thus, propellant mass could be saved and the CubeSats would not need to consume propellant to slow down their speed for the final orbit. A completely new study would be required for determining how the CubeSats would fly to their final orbit, and this thesis can provide only this brief background into the field.

3.5.3 Payload: Magnetometer

Magnetometers have been used in many NASA and European Space Agency's (ESA) deep-space missions to explore the magnetic conditions in their target. The magnitude of the magnetic fields is typically very weak, in the order of nT, which demands good sensor sensitivity and accuracy [10, 47]. However, there is another, even larger challenge. Since the interplanetary magnetic fields are so weak, the spacecraft's own magnetic field can disturb the measurements. The disturbances are due to the electrical equipment and structure of the spacecraft. Therefore, it is necessary to minimize magnetic disturbances under a certain level of magnitude. Further benefit is also achieved by placing the magnetometer sensor away from the spacecraft's structure, and thus, farther away from the disturbances. The placing is often done by setting a boom out of the spacecraft. These booms can be several metres long [10, 47]. In addition, there can be additional magnetometer sensors inside or closer the spacecraft and they can be used for more efficient mitigation of background noise. The boom can be either fixed or deployable. The sensor is connected to a board (typically inside the spacecraft) which is responsible for the power supply for the sensor and the handling of the measurement data. [47]

Magnetometers have also been used in most CubeSats, but for a different reason, namely to determine the attitude of the satellite. The Earth produces a magnetic field of many orders of magnitude higher that of the solar wind or a CME, and one does not need the same accuracy for the sensor as in typical deep-space missions. The magnetic cleanliness is also not a concern in LEO, since the Earth's magnetic field is several orders of magnitude stronger than the magnitude of disturbances. [48]

Huge progress has recently been made using CubeSats in the measurement of

the properties of weak magnetic fields [48]. Some CubeSats have had a sensitive magnetometer as payload, such as the CubeSat for Ions, Neutrals, Electrons, & MAgnetic fields (CINEMA) 3U CubeSat (launched in Sep. 2012 into LEO) [48]. CINEMA's magnetometer sensor was deployed with a wire by centrifugal force. This CubeSat uses a sensor called MAGnetometer from Imperial College (MAGIC) [49], which can also be considered for the HelioRing CubeSats. Its calibrated sensitivity of 2 nT gives a good baseline for developing the magnetometers for the HelioRing CubeSats. In addition, recent years have shown that high accuracy (absolute uncertainty < 1 nT) and sensitivity (< 10 pT/$\sqrt{Hz}$) are achievable with small sensor board areas (tens of cm^2) [50]. Furthermore, spaceborne magnetometers have also demonstrated wide dynamic ranges (hundreds of nT) and good radiation tolerance, which makes the demonstrated systems promising for space weather forecasting [50].

In addition to CINEMA, the Dellingr 6U CubeSat will represent the state-of-the-art CubeSat magnetometer system (expected to be launched in mid-2016 into LEO) [51]. Dellingr uses a deployable boom of 76 cm in length when extended. Dellingr and its deployed boom are shown in Figure 8 and the same system would offer a good baseline for designing the boom for a HelioRing CubeSat. Finding out how the sufficient magnetic cleanliness and required accuracy could be achieved for a sensor system would require a study of its own.

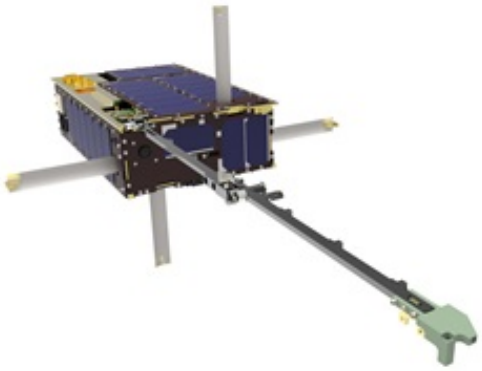

Figure 8: An artist's impression of the Dellingr 6U CubeSat developed by NASA's Goddard Space Flight Center. The boom for the magnetometer is deployed in the bottom right. [Courtesy: NASA, Luis H. Santos]

The volumetric allocation of subsystems for a HelioRing CubeSat is presented in Chapter 4 in order to determine the volume limit for the main communication system. The thesis considers the following main subsystems to be used in a 6U HelioRing CubeSat:

1. Housekeeping subsystems, including on-board computer, batteries and electrical power supply system.
2. Attitude determination and control system (ADACS).
3. Propulsion system.

4. Ultra high frequency (UHF) communication system for the initial phase of the mission (to be used before flying out of Earth orbit).

5. Science payload, i.e. the magnetometer and its board.

6. Main communication system.

UHF communication systems are typically used when CubeSats are dispensed from the launcher [15]. They allow contact to the ground station independently on the attitude of the CubeSat.

3.6 Challenges

Despite several ambitious objectives and a significance for humanity, the HelioRing mission has some unique challenges in space that no CubeSat has faced to date. One of the major challenges is the communication between the CubeSats and ground stations. No CubeSat has been farther than the HelioRing CubeSats would be, even if one took the MarCO Cubesats into account [19]. Also, it is necessary to communicate with the HelioRing CubeSats more frequently, actually many times within 24 hours with the closest CubeSats (see Requirement 1). This leads to the need to have several ground stations all around the world, since if only one ground station was used, it would sometimes be on the night side and continuous space weather forecasting would not be possible. Furthermore, communication with a fleet of ten CubeSats is also challenging due to little experience of fleet space missions. This requires well-designed timing for communication where the communication delay can be several minutes due to the long distances involved.

The second major challenge is reaching the final orbit for the HelioRing CubeSats (see subsection 3.5.2 for details). One challenge is also particle radiation in space. The HelioRing CubeSats must withstand ionizing radiation at least for three years and preferably even longer. All CubeSats have been in LEO [16] where radiation conditions are less of concern [15]. In LEO, the Earth's magnetic field provides protection against galactic cosmic rays as well as against particle radiation originating from the Sun [15]. Additionally, typical CubeSat missions last from several months to a few years, whereas the HelioRing CubeSats will be exposed to radiation for much longer, which makes the problem even more challenging [15]. However, there is extensive experience in space radiation protection from several deep-space missions and, thus, this challenge is considered less problematic than the first two. Nevertheless, there will most likely be a need for radiation-hardened components for critical subsystems and radiation shielding might became challenging due to the limited CubeSat size and mass [15].

The last challenge is to achieve sufficient magnetic cleanliness for the CubeSats and the required accuracy for the magnetometer. However, this challenge is estimated less problematic compared to the others as there is long experience in spaceborne magnetometer instruments [10, 50]. The following list summarizes briefly the major challenges for HelioRing, of which the first two are considered the most difficult:

1. How can all CubeSats communicate with the Earth from deep space in near real-time?

2. How to place the CubeSats in their final orbit?

3. How to ensure that the CubeSats will endure the radiation conditions in deep space for at least three years?

4. How to achieve sufficient magnetic cleanliness for the CubeSats and the required accuracy for the magnetometer?

3.7 Schedule

The activity of the Sun varies in 11-year cycles, which are counted from one solar minimum to the next [52]. In a solar maximum period, there are more CMEs released from the Sun, as discussed in Chapter 2. During a solar minimum period, the Sun's activity is low and large CMEs are rarer, even though a massive eruption can occur at any time [2]. Thus, the thesis suggests the beginning of a solar maximum period for the starting point of the operation at 0.72 AU.

The last solar maximum was in the year 2013, and thus, the near-maximum period can be considered to occur during the period from 2013 and 2015. It is expected that the next near-maximum periods will occur around 2024–2026 and 2035–2037 [52]. Therefore, the ideal year for starting the operation at 0.72 AU would be in 2024 (or 2034). However, the exact date and year also depend on many other things, and determining the most beneficial starting point would require further work. Moreover, due to the several substantial challenges and probably demanding subsystems, the mission may require a precursor mission. In the pre-mission, subsystem and some operational tests would take place, e.g., in near-Earth space. In addition, the number of CubeSats would probably be only a few, in order to reduce costs.

3.8 Research questions on data communications

This thesis aims to solve the aforementioned Challenge 1 (see subsection 3.6). The most critical open questions regarding communication are the following:

1. What is the size of the data that the magnetometer produces for a single measurement?

2. What other information is needed in addition to a magnetic field measurement?

3. How often will the measurement data packets be transmitted?

4. What housekeeping data is worth transmitting? How big is this data and how often will it be transmitted?

5. Eventually, once the above questions have been solved, what is the minimum data rate for communication?

6. What is the maximum communication delay from the nearest 36° heliospheric longitude at 0.72 AU to the Earth?

7. What systems will be used for communication and how much volume will they occupy?

3.9 Generated data to be transmitted from one CubeSat

It is worthwhile to determine the minimum data rate to be transmitted from one HelioRing CubeSat by estimating the data rate generated. Data that will eventually be transmitted to the ground stations is comprised of the payload and housekeeping (H/K) data of the CubeSats. The payload data consists of 3-axis magnetic field measurements, which are taken every second. For the final payload data, the measurements are averaged to one minute. A one-axis measurement contains 16 bits of data, which is sufficient according to Requirement 2.

If measurements were taken for one minute, the 3-axis measurement data would then contain data of 3×16 bits $= 48$ bits. For the final payload packet, there is an estimated 10 % overhead, which contains system information of the measurements (e.g., time stamps) [53]. Finally, the final size of payload data for a single CubeSat is about 53 bits from one-minute measurements and the generated payload data rate is thus about 1 bit/s.

H/K data contains information about the status of the spacecraft. Some relevant H/K data points are the following [54, p. 442–443]:

1. Temperature measurements at several points in the spacecraft.

2. The status of payload and other subsystems.

3. Power system parameters such as voltages in different systems, and the health of batteries and solar panels.

4. ADACS data, such as pointing history and data from sensors.

As was discussed in subsection 3.5, there are only proposals for the type of the subsystems, the H/K data rate (generated) cannot be estimated accurately. There are, however, some small-satellite space missions that could be used as a baseline. H/K data from the TUGSAT-1 satellite was the only reference [55] that was found, but it is sufficient to give a reasonable baseline for estimating the H/K data rate for a HelioRing CubeSat. TUGSAT-1 is a cube whose one side is 20 cm long. It has also several same subsystem types, such as a star tracker, as proposed for the HelioRing CubeSats. TUGSAT-1 generates H/K data of about 6.0 Mbits (compressed) per day. Thus, the H/K data rate is 69.4 bits/s. For a HelioRing CubeSat, a 15 % margin is added. Therefore, the estimated H/K data rate for a single CubeSat is 80 bits/s.

After all, the final data rate (including payload data) generated for a HelioRing CubeSat is estimated to be 81 bits/s. Table 1 summarizes the data rates generated by a CubeSat at 0.72 AU for data transmission. It can be seen that the H/K data rate clearly dominates the final generated data rate. Therefore, according to these

calculations, the time resolution of magnetic measurements could be much lower, e.g. ten seconds, if necessary. Finally, Table 2 summarizes the HelioRing mission briefly.

Table 1: The generated data rates estimated for a HelioRing CubeSat at 0.72 AU for data transmission.

Data	**Generated data rate (bits/s)**
Payload	1
Housekeeping	80
Total	81

Table 2: A summary of the HelioRing mission

Subject	**Description**
Mission statement	To provide magnetic field properties of Earth-directed coronal mass ejections by using a CubeSat fleet in a heliocentric orbit for increasing the prediction lead time of geomagnetic storms on the Earth.
Objectives 1.–4.	Primary objectives: 1. To warrant a prediction lead time of at least three hours for the most extreme geomagnetic storms based on in-situ magnetic field measurements. 2. To use only CubeSats as spacecraft in the mission in order to reduce costs. 3. To have a minimum operational lifetime of three years in the final heliocentric orbit for each CubeSat. Secondary objectives: 4. To provide magnetic field properties of the solar wind around the Sun in near real-time for scientific purposes.
Orbit	Heliocentric at around 0.6–0.8 AU. This thesis focuses on the orbit at 0.72 AU.
Number of CubeSats	10
Configuration for CubeSats	6U (12 cm × 24 cm × 36 cm, max. 12 kg)
Payload	Magnetometer

4 Laser communication concept design for the HelioRing mission

The previous chapter presented the HelioRing mission, including its objectives and requirements. Given these descriptions, communication can be designed between the CubeSats and the Earth according to the mission requirements. This chapter discusses different options to communicate and ends up using a laser wavelength in communication. In fact, the main benefit in using laser communication (lasercom) is that this technology offers an opportunity to design inter-CubeSat communication for the mission. This communication method can then be used for delivering the data from all HelioRing CubeSats to the Earth. The closer distance to the Earth leads eventually to a lower free-space loss for downlinking the data to the ground stations. The thesis suggests an additional CubeSat to be used in a Sun-synchronous dusk-dawn orbit and this satellite would downlink the mission data using RF instead of laser communication. Finally, the free-space loss will be so low that very inexpensive amateur RF ground stations can be used instead of expensive large optical or RF ground stations. The inexpensive ground station network is one of the major advantages of the laser communication concept.

This chapter begins with the introduction to the advantages and challenges of deep-space laser communication, following a discussion in the communication scenarios. After this, the laser link budgets are calculated. Next, data communications is designed in order to show that the laser communication concept fulfils the mission requirements. At the end of this chapter, the laser concept is evaluated in comparison with a possible RF communication concept in order to highlight the advantages and disadvantages of both concepts. Finally, the laser concept is briefly summarized in a tabulated form (see page 64).

4.1 Advantages and challenges of deep-space laser communication

Laser communication has been demonstrated in many space missions [57]. Typically, these have been satellite–ground links, but also inter-satellite lasercom has been demonstrated in some missions, such as the Semiconductor-laser Intersatellite Link EXperiment (SILEX) [58]. This inter-satellite lasercom is depicted in Figure 9. In this program, data was relayed between the ARTEMIS and SPOT-4 satellites.

However, deep-space lasercom has not been demonstrated, even though there have been laser beam pointing demonstrations from as far as 24 million km from the Earth [21]. Several deep-space lasercom missions have been designed to date, but none of them have yet been realized as a space mission [21]. Lasercom using a CubeSat will probably be demonstrated for the first time by the OCSD mission in the upcoming years [22]. In this mission, a 1.5U CubeSat will communicate with a laser with the ground station from LEO. Furthermore, there are several deep-space CubeSat mission proposals where lasercom is used, such as [39, 42].

Deep-space lasercom imposes a number of challenges, but also several major

Figure 9: An artist's illustration of inter-satellite laser communication between ARTEMIS and SPOT-4 satellites. In reality, the distance between the satellites was much larger as ARTEMIS communicated from geostationary orbit (GEO) to LEO. [58]

advantages. Both are shown in Table 3. One of the major advantages is a more lightweight communication system on a spacecraft [59]. This is mainly because an optical antenna aperture can be small, but still the antenna gain is much higher compared to traditional RF approaches [59]. Also, there are no frequency restrictions in lasercom unlike in RF communication bands. [21]

One of the major challenges in deep-space lasercom is the stringent pointing accuracy requirement [21]. Due to a more narrower beamwidth compared to RF communication, an even small miss-point can result in a total loss of the signal [21]. Another major challenge is the atmosphere of the Earth [21]. The uplink beam is refracted and broadened by the atmosphere, which leads to difficulties in directing the beam correctly and achieving sufficient transmit power into deep space. These challenges do not take place in the laser downlink on the same scale [59]. However, there are still large losses due to the atmosphere (especially from clouds) [59].

Table 3: The major advantages and challenges of deep-space laser communication.

Advantages	**Challenges**
More lightweight communication system	Stringent pointing requirements
Higher data rates	The atmosphere of the Earth
Unrestricted use of optical spectrum band	

4.2 Communication scenarios for the mission

Communication between the HelioRing CubeSats and the ground stations, i.e. the Earth, can be designed in several ways. There are three scenarios for communicating with the Earth that have been found to date, of which the thesis recommends the first one:

1. Laser communication (lasercom) between the CubeSats and the use of a relay-CubeSat (RelayCube) for delivering the data to the Earth.
2. Laser communication between the CubeSats and the ground stations.
3. Radio frequency (RF) communication between the CubeSats and the ground stations.

4.2.1 Laser communication between the CubeSats

The first scenario utilizes laser crosslinks between CubeSats, where each CubeSat communicates with its neighbouring CubeSats. The method is depicted in Figure 10. The ten CubeSats are distributed uniformly along the orbit, which leads to the angular separation of 36°. The 36° sector represents the critical sector from the mission point of view as it is required the CubeSats inside (or on edges of) this sector will be transmitting data to the ground station within 120 minutes from the latest measurement. The orbital planes of the Cubesats equal to the orbital plane of the Earth. The orbital plane of Venus differs slightly from that of the Earth, but it does affect the performance of the communication concept.

The CubeSat closest to the Earth communicates with a CubeSat called RelayCube, which orbits the Earth in a Sun-synchronous dusk-dawn orbit and is almost always visible to the other CubeSats. An altitude of 730 km would be ideal for RelayCube as, in this case, the duration of a solar eclipse is at minimum [56]. In this orbit and altitude, there is an eclipse period of 18 minutes per orbital period for about two months of a year. This duration is acceptable as the maximum communication delay is two hours. It is, however, necessary to take this into account in the design process.

When RelayCube communicates with the closest CubeSat, the background noise from the Sun will increase at some point so high that communication is no longer possible. For this problem, RelayCube communicates with the second closest CubeSat. RelayCube relays data from all CubeSats to the ground stations using RF communication. The major advantage of this scenario is that the construction and operations of the ground stations are significantly more affordable compared to the RF communication scenario (see subsection 4.2.3). The RF ground stations can have just simple and inexpensive UHF amateur RF systems in order to achieve a sufficient data rate (see subsection 4.7.4). It should be noted that the details of the RF communication and required RF systems for this link are beyond the scope of the thesis and, therefore, they are only briefly discussed in subsection 4.7.4. The detailed RF link budget should be calculated in future work.

The data flow from the CubeSats towards RelayCube depends on which side of the Sun the CubeSats are seen from Earth. The CubeSats on the right side deliver data

to the closest CubeSat clockwise and those situated on the left side counter-clockwise. The data to the Earth consists of payload and housekeeping (H/K) data. The data from the Earth to the CubeSats contains commands and different status messages of data transmission, such as "data received successfully", as well as updates of orbital parameters. The parameters are needed in navigation and directing a laser beam during communication in the right direction.

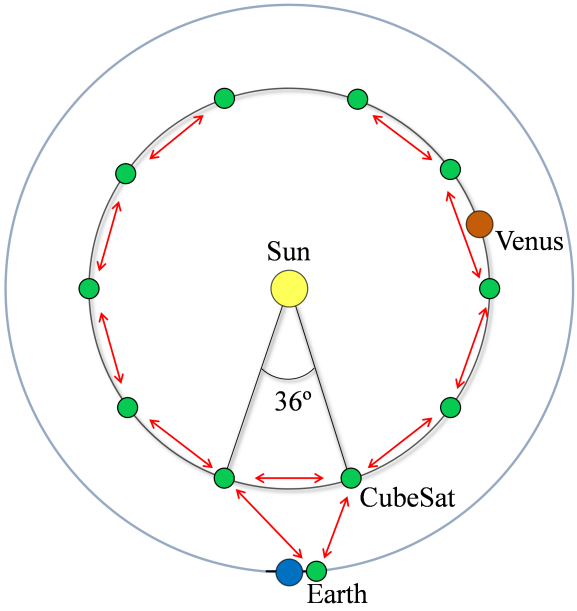

Figure 10: A representation of the heliocentric orbit and laser communication between the CubeSats (figure not to scale). The ten CubeSats are orbiting the Sun at 0.72 AU, i.e., at the same distance as Venus.

4.2.2 Laser communication between the CubeSats and the ground stations

The second option for communicating is to construct four to six optical ground stations uniformly distributed over the world in order to communicate with the closest CubeSats several times per day. All other CubeSats also communicate with the Earth, but less frequently (e.g., once per day). This number of ground stations is needed due to the fact that the ground stations must communicate with the nearest CubeSats several times per day and communication is not possible from the night side of the Earth. This scenario has enormous challenges due to the atmosphere of the Earth [21]. Therefore, this scenario is not recommended because of the major challenges in the uplink processes that were discussed in subsection 4.1.

4.2.3 Radio frequency (RF) communication between the CubeSats and the ground stations

The third scenario is similar to the second, but RF communication systems are used instead of optical systems. A link budget for this scenario is calculated in Appendix

A. By using state-of-the-art communication systems in a HelioRing CubeSat, the ground stations would still need to have about a 21-m dish in order to communicate with the farthest CubeSats from about 1.72 AU even with a very low data rate of about 85 bits/s. As the generated data rate was estimated to be about 81 bits/s in subsection 3.9, it becomes clear that a data rate for data transmission must be higher. This is because the ground stations will also communicate with the other CubeSats and new data is generated during the communication process.

Three ground stations is the minimum number that enables one to communicate continuously with a deep-space spacecraft. Otherwise, by using only two, there will be a point when the ground station antenna should point to the horizon, which would lead to too high losses due to the atmosphere. The construction and operations of three of these kinds of large stations have significant costs. For example, the construction and implementation cost of one of Deep Space Network's (DSN's) 34-m antennas was approximately 33 million dollars [60, p. 7]. Also, the annual operations cost is about 2 million dollars. The antenna is larger than the estimated minimum size for HelioRing, but it gives a baseline for estimating the possible costs for at least three RF ground stations needed for the mission.

In addition, the ground segment of the CARETAKER has been estimated to be around 400 million euros [9]. If one compares the ground segment of six ground stations to HelioRing in which three stations would be used, the HelioRing ground segment would cost roughly 200 million euros and still the dish size of 15 m would be too small. In the light of this, CubeSat missions can be considered relatively affordable space missions. Even though the total mission cost depends on the destination, a deep-space CubeSat mission has been estimated to cost roughly 30 million euros [42]. In this regard, the ground segment cost of HelioRing would significantly increase the total cost of the HelioRing mission in this scenario.

Another disadvantage of the RF concept is that there would be a communication outage at some point when the CubeSat orbits closer to the Sun seen from the Earth (see Appendix B for further details and calculations). It is estimated that this point occurs when the spacecraft is 1.5° to the Sun seen from the Earth. At this angle the background noise is significantly increased. Thus, if the diameter of the ground station antenna was not increased to overcome this noise, it is estimated that communication would be blocked. This leads to the situation that one cannot forewarn of CMEs for approximately two days. That is a long time from the standpoint of space weather forecasting, since there are about six communication outages per year. These outages occur almost equal time intervals in a year as it takes some time when the next CubeSat orbits close to the Sun seen from the Earth. It is calculated in Appendix B that the durations of the communication outages comprise 3.2 % of the mission lifetime. This is a disadvantage, but it is not considered too considerable as forecasting is estimated to be possible 96.8 % of the mission lifetime.

There could be one scenario more in which the CubeSat crosslinks are at RF instead of optical wavelengths. It was, however, realized during the communication design process that even by using the state-of-the-art RF systems in the CubeSats, crosslink communication would not be possible as the free-space loss is too high. It is beyond the scope of this study to provide a demonstration of the RF CubeSat

crosslink. Instead, another study is needed, in which this is shown by calculations.

After the presentation of all three scenarios, the first, i.e., the lasercom concept, is recommended to be used for communication in the HelioRing mission. In addition, an RF communication system is included in each CubeSat as a secondary communication system. It is assumed that the large existing RF ground stations, such as the DSN, are available for use from time to time (e.g., in an emergency situation) within the same concept. Furthermore, it is also assumed that they can be used in the initial phase of the mission in order for the CubeSats to be guided to the final orbit, as well as for obtaining the location and velocity of the CubeSats from the Earth.

4.3 Link budget design for the crosslinks between the CubeSats at 0.72 astronomical unit (AU)

Link budget design is typically an iterative process and so it is also for the laser communication link budget. The lasercom link budget design is presented in this subsection. It took numerous iterative times in order to obtain a link budget that is feasible. The main steps in the design process [61, 62] are the following:

1. to obtain the received power,
2. from the received power to obtain the number of detected photons,
3. to determine the background noise, and
4. to determine the data and bit error rate.

4.3.1 Link equation and received signal power

The first step is to determine what is the received power when a laser pulse is transmitted from one CubeSat to another. The received power P_r is given [59] by

$$P_\mathrm{r} = P_\mathrm{t} G_\mathrm{t} G_\mathrm{r} L_\mathrm{s} \eta_\mathrm{pt} \eta_\mathrm{pr} \eta_\mathrm{t} \eta_\mathrm{r} \tag{1}$$

where

P_t is the average (root mean square) transmit power
G_t is the transmitter gain
G_r is the receiver gain
L_s is the free-space loss
η_pt is the pointing efficiency of the transmitter
η_pr is the pointing efficiency of the receiver
η_t is the transmitter efficiency, and
η_r is the receiver efficiency.

The free-space loss L_s is

$$L_\mathrm{s} = \left(\frac{\lambda}{4\pi R} \right)^2 \tag{2}$$

where

λ is the carrier wavelength, and
R is the range between two CubeSats.

The carrier wavelength for deep-space lasercom is typically considered in the range of around 500 to 2000 nm [63, p. 354]. The angular separation of 36° between two CubeSats leads to R of about 67×10^6 km. This distance is assumed to be a fixed value, since there is no significant variation in R in the long term.

The transmitter gain can be approximated [59] as

$$G_{\mathrm{t}} = \left(\frac{\pi D_{\mathrm{t}}}{\lambda}\right)^2 \tag{3}$$

where D_{t} is the aperture diameter of the transmitter. The same applies to the receiver gain and is given similarly as in equation (3).

As a result of the iterative process in the laser link design, the parameter values listed in Table 4 are recommended for equation (1). Thus, the obtained $P_{\mathrm{r}} = -133.92$ dBW. The reasons for these values are further discussed in the following subsections. In deep-space lasercom, there is a need for a high peak transmit power in order to circumvent the enormous free-space loss. Typically, in such a case, one uses Pulse-Position modulation (PPM), which is widely proposed for deep-space lasercom. In PPM, data is transmitted via short pulses. PPM is discussed in more detail in subsection 4.3.4. Therefore, the objective was to achieve as high P_{r} as possible with the trade-off between volume, mass, complexity and power achievable for the transmitter. [63, p. 331–332]

The efficiencies of the transmitter and receiver were approximated and concluded from some deep-space lasercom studies representing similar values as in Table 4 [64], [65] and [63, p. 175]. The transmitter efficiency, η_{t}, is mainly composed of the efficiency of the optics, laser beam coupling to the optics and the far field. The receiver efficiency, η_{r}, is mainly comprised of the efficiency of the optics, laser scattering, the polarization loss, and the transmission loss through a narrow-bandpass filter. The filter, situated before the photon detector, is used for minimizing background light. [21]

4.3.2 Laser transceiver

A transceiver is composed of a transmitter and a receiver. This subsection focuses on a transmitter. The most important component of the receiver is a detector that is chosen in subsection 4.3.5. In seeking an efficient laser transmitter, there are many options for deep-space laser communication, such as pulsed lasers, fiber-waveguide amplifiers and pulsed-diode lasers [63, p. 337–345]. One choice for pulsed-diode lasers could be a Q-switched laser (at around 1064 nm), which is widely considered for deep-space lasercom missions because of its inherent ability to produce short but high peak power pulses [63, p. 235]. The Q means here the quality factor of the laser resonator. In laser transmitting, the length of pulses is typically tens of ns and the peak power some or tens of kW.

Table 4: Proposed link budget values for the received power P_r.

Parameter	**Value**	**Value (in dB)**
P_t	22 W	13.42 dBW
G_t		107.79
G_r		107.79
D_t and D_r	8.3 cm	
λ	1064 nm	
L_s		−357.91
R	67×10^6 km	
η_pt	0.92	−0.75
η_pr	0.92	−0.75
η_t	0.79	−2.0
η_r	0.75	−2.5
P_r		−133.92 dBW

There are two types of Q-switched lasers: passively and actively Q-switched lasers. In a passively Q-switched laser, the repetition frequency of pulses is fixed and therefore, this laser type cannot be used for encoding data [66]. Instead, many deep-space lasercom designs that have been developed are based on an actively Q-switched laser. However, actively Q-switched lasers are inherently bulky systems [67] and, thus, it is not advisable to consider that technology for a CubeSat mission.

Another laser option for the transmitter could be a pulsed-diode laser. This type of laser contains a laser diode that can be amplitude-modulated. The transmit power of the diode is too weak for a deep-space mission, and thus, its laser pulse needs to be amplified. The amplification can be done, e.g., with a fiber laser amplifier, which is considered a relatively compact way of achieving high-energy laser pulses [67]. [63, p. 338]

One choice for a pulsed-diode laser design is presented here. The design is based on the fiber-based master oscillator/power amplifier (MOPA). The detailed MOPA design is presented in [68]. The design can also be considered as a laser transmitter as the position of the laser pulses can be controlled in time. The performance of the amplifier is shown in Table 5. The carrier wavelength is 1064 nm, which is widely used for achieving short and high peak power pulses [63, p. 337]. The average output power is 22 W and the peak power 1.42 MW. The pulse width of 1.55 ns represents the effective pulse width, since the shape of the pulse is not rectangular but decreases continuously from the peak power. Thus, the total pulse width is about 2.6 ns. For calculations, the effective pulse width is used.

The repetition frequency of pulses can be continuously adjustable, but it was kept to 10 kHz. The reference does not state why it was kept to this value, but if it had been changed, it might have affected adversely other parameters of the design, such as output noise and pulse time jitter. Beam quality is an important parameter of the transmitter, since a too poor beam quality broadens the beam and leads to high transmission and coupling losses [63, p. 335]. A beam quality of 1.0 means that the beam shape is diffraction limited. A beam quality of 1.2 or less is

typically desired for deep-space lasercom missions [63, p. 335]. The MOPA design achieves this requirement as the beam quality is 1.2 or less [68]. The electro-optic efficiency represents the efficiency of the amplifier, so about four fifths of the energy is converted into heat.

Table 5: Values for the MOPA design [68].

Parameter	**Value**
λ	1064 nm
Average output power	22 W
Pulse width	1.55 ns
Output pulse energy	2.2 mJ
Pulse repetition frequency	10 kHz
Peak power	1.42 MW
Beam quality	≤ 1.2
Laser linewidth	0.2 nm (about 92 % energy in this linewidth)
Electro-optic efficiency	0.19
Dimensions	It is possible to be fit into a volume of 0.6U

The schematic of the MOPA from [67, Figure 5a], is depicted in Figure 11. The MOPA is otherwise the same as in [68], but the system schematic is simplified. However, the performance of the system is the same as before. The function of this pulsed-diode laser transmitter is described here. The pulse driver controls the laser seeder and the MOPA. The laser seeder is comprised of a master oscillator (MO), a fiber-coupled phase modulator (FM) and a semiconductor optical amplifier (SOA). The MO contains an amplitude-modulated diode laser and the FM is used to broaden the laser linewidth of the seeder and to minimize scattering from the optical fibers. The laser pulse is amplified by the SOA. Next, there is an optical isolator to prevent backward laser feedback and a filter, mainly to remove the amplified spontaneous emissions. These emissions are generated in the time intervals between laser pulses. After these two components, the laser pulse is amplified by three fiber amplifier chains. Between those amplifiers, the laser pulse is isolated and filtered in order to maintain a low noise level. [68]

The last amplifier comprises of straight photonic crystal fibers (PCFs). The core thickness of the PCFs is so large that they must be kept straight in order to avoid bending losses. In the MOPA design, a single PCF with a length of 72 cm was laid out into two parallel 36 cm long segments in order to obtain a more compact design. In this case, the laser beam is turned 180° by two mirrors. At the output of the PCF chain, the laser beam is pumped by a fiber-coupled diode at 975 nm. The laser pumping here means that the energy of the pumping laser is transferred into the gain medium of a laser.

The MOPA has no space heritage and the article does not state how much volume it needs. At this point, it is advisable to compare the design with other laser transmitter designs. Then, it is possible to estimate whether the amplifier is

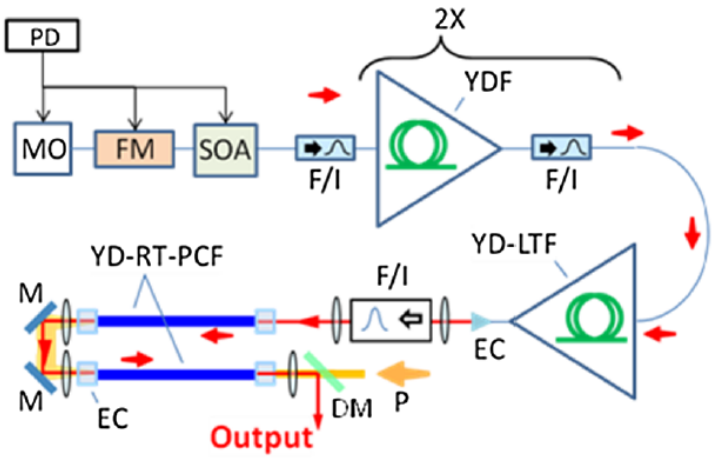

Figure 11: The schematic of a fiber-based MOPA architecture to be used as a laser transmitter for a HelioRing CubeSat. PD: Electronic pulse driver; PM: polarization maintaining; MO: master oscillator (amplitude-modulated diode laser); FM: PM fiber-coupled phase modulator; SOA: PM fiber-coupled semiconductor optical amplifier; F/I: PM fiber-coupled band-pass filter and optical isolator; YDF: Yb-doped, PM fiber preamplifiers (10-μm core); YD-LTF: Yb-doped, PM, longitudinally tapered fiber having 25/40-μm input/output core diameter; EC: endcap; YD-RT-PCF: rod-type, Yb-doped, 100-μm-core PM photonic crystal fiber; M: Mirror; DM: shortpass dichroic filter; P: 975 nm wavelength pump beam from a laser diode. [67]

possible to be fitted to the required volume. There are not many CubeSat laser transmitter references, since laser communication is a new field for CubeSats [22]. However, the AeroCube-OCSD 1.5U CubeSat [22] is one of these rare small satellites to communicate optically. The transmitter of the AeroCube-OCSD CubeSat has been demonstrated to fit into a volume of 10 cm $\times$ 10 cm $\times$ 2.5 cm (0.25 U).

The schematic of the AeroCube-OCSD CubeSat's transmitter is shown in Figure 12. It can be seen that the schematic comprises many of the same components as the MOPA in Figure 11, even though the transmitter of the AeroCube-OCSD CubeSat has been designed for transmitting continuously instead of in short pulses [22]. The output power of 10 W is significantly lower than in the MOPA. However, the same component types can be found in it, such as a master oscillator, optical isolators, fiber preamplifiers, optical filters and pump lasers. For simplicity, the comparison in the numbers of component types is shown in Table 6. There are two components that are not included in the AeroCube-OCSD CubeSat's design: straight photonic crystal fibers (PCFs) and laser mirrors. However, instead of slicing one PCF into two, the same single PCF could be sliced into three parallel 24-cm long segments. By doing so, these segments can be fitted into a 6U CubeSat.

There are master oscillator boards designed for deep-space laser communication that handle PPM and can be considered for a deep-space CubeSat mission [42, Figure 6]. The board sizes are more or less the same as in the AeroCube-OCSD design.

Another issue of the MOPA design is the mirrors. That is, after modifications for the PCF segments, there are four mirrors that turn the laser beam two times

Table 6: The numbers of component types in the MOPA and AeroCube-OCSD laser transmitter.

Component	**MOPA**	**AeroCube-OCSD laser transmitter**
Master oscillator	1	1
Optical isolator	4	1
Optical filter	4	2
Pumping laser	1	2
Straight photonic crystal fiber	2	0
Laser mirror	2	0

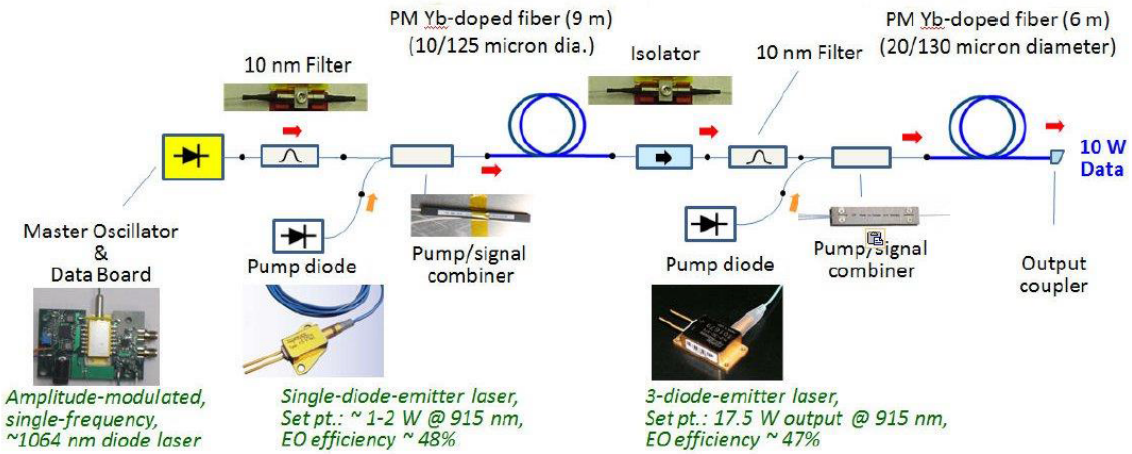

Figure 12: The schematic of the laser transmitter for the AeroCube-OCSD CubeSat. EO: electro-optic, Yb: Ytterbium. [22]

180 degrees. The turns can be achieved with corner cubes [69]. A corner cube is an optical component that is meant to make total reflection for a laser beam. Therefore, there would be two corner cubes in the MOPA design. The design can be achieved all-in-fiber before the mirrors, which means that it is not possible to see the laser beam and the beam travels inside the system. This may be beneficial in the implementation process of the MOPA to a 6U CubeSat. It would be advisable to have a custom design of the two corner cubes in order to maintain all-in-fiber type. Finally and most importantly, it is possible to fit the MOPA design into the volume of 0.6U after some modifications. [69]

When a laser pulse has been sent from the MOPA, the pulse goes through the optics and is finally sent to free space by an optical antenna. Some conventional optics solutions having a diameter of the antenna typically around 20–30 cm [63, p. 315, 332] [62] or larger are too massive for a 6U CubeSat. Thus, different approaches are needed in order to achieve a sufficient antenna gain. Figure 13 shows a miniature laser transceiver proposed to be used in deep-space CubeSat missions. From the transceiver model, a prototype (shown bottom in Figure 13) was developed for the

Lunar CubeSat. However, the average transmit power of 1.2 W of the transmitter is too poor for the lasercom concept as this power does not lead to a sufficient number of detected photons (see page 39 for the definition). Nevertheless, the same optics in the receiver system can be used for a HelioRing CubeSat. In addition, a more advanced low-noise photon detector is used (see subsection 4.3.5).

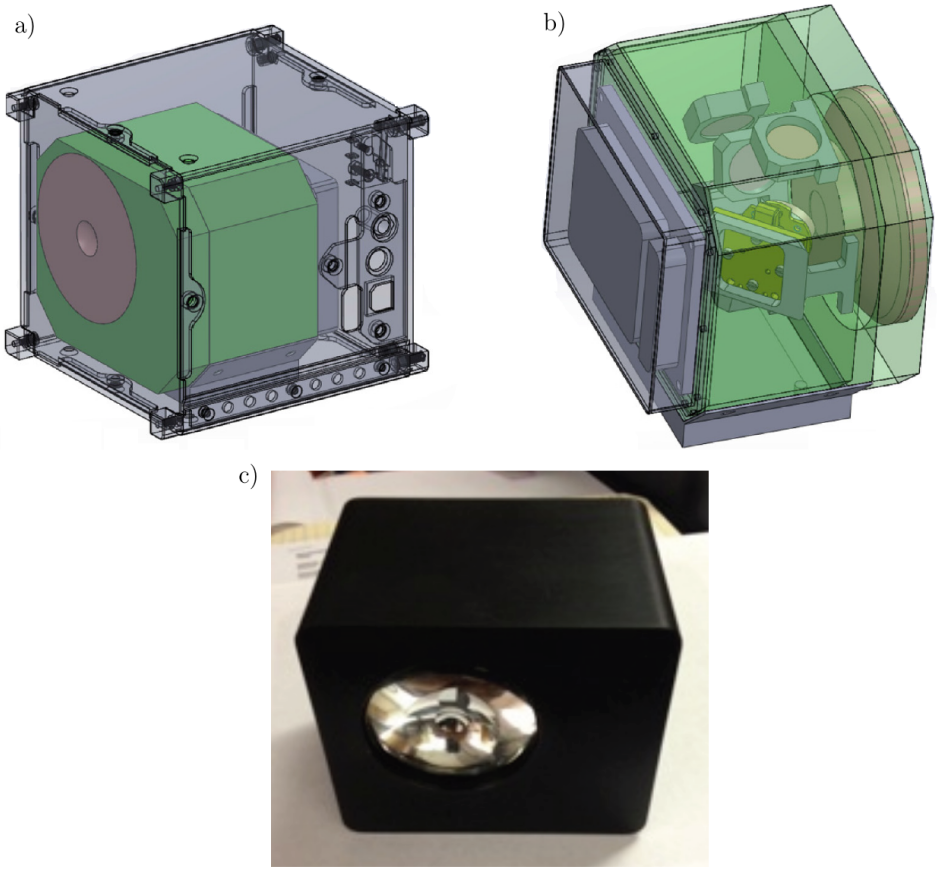

Figure 13: A 1U transceiver (including optics and antenna) design for a deep-space CubeSat for laser communication. a) The transceiver seen from the front where the brown circle represents the optical antenna [42]. b) The same system seen from the side. A transmitter is shown as a grey box on the left [42]. c) A prototype of the transceiver having a 7-cm optical antenna for the Lunar CubeSat [70].

4.3.3 Pointing accuracy

An optical antenna produces a laser beam at 1064 nm whose beamwidth (full width at half maximum) is about $\lambda/D_\mathrm{t} = (1064\,\mathrm{nm})/(8.3\,\mathrm{cm}) \approx 12.8\,\mu\mathrm{rad}$ [63, p. 354]. Every transceiver has some mispoint loss, which needs to be taken into account in the link budget. Figure 14 shows the mispoint loss as a function of the mispoint angle. The mispoint angle in the figure represents what a portion of the beamwidth is mispointed. The larger the mispoint angle is, the larger the mispoint loss becomes. Therefore, there is a trade-off between the diameter of the antenna and the mispoint

loss, if the carrier wavelength is fixed. If one increases the diameter too much, it results in a large mispoint loss and the achieved asset of the increased antenna size will be lost.

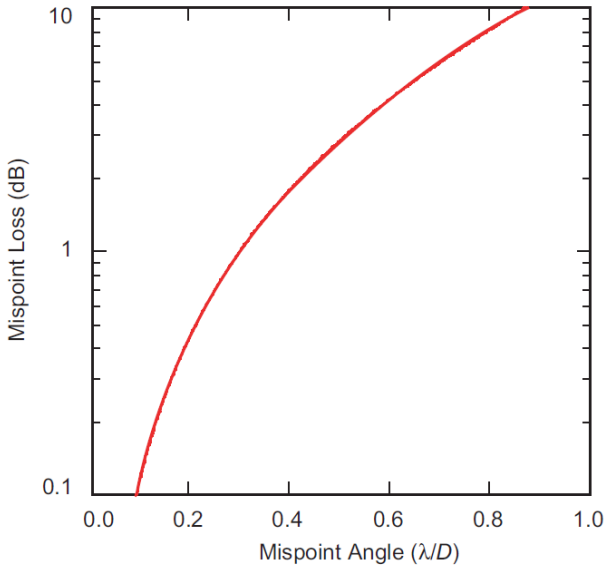

Figure 14: Pointing loss of the laser transceiver as a function of the mispoint angle. The mispoint angle, λ/D (antenna diameter of the transmitter or receiver), is shown with relation to the beamwidth. The figure is from [63, p. 354] which also gives further details of the pointing loss.

The required pointing accuracy for the attitude control was determined to be 3.33 μrad to avoid large mispoint losses. That is, a maximum mispoint angle of 3.33 μrad is allowed. This pointing accuracy would lead to a 0.75 dB mispoint loss deduced from Figure 14 (mispoint angle with relation to the beamwidth = 3.33 μrad/12.8 μrad = 0.26). The required pointing accuracy is of the same order as has been required from some other future CubeSat missions. However, no CubeSat has yet demonstrated sub-10-μrad-level pointing accuracy.

A 3U optical telescope CubeSat is under development and has a goal for a pointing accuracy of less than 5 μrad for ten minutes for Earth observation [71]. Its pointing accuracy will be achieved with the aid of a fine-steering mirror system including sophisticated algorithms. Similarly, many deep-space lasercom systems are included with a fine-steering mirror mainly because of more stringent pointing accuracy requirements [63, p. 11, 362, 376]. In addition, Exoplanetsat (3U CubeSat) is also under development and simulations have indicated that a pointing accuracy of 5 μrad can be possible with some modifications [72].

There are different models for defining the beamwidth of laser, and if the losses of the optical antenna are taken into account, one can find a wider beamwidth for the 8.3-cm aperture than calculated above. Using the model from [61], the beamwidth has increased so that the required pointing accuracy can be 5 μrad.

After all, a pointing accuracy of 3 to 5 μrad for the HelioRing CubeSats is estimated to be achievable, since other CubeSat missions discussed above require

nearly the same accuracy and the scale for the required pointing accuracies in space missions is vast. For instance, the AeroCube-OCSD CubeSat has the required pointing accuracy of about 3 mrad. On the other hand, many deep-space lasercom missions require a pointing accuracy of 0.3 μrad or lower, which is an order of magnitude more accurate than for the HelioRing CubeSats [59],[63, p. 353], [64]. However, for those missions, spacecraft are larger than 6U CubeSats and more advanced pointing control systems can be accommodated. Therefore, achieving the required pointing accuracy for the HelioRing CubeSats demands an extensive investigation and effort.

The attitude control system for the HelioRing CubeSats probably requires at least a fine-steering mirror for fine pointing control and reaction wheels for coarse pointing. As in the CubeSat missions mentioned in this subsection, a star tracker and inertial sensors (such as gyroscopes) are also proposed for attitude determination.

4.3.4 Pulse-Position Modulation (PPM)

Pulse-Position modulation (PPM) is explained in this subsection, and it is proposed to be used in lasercom of the HelioRing mission. A more detailed principle of PPM is presented in [63, p. 234] and [73].

PPM is a type of signal modulation in which k bits are encoded onto one of $M = 2^k$ time slots. The sequence of M slots is referred to a word. That is, there is only a single pulse in a word. The slot location of the laser pulse indicates the bit value. For example, with $M = 256$, the laser pulse represents $\log_2(M) = 8$ bits. A pulse occurring in the first slot indicates zero and in the last slot the bit value would be 255. If necessary, one can also add guard-time slots onto the word if there is a requirement to have a break between the words [73]. This is depicted in Figure 15 where $M = 16$ and there are also some guard slots. In laser transmitting with PPM, the pulse lengths are typically in order of 10 ns and the peak power some or 10 kW. [73]

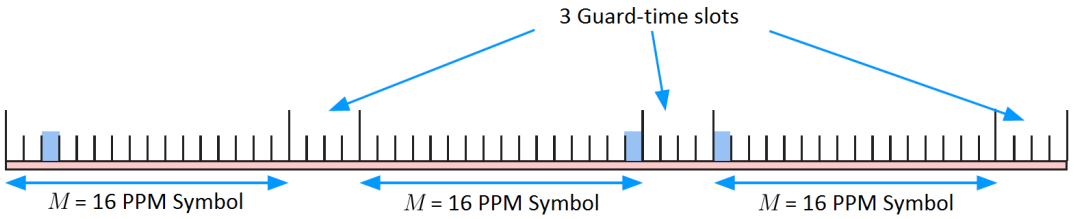

Figure 15: Pulse-Position modulation (PPM) with $M = 16$ and guard-time slots. Adapted from [74].

In PPM, the word time T_w is given [75] by

$$T_\mathrm{w} = \frac{R_\mathrm{ECC} \log_2(M)}{R_\mathrm{b}} = MT_\mathrm{s} + T_\mathrm{d} \tag{4}$$

where

R_{ECC}	is the error correction coding rate [65]
M	is the PPM alphabet size
R_{b}	is the data rate
T_{s}	is the slot width, and
T_{d}	is the guard time.

If the transmitted data is uncoded, $R_{\mathrm{ECC}} = 1$, otherwise $R_{\mathrm{ECC}} < 1$, since the data rate is reduced due to error correction coding. The average power transmitted P_{t} is [63, p. 339]

$$P_{\mathrm{t}} = \mathrm{PRF} \times P_{\mathrm{peak}} T_{\mathrm{p}} = \frac{P_{\mathrm{peak}} T_{\mathrm{p}}}{T_{\mathrm{w}}} = \frac{P_{\mathrm{peak}} T_{\mathrm{p}} R_{\mathrm{b}}}{R_{\mathrm{ECC}} \log_2(M)} \tag{5}$$

where PRF is the pulse repetition frequency, P_{peak} is the peak transmit power and T_{p} is the pulse width. It should be noted that typically $T_{\mathrm{p}} < T_{\mathrm{s}}$ in order to minimize jitter and synchronization losses in receiving. For this, there are some margins in order to match the pulse onto the slot [73]. In [73], T_{s} was made 20 % larger than T_{p} when T_{s} and T_{p} could be around 5–10 ns. Therefore, for the lasercom concept, it was decided that there are 2.2 ns margins on both sides of the pulse, and $T_{\mathrm{s}} = 7$ ns. Thus, they are sufficient margins in order to minimize the losses. The word time T_{w} can then be expressed from equation (5) as

$$T_{\mathrm{w}} = \frac{P_{\mathrm{peak}} T_{\mathrm{p}}}{P_{\mathrm{t}}} \tag{6}$$

The number of detected signal photons per PPM word or per pulse, n_{s}, is given [21] by

$$n_{\mathrm{s}} = P_{\mathrm{r}} T_{\mathrm{w}} \frac{\lambda \eta_{\mathrm{det}}}{hc} = \frac{P_{\mathrm{r}} P_{\mathrm{peak}} T_{\mathrm{p}} \lambda \eta_{\mathrm{det}}}{P_{\mathrm{t}} hc} \tag{7}$$

where η_{det} is the photon detection efficiency of the detector. A value of 0.5 is used for η_{det} as in [76]. T_{w} is kept at 100 μs, which is the result of PRF $= 1/T_{\mathrm{w}} = 10$ kHz from the MOPA design. h and c are Planck's constant and the speed of light, respectively. It can be seen in equation (7) that n_{s} increases with $P_{\mathrm{peak}} T_{\mathrm{p}}$, i.e., the output pulse energy. This product is limited by the transmitter [68]. Table 5 shows 2.2 mJ for pulse energy, which limits the $n_{\mathrm{s}} = 8.625$ according to equation (7) with values from Table 4.

Typically in space communication, there is a link margin (around 3 dB is commonly used [62], [63, p. 332, 543]) in a link budget and the same is used in this design. Furthermore, there are some coding efficiency η_{code} and synchronization losses taken into account, which reduces the required n_{s} [62]. These losses are estimated to be 1.0 dB similarly as in [62] and [63, p. 100], but the real value for η_{code} depends on the coding method. Thus, due to a total of 4 dB reduction, $n_{\mathrm{s}} = 3.43$ is achieved as a result of the iterative design process. The values for equation (7) are from Tables 4 and 5.

4.3.5 Background noise

The number of detected background noise photons per slot width, n_{b}, is given by [21, 62]

$$n_{\mathrm{b}} = \frac{\pi L(\lambda) D_{\mathrm{r}}^2 \Delta\lambda_{\mathrm{nf}} \eta_{\mathrm{r}} \eta_{\mathrm{det}} T_{\mathrm{s}} \lambda}{4hc} + N_{\mathrm{dc}} T_{\mathrm{s}} \tag{8}$$

where

$L(\lambda)$	is the background irradiance from planets and stars
D_{r}	is the aperture diameter of the receiver
$\Delta\lambda_{\mathrm{nf}}$	is the narrowband noise filter bandwidth, and
N_{dc}	is the dark count rate, i.e, noise photons per second produced by the detector.

There are many background irradiance sources in space where planets, the Sun and other stars are the most relevant. The background irradiance $L(\lambda)$ from planets is [77]

$$L(\lambda) = \frac{H_\lambda}{R_{\mathrm{AU}}^2} \left(\frac{R_{\mathrm{p}}}{Z_{\mathrm{pr}}} \right)^2 A(\lambda) \tag{9}$$

where

H_λ	is the Sun spectral irradiance at 1 AU at the desired wavelength (different values can be found in [77])
R_{AU}	is the planet-Sun distance in AU
R_{p}	is the radius of the planet or the footprint of the beam on the planet
Z_{pr}	is the planet-receiver distance, and
$A(\lambda)$	is the planet spectral albedo.

Concerning the crosslinks, the Earth is one of the most powerful background sources. The Sun and Venus can be omitted, since they are not in the field-of-view during communication. Venus is about 9° from the line-of-sight to another CubeSat. It was discovered that the Earth is in the field-of-view in certain cases. These cases are illustrated in Figure 16. The average time when the Earth is in the field-of-view is very short compared to the total communication time within the mission lifetime. However, it is of interest to achieve a time-independent opportunity for crosslink communication at 0.72 AU. Furthermore, this reduces the complexity, since one does not then need to take into account where the Earth is exactly.

Concerning the Earth as background noise, as in Figure 16, the distance between the receiver and the Earth is about 123×10^6 km. Also, the Earth cannot be considered as a point source when the beamwidth (12.8 μrad) is taken into account. The footprint of the beam has a diameter of 1577 km on the Earth, which is less than the radius of the Earth.

Table 7 shows parameters and their values for equation (9) to obtain a value for the background irradiance. The spectral albedo of the Earth depends on the

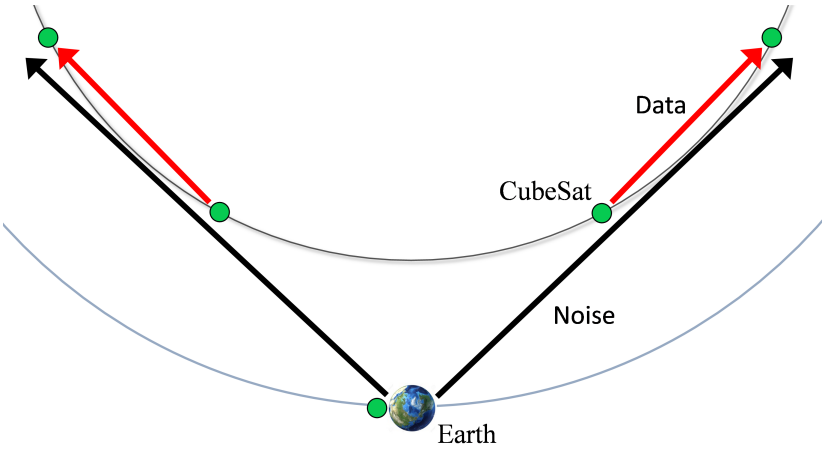

Figure 16: An illustration of the Earth as background noise for the crosslinks (figure not to scale). There are two times in the orbital period for a single CubeSat when the Earth is in the field-of-view during communication.

wavelength, but it was approximated to be about 0.36 (measured at around 600 nm) [77]. Nevertheless, high-altitude aircraft measurements have shown that the albedo does not increase from its peak value at around 600 nm to 1064 nm [78] when the irradiance difference of the Sun is taken into account at these wavelengths [77]. Therefore, there is good reason to assume that the Earth's albedo of 0.36 represents the maximum value for this design. Therefore, the maximum irradiance of the Earth is in this link budget 4.0 $\times 10^{-12}$ W/(cm^2 μm). Nevertheless, further investigations are needed in order to determine the real order of magnitude of the value and variations. Background noise from the full Moon is assumed to be insignificant, since its albedo is low compared to the Earth (about 0.08 at around 600 nm) and its spectral irradiance decreases towards 1064 nm [79].

There are a few planets whose irradiance is higher that of the Earth: Mars, Jupiter and Saturn. Their irradiance is at most 10^{-11} W/(cm^2 μm) or less at 1064 nm [79]. But when the beam divergence is taken into account, the beam footprints on these planets are so small that the irradiances are eventually lower than 4.0 $\times 10^{-12}$ W/(cm^2 μm). The irradiance from stars is at most about 5.0 $\times 10^{-12}$ W/(cm^2 μm) [79]. The irradiance from the stars of Mira, Alpha Crucis and Betelgeuse is larger than from the Earth, but their declination differs tens of degrees or more from the orbital planes of the CubeSats and Earth[6]. Thus, these stars are not considered as background noise. After all, the highest irradiance is from the Earth. Therefore, $L(\lambda) = 4.0 \times 10^{-12}$ W/(cm^2 μm) is used for equation (8).

Before determining the number of detected background noise photons, n_b, the dark count rate N_{dc} of the detector needs to be determined first. There are several photon detector options for the receiver. For a low data rate lasercom, Geiger-mode avalanche photon detectors (GM-APDs) may be considered [80, p. 211]. GM-APDs allow only a low data rate due to the required reset time (typically around tens of

[6]To obtain the declinations of the stars from the ecliptic, the SIMBAD Astronomical Database was used. See the link for further details: `http://simbad.u-strasbg.fr/simbad/`

Table 7: Parameter values for the received irradiance from the Earth in crosslink at 0.72 AU.

Parameter	**Value**
H_λ at 1064 nm [77]	0.067 W/(cm^2 μm)
R_{AU}	1
R_{p}	1577 km (footprint)
Z_{pr}	123 $\times 10^6$ km
$A(\lambda)$	0.36
$L(\lambda)$	4.0 $\times 10^{-12}$ W/(cm^2 μm)

microseconds) to able to function again. A GM-APD design presented in [76] has $\eta_{\mathrm{det}} = 0.5$ and $N_{\mathrm{dc}} = 20$ kHz at room temperature (about 25°C). This design is proposed for the receiver. The required reset time is about 1 μs.

Table 8 shows values for equation (8) to obtain n_{b}. The narrowband noise filter bandwidth, $\Delta\lambda_{\mathrm{nf}}$, is 0.6 nm and larger than the laser pulse linewidth of about 0.2 nm. The link budget calculations for lasercom between a spacecraft in Mars orbit and the Earth used a 0.1 nm filter bandpass [62]. In the same calculations, the maximum radial velocity between the transmitter and receiver was determined to be of the order of 20 km/s. This corresponds to a Doppler shift of 0.07 nm at 1064 nm. There is approximately no radial velocity in the crosslinks at 0.72 AU, whereas in the crosslinks from 0.72 AU to the Earth, there is the same order of magnitude of the radial velocity as in the Mars link budget calculations. Therefore, there is a good reason to assume that the Doppler shift in lasercom in HelioRing would not be a problem, since $\Delta\lambda_{\mathrm{nf}}$ of 0.6 nm would clearly exceed the Doppler shift of around 0.07 nm.

Table 8: Values for the number of detected background noise photons per slot width n_{b}.

Parameter	**Value**
L(1064 nm)	0.040 W/m^2
D_{r}	8.3 cm
$\Delta\lambda_{\mathrm{nf}}$	0.6 nm
η_{det}	0.5
T_{s}	7 ns
N_{dc}	20 kHz
n_{b}	0.00137 + 0.00014 = 0.0015

It can be seen in Table 8 that background noise clearly dominates over dark noise in the presence of the maximum noise photon condition. It should be noted that for most of the communication time, the dark count rate dominates the number of noise photons. If it is necessary to have smaller n_{b}, T_{s} can be shortened, but then there might be an issue with synchronization of the pulse and slots. In addition, $\Delta\lambda_{\mathrm{nf}}$ can be narrower and closer to the laser pulse linewidth, but then there might be an issue with the stability of the linewidth. Therefore, there are some margins in order to

allow some variation in the systems.

4.3.6 Bit error rate

Concerning the crosslink, the detected signal and background noise photons per slot are 3.43 and 0.0015, respectively. How low a bit error rate (BER) is achievable depends on these values and the PPM alphabet size M. The symbol error rate (SER) for PPM is given [81] by

$$\begin{aligned}\mathrm{SER}(M, n_\mathrm{s}, n_\mathrm{b}) =& 1 - \frac{1}{M} e^{-(n_\mathrm{s}+Mn_\mathrm{b})} - \sum_{j=1}^{\infty} \frac{(n_\mathrm{s}+n_\mathrm{b})^j}{j!} e^{-(n_\mathrm{s}+n_\mathrm{b})} \\ & \left[\sum_{m=0}^{j-1} \frac{n_\mathrm{b}^m}{m!} e^{-n_\mathrm{b}}\right]^{M-1} \frac{1}{aM}\left[(1+a)^M - 1\right]\end{aligned} \tag{10}$$

where

$$a = \frac{n_\mathrm{b}^j/j!}{\sum_{m=0}^{j-1} n_\mathrm{b}^m/m!}$$

BER (uncoded) can be determined from SER as follows [63, p. 254]

$$\mathrm{BER}(M, n_\mathrm{s}, n_\mathrm{b}) = \frac{M}{2(M-1)} \mathrm{SER}(M, n_\mathrm{s}, n_\mathrm{b}) \tag{11}$$

When the uncoded BER is low enough, the final (end-to-end) BER can be achieved with error correction coding. Typically, the final BER of around 10^{-6} or less is desired for a space mission [81], and it is also set as a goal for this lasercom concept design. There is a number of coding methods available for lasercom, of which the Reed Salomon PPM (RSPPM) and serially concentrated PPM (SCPPM) methods are widely considered for deep-space lasercom missions [21, 81]. Figure 17 shows the performance of these methods and the uncoded BER. The most important finding from the figure is what an uncoded BER is needed to achieve the final BER around 10^{-6}. For simulations that results can be seen in Figure 17, values of $M = 64$ and $n_\mathrm{b} = 1.0$ were used [81].

With the RSPPM coding, the uncoded BER can be something like 0.05 or below to achieve the required final BER. This can be seen in Figure 17. Even with the uncoded BER close to 0.2, it is possible to achieve BER = 10^{-7} or less with the SCPPM coding.

Since no coding has yet been applied to the lasercom concept, it is estimated that a BER of about 0.03 as the baseline would be a sufficient goal. Thus, there is some margin compared to the RSPPM example above. Also, it could turn out that RSPPM is a more favourable choice over SCPPM under different parameter values. For example, n_b of 1.0 was used for the simulations in [81], whereas for this link budget $n_\mathrm{b} = 0.0015$. Thus, there is some margin between the required uncoded BER and both of these coding examples. Further simulations are needed to determine which coding method would be the most advisable to implement.

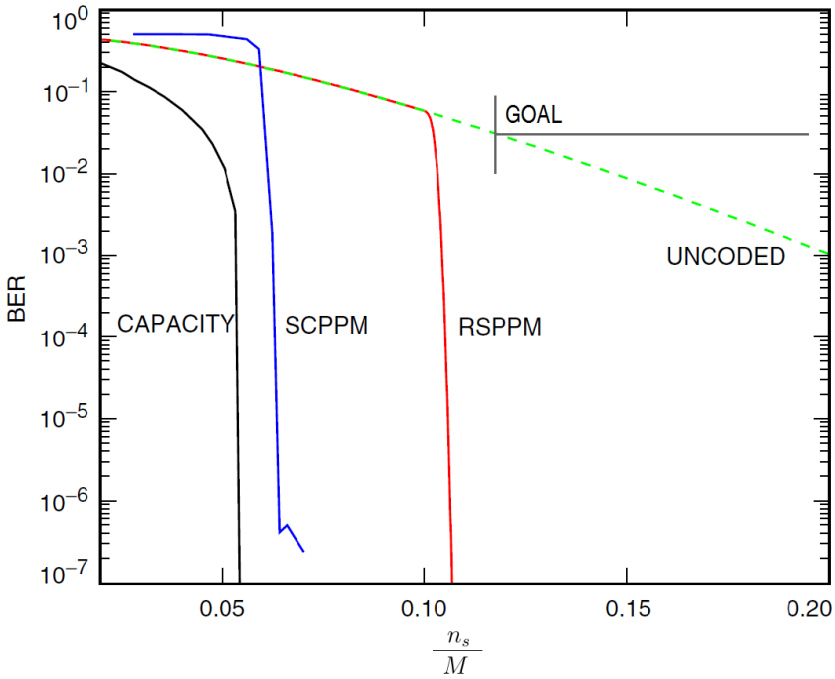

Figure 17: Bit error rate (BER) as a function of n_s/M (adapted from [81]). Uncoded BER and BERs with error correction coding methods, of which Reed Salomon PPM and serially concentrated PPM (SCPPM) are presented. Also, theoretical capacity limit is shown. The goal of the uncoded BER = 0.03 for the laser crosslink at 0.72 AU can be seen above.

Table 9 shows uncoded BERs with different values of $n_\mathrm{s}, n_\mathrm{b}$, and M. These BERs were calculated according to equation (11). The indexes of the table are just for pointing out the parameter values for obtaining a certain uncoded BER. With current n_s and n_b values, BER = 0.0163 with $M = 2$ (index 1), which fulfils the requirement of the uncoded BER. If $M = 64$ was used as in the coding examples above, an uncoded BER = 0.0188 would be achieved. The highest possible M in this link budget is estimated to be 256 in which case the uncoded BER = 0.0256 (index 3).

According to equation (11), BER increases with M (see indexes 1–4 in Table 9). But it increases so little (from about BER = 0.01 to 0.0264) that with $M = 256$, the data rate has increased by eight compared to the original case (index 1). This is a significant result as by increasing M, the data rate is also increased with a minimal cost in the uncoded BER at low background noise.

At low background noise, it can be clearly seen that BER does not improve much if n_b is reduced to zero (index 5) when $M = 2$. But when M is increased, the advantage of low background noise can be seen. If $M = 512$ and assuming $n_\mathrm{b} = 0$, BER is still 0.162 (index 6). That is, the lower n_b is, the higher M one can use in principle. However, one can attempt to increase η_det with the same GM-APD design [76], even though there is some increase in N_dc. Typically, if one tries to increase η_det by raising the bias voltage of the detector, it also raises N_dc [76]. For illustration,

if η_{det} could be increased from 0.5 to 0.6 and then N_{dc} from 20 kHz to 200 kHz for example, BER would be 0.0249 at $M = 512$ (index 7).

A CubeSat, as any spacecraft, can undergo a malfunction during its mission. If the lasercom system of a CubeSat was unable to communicate with its neighbour, the requirements of the mission would not be fulfilled as this CubeSat could not provide its payload data eventually from the Sun-Earth line. However, the requirement of making measurements with the angular separation of 36° could be relaxed in this case. Therefore, the propulsion system could be designed so that one takes this malfunction probability into account and allocates propellant for transforming nine CubeSats so that the angular separation changes into 40°. In this case, $R = 73.68 \times 10^6$ km, which results in $n_{\mathrm{s}} = 2.80$. In this case, BER = 0.0307 (index 8) with $M = 4$. This does not fulfil the requirement for the uncoded BER, but obtaining a sufficient final BER is still estimated to be possible, since there may still be margin in the RSPPM coding example above. However, further simulations are needed for determining how low the final BER could be achieved.

Table 9: Different uncoded BER values as a function of $n_{\mathrm{s}}, n_{\mathrm{b}}$ and M for the laser crosslink at 0.72 AU.

Index	**BER**	$\boldsymbol{n_{\mathrm{s}}}$	$\boldsymbol{n_{\mathrm{b}}}$	$\boldsymbol{M}$
(1)	0.0163	3.43	0.0015	2
(2)	0.0188	3.43	0.0015	64
(3)	0.0256	3.43	0.0015	256
(4)	0.0330	3.43	0.0015	512
(5)	0.0162	3.43	0	2
(6)	0.0162	3.43	0	512
(7)	0.0249	4.12	0.0310	512
(8)	0.0307	2.80	0.0015	4

4.3.7 Localization of the CubeSats for communication

In a crosslink at 0.72 AU, the diameter of the imaginary footprint at another CubeSat is about $\lambda/D_{\mathrm{t}} \times R = 860$ km. Since the required pointing accuracy (3.33 μrad) is smaller than the beamwidth, the transmitting CubeSat has to be able to determine whether the receiving CubeSat is on a footprint of about 223 km. The same requirement applies to the receiving CubeSat as it must point in the required direction and know that the transmitting CubeSat is really there in order to detect the signal without large mispoint losses.

The current RF communication technologies of the DSN are capable of determining the range and velocity of a deep-space spacecraft in the order of one metre and about one mm/s, respectively [82, 83]. Additionally, the location perpendicular to the range vector from the Earth can be determined with the DSN with an accuracy of about 2.5 nrad [82]. In addition, ESA deep-space communication systems can do the same with an angular accuracy of 25 nrad [84]. Therefore, localizing the farthermost CubeSat (about 1.72 AU from the Earth) can be determined with an accuracy of

about 6 km with the ESA systems. The position estimate can be improved when the CubeSat orbits closer to the Earth (for laser beam pointing purposes). After all, the orbital parameters of all CubeSats could be delivered by the DSN to each CubeSat. Therefore, locating another CubeSat for a crosslink would be feasible from the point of view of communication. Laser ranging can also be considered instead of using RF communication, but it is anticipated to be too difficult to be accomplished without RF communication in deep space. Deep-space navigation is discussed in more detail in [83].

4.3.8 Acquisition, tracking and pointing

There are three important steps in deep-space lasercom: acquisition, tracking and pointing [63, p. 351]. In typical deep-space lasercom designs, a beacon signal continuously sent from the Earth is captured by the lasercom system of the spacecraft during communication. First, the spacecraft must find the beacon signal, and this process is called acquisition. Next, the lasercom system tracks this beacon signal in order to point in the right direction during communication.

For deep-space lasercom missions, there are also other options, such as beaconless tracking. In this method, passive sources are tracked, such as the Earth and stars, and they are used as pointing references. In this crosslink design, a star tracker is used for tracking. This topic is discussed in more detail in [63, p. 316, 351]. By using an on-board model where the location of each Cubesat is known, pointing directions are calculated from the star tracker data during communication.

Typically in deep-space missions, there are large transverse velocities between the spacecraft and the ground stations on the Earth [62]. When the receiver receives a signal from the transmitter, and if the receiver were to sent a signal back, the transmitter would not be in the same direction any more. Therefore, the transmitter has to take the point ahead into account in order to determine the position of the receiver when it receives data. The same rule applies to the receiver. The point ahead between the CubeSats at 0.72 AU is around 72 μrad in one-way. Thus, a CubeSat needs to track the predicted location reference of another CubeSat when it is going to receive data. Data communications between CubeSats is discussed in more detail in subsection 4.7.

4.4 Link budget design for the crosslink between a CubeSat at 0.72 AU and a CubeSat orbiting the Earth

In order to deliver data from the CubeSats at 0.72 AU to the Earth, the CubeSat orbiting the Earth (RelayCube) receives this data from the nearest CubeSat at 0.72 AU and transmits it to the ground station. It is assumed that RelayCube is equal to the other CubeSats. That is, it consists of the same optical communication system as the others, except that the diameter of the aperture of the antenna can be changed. However, the propulsion system for RelayCube can be less demanding. Some thrust might be needed for possible station keeping, but the amount of propellant would be

much less than for the other CubeSats. Furthermore, a less demanding and expensive RF communication system is required. Other subsystems can be the same.

Figure 18 depicts communication between a CubeSat at 0.72 AU and RelayCube. From the viewpoint of communication it is assumed that RelayCube and the Earth remain located at the same point, as the distance differences are large (RelayCube – Earth vs. CubeSats at 0.72 AU – RelayCube). There is a point when the angle between the nearest CubeSat at 0.72 AU and the Sun seen from the Earth becomes so small that communication is blocked by too high background noise from the Sun. This angle is referred to as the Sun-probe-Earth (SPE) angle. For other deep-space lasercom missions, communication is typically designed so that one can handle even as small SPE angles as 2° [63, p. 309], [62].

For the lasercom concept, communication with an SPE angle of 5° and more is estimated to be possible and, thus, some margin is added compared to other mission proposals. Therefore, there is a 10° sunlit sector seen from the Earth to the Sun, and if a CubeSat is inside this sector, lasercom is assumed to be impossible. This CubeSat will stay inside the sector for approximately 16 days before communication is possible again (the same calculation method was used as in Appendix B). This is too long a time to wait for the next communication period with the CubeSat. Therefore, the CubeSat inside the sector must transmit data to the second nearest CubeSat to the Earth, and thus that CubeSat will communicate with RelayCube. Even if one CubeSat is inside the sunlit sector, there is always a CubeSat inside the nearest 72° sector (see Figure 18). Thus, this laser crosslink must be designed so that RelayCube must be able to communicate with a CubeSat that is located at 36° seen from the Sun to the Earth. In this case, $R \approx 89 \times 10^6$ km, and the CubeSat at 0.72 AU is then about 45° seen from the Earth to the Sun.

4.4.1 Link equation and received signal power

Table 10 shows the parameter values chosen in order to obtain the received power P_r for RelayCube. P_r was calculated according to equation (1). In the crosslink, the transmitter is at 0.72 AU, and the receiver is RelayCube. The diameter of the optical antenna for RelayCube was increased in order to circumvent the larger free-space loss. This change led to a narrower beamwidth, but the same pointing accuracy was still required. Thus, the pointing loss has also been increased for RelayCube due to the narrower beamwidth. The P_r results in $n_\mathrm{s} = 3.48$ according to equation (7). The obtained n_s is close to 3.43 of the first link calculation.

4.4.2 Background noise

The next step is to determine the maximum n_b in the field of view for the link (RelayCube still as the receiver). The Earth is not considered as a background noise source, since the other CubeSats are almost always visible to RelayCube and the Earth is then not in the field of view (see page 27). The most powerful background irradiance sources apart from the Sun are Venus and the Moon. Irradiance from other planets is still relatively low, since the planets of the solar system cannot be considered as point sources due to the narrow beamwidth of RelayCube. See

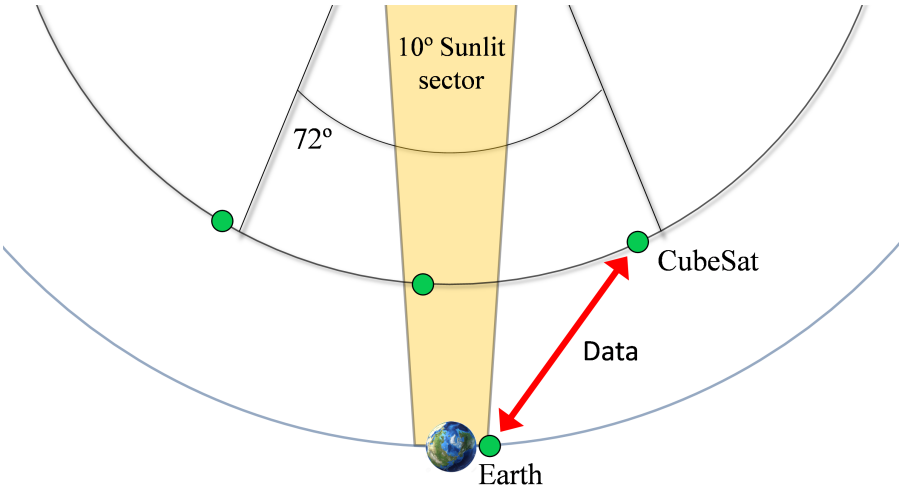

Figure 18: An illustration of laser communication between the CubeSats (figure not to scale). A CubeSat at 0.72 AU communicates with a CubeSat that orbits the Earth (RelayCube). If a CubeSat is inside the 10° sunlit sector seen from the Earth to the Sun, communication is estimated to be blocked by too high background noise from the Sun. Therefore, the laser communication concept is designed so that it permits a CubeSat to communicate with RelayCube from the edge of the 72° sector seen from the Sun to the Earth in order for RelayCube to obtain the critical payload data from inside the 10° sunlit sector.

Table 10: Parameter values for laser systems and the received power P_r.

Parameter	**Value**	**Value in dB**
P_t	22.00 W	13.42 dBW
G_t		107.79
G_r		111.00
D_t	8.3 cm	
D_r	12.0 cm	
λ	1064 nm	
L_s		-360.43
R	88.94×10^6 km	
η_{pt}	0.92	-0.75
η_{pr}	0.85	-1.40
η_t	0.79	-2.0
η_r	0.75	-2.5
P_r		-134.87 dBW

section 4.3.5 for more details. Of the planets, Venus is the most powerful source of background irradiance above the atmosphere of the Earth at the operating wavelength [79].

The irradiance graph in [79] does not state the distance from planets to the Earth when they reach their maximum irradiance value. Therefore, it is assumed that the

maximum irradiance from Venus is obtained from its farthermost point, i.e., when Venus is located at 1.72 AU from the Earth, since the footprint diameter of the beamwidth on Venus is at maximum and gives the maximum n_b. Thus in this case, the diameter of the footprint of the beamwidth is about 2800 km while the diameter of Venus is about 12100 km. Therefore, $n_b = 0.0026$ according to equations (8) and (9).

The orbital plane of the Moon differs about 5° from the ecliptic, i.e., from the plane of CubeSats at 0.72 AU and RelayCube. Looking from RelayCube, the angular width of the Moon is about 0.5°. In addition, a margin of one angular width of the Moon is estimated as a reliable separation to begin communication. Thus, communication is assumed to be possible 0.75° from the centre of the Moon. Since the orbital orientation of the Moon is fixed with respect to the Earth while the Earth takes one orbit around the Sun, the angular separation of the Moon from the ecliptic is for long periods of a year so large that there is no risk of a communication outage. However, there are also periods in a year when the risk is increased, when the maximum inclination angle of the Moon is perpendicular to the Sun-Earth vector. Then, from the viewpoint of communication, the Moon stays for longer periods closer to the ecliptic and so also to the field-of-view during communication.

After all, the average risk of a communication outage caused by the Moon is very small. However, it is estimated that a communication outage by the Moon will happen during the mission. But due to its low probability, the effect to the performance of the communication concept is low and it is not considered as a significant factor (see next subsection for more details). Simulations of the communication outages are, however, needed and they are recommended to be done in future studies. It is also advisable that RelayCube and the other CubeSats should have an on-board model to predict possible communication outages beforehand.

4.4.3 Bit error rate

Table 11 shows BERs for the link in different situations, and they were calculated according to equation (10). The requirement for BER stays the same, i.e., the uncoded BER shall be 0.03 or lower. In the downlink (from 0.72 AU to RelayCube), the maximum possible M that can be used is 256 (index 3) as in the previous link budget. When a CubeSat orbits closer to the Sun seen from the Earth, n_b is increased due to higher background noise from the Sun. However, n_s has also been increased due to the smaller free-space loss. When the CubeSat has the critical SPE angle of 5°, n_s has been increased to 15.67. In this case, n_b may increase by a factor of about 2450, i.e., to 6.37, and the BER requirement can still be achieved (index 4).

Index 5 illustrates the situation when communication is blocked by the Moon, and there is a CubeSat at the edge of the sunlit sector. If RelayCube attempts to communicate with the nearest CubeSat outside the 72° sector, communication is possible with the required BER. However, the maximum M can be only 64 in this case. This is a special case, but it demonstrates that critical data from at least the nearest three CubeSats can be transmitted to the Earth even if the Moon would be a problem from the standpoint of communication.

In the uplink, when a CubeSat at 0.72 AU receives a signal from RelayCube, background irradiance from the Earth in the field of view has not been increased from the previous link (index 6). This is due to the smaller footprint of the beamwidth on the Earth, since the CubeSat is closer to the Earth. After all, the required BER can be achieved for the link.

Index 7 shows a BER in the case of a loss of a single CubeSat at 0.72 AU. Again, the angular separation of the CubeSats is assumed to be changed into 40°. Then n_s would drop to 2.95 in which case BER = 0.0293 and the requirement would be still achieved. But the highest value of M can only be 32 in this case. After all, the BER requirement would be fulfilled in all cases presented in this subsection.

Table 11: Different uncoded BER values as a function of n_s, n_b and M for the laser crosslink from 0.72 AU to RelayCube.

Index	**BER**	$\boldsymbol{n_s}$	$\boldsymbol{n_b}$	$\boldsymbol{M}$
(1)	0.0155	3.48	0.0026	2
(2)	0.0196	3.48	0.0026	64
(3)	0.0299	3.48	0.0026	256
(4)	0.0300	15.67	6.37	256
(5)	0.0255	3.20	0.0026	64
(6)	0.0250	3.48	0.0015	256
(7)	0.0293	2.95	0.0026	32

4.4.4 Acquisition, tracking and pointing

Concerning lasercom with the Earth, beaconless tracking from deep space is typically based on optical images of the Earth in visible band, thermal images of the Earth or star tracker and inertial sensor measurements (see section 4.3.8). To be able to point the laser beam accurately to the ground station, images of the Earth can be used for determining the centroid of the Earth. From the centroid, it is possible to calculate the location of the ground station by using some algorithm. Instead of pointing to a ground station, a CubeSat at 0.72 AU points to RelayCube. The pointing direction is calculated from the centroid of the Earth and the orbital parameters of RelayCube. [63, p. 375–399].

Figure 19 shows an example of the difference between optical and thermal images (in the band of 8–13 μm) of the Earth taken by Mars Odyssey at a distance of about 3.6 million km from the Earth on 19th Apr. 2001 [88]. When there is a large phase angle between a space probe and the Earth–Sun line, determining the centroid of the Earth becomes more difficult, and there is a larger error in the calculated centroid.

If a CubeSat at 0.72 AU resides at the edge of the 72° sector, the angle between the Earth and Earth–Sun line would be about 45° seen from the CubeSat. The Earth is then more visible optically than in the visible image in Figure 19. However, a significant portion of the Earth is still invisible and there could be a considerable bias error in the pointing, which would result in a too large pointing loss. This problem

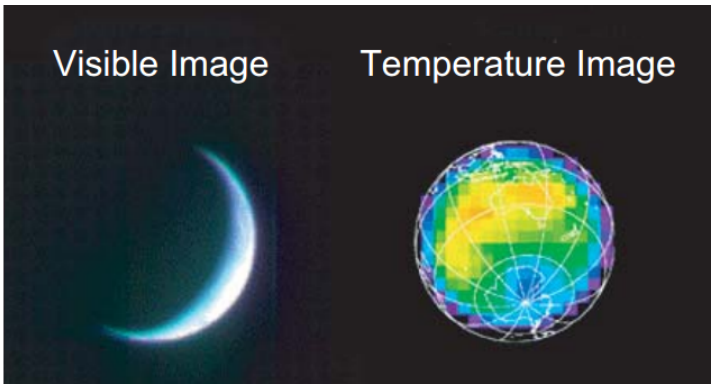

Figure 19: Images of the Earth at visible optical and thermal (infrared) bands taken by Mars Odyssey [88].

does not take place in thermal images. The performance of thermal images of the Earth is independent of the phase angle.

There is also another issue of visible images, namely the unpredictable albedo variations of the Earth resulting from cloud coverage [88, 89]. This leads to magnitude variations in images, which can cause large errors in the calculated centroid. Simulations indicate that thermal images of the Earth are worth measuring at a wavelength range of 8 to 13 μm [89]. The thermal-image-based tracking method might achieve 0.150 μrad bias error from the centroid of the Earth from a distance of 2.7 AU. The detector could be an uncooled sensor, such as a microbolometer or a microcantilever. [89]

However, in these simulations in [89], a 30-cm aperture was used for tracking, which is too massive for the HelioRing CubeSats. However, the distance of 2.7 AU is much longer compared to the maximum distance of 0.59 AU in the this lasercom link design. Thus, a significantly smaller aperture can be used in order to achieve the same performance. Finally, it is estimated that thermal images offer better choice for tracking in the HelioRing mission than visible images.

Nevertheless, the results of references [88, 89] demonstrate that further studies would be desirable for the thermal image-based tracking. However, tracking of RelayCube could also be done with star trackers and inertial sensors as in the previous link. Tracking of a CubeSat at 0.72 AU is proposed to be done also by using star trackers and inertial sensors. That is, there are no objects close to the other CubeSats and, thus, images would not help in the tracking processes.

4.5 Secondary RF communication design

In this subsection, the preliminary secondary RF communication system is introduced for communicating between the farthermost CubeSats and the DSN. Since this thesis mainly focuses on laser communication, it is beyond the scope of the thesis to design a detailed link budget for the secondary RF communication. Therefore, the designing of the secondary RF link budget is recommended to be done in more detail in a future study. However, one can use the downlink of the MarCO mission as a baseline

for illustrating the feasibility of the RF link for the HelioRing mission at a high level.

In the MarCO mission, both CubeSats are capable of transmitting data at 8 kbits/s from Mars to the DNS's 70-m dish in Spain [19]. In this case, the distance to the Earth is 1.05 AU. The gain of the high-gain antenna of the CubeSat is about 28 dB [86]. According to the RF link equation (see Appendix A), the signal-to-noise ratio (SNR) is directly proportional to the antenna gain. Also, SNR is inversely proportional to the square of the range and proportional to the data rate.

Therefore, if the communication systems of the MarCO CubeSat were used in the HelioString mission, one would be able to communicate from the farthest point (of 1.72 AU) at a data rate of about $(1.05\,\mathrm{AU}/1.72\,\mathrm{AU})^2 \times$ 8 kbits/s = 2.98 kbits/s (in the real case, operating at small Sun angles reduces the data rate). The high-gain antenna of the MarCO CubeSat is probably too large for a HelioRing CubeSat as a secondary communication antenna. Thus, it would be advisable to use a more compact antenna, but then the gain is probably lower. One option is to use a patch antenna whose dimensions are smaller than those of the MarCO CubeSat's antenna. One example of a patch antenna (15 dB gain) can be found in [87]. It would require only little space on the side of a HelioRing CubeSat. The gain difference between antennas is 13 dB, which reduces the data rate by the same amount, i.e., to $10^{-13/10} \times$ 2.98 kbits/s = 150 bits/s. This data rate is estimated to be sufficient for secondary communication of transmitting housekeeping data to the Earth as well as for providing orbital parameters for the CubeSats. By using the same simple model, the downlink data rate can be increased to about 1.3 kbits/s or more from inside the closest 72° sector. [54, p. 420-421]

4.6 Volumetric budget for CubeSats

It is advisable to produce a volumetric budget for a HelioRing CubeSat in order to demonstrate that the proposed lasercom system is feasible to be fit into the spacecraft. The volumetric budget model of a deep-space lasercom 6U CubeSat from [42] is used as a baseline with some modifications. That 6U CubeSat model is only a proposal and has not been demonstrated in space. Table 12 shows the volumetric budget proposal for the HelioRing CubeSats at 0.72 AU with allocated subsystem volumes. The subsystems were discussed in more detail in subsection 3.5.

An attitude determination and control system (ADACS) was included in the housekeeping (H/K) subsystems in the original model [42], but here it is separated from those into a system of its own. There is an allocation increase for the H/K subsystems (without the ADACS) as it was estimated that the batteries occupy a larger volume.

For the lasercom system, 1.8U is allocated, of which 0.6U is for the transmitter. The same optics concept as was presented in [42] is also proposed for a HelioRing CubeSat. The laser transceiver requires a volume of 1U in total including a miniature transmitter, optics, an optical antenna having a diameter of 6 cm, and a receiver. The optics of the lasercom system clearly take the majority of volume. Thus, since the diameter for the optical antenna would be slightly larger (8.3 cm) for HelioRing, about 1.2U is allocated for the antenna, optics and receiver, with some margin. These

allocations make the total volume of 1.8U. The volume of 0.4U for the secondary communication RF transceiver originates from [84]. The presented RF transceiver is intended for CubeSats for deep-space communication at X-band, such as for the future MarCO CubeSats [85].

Table 12: The volumetric allocation of HelioRing CubeSat subsystems.

Volume in Units (U)	**Subsystem**
0.8	Housekeeping subsystems (UHF system included)
0.7	Attitude determination and control system
2.1	Electrical propulsion
1.8	Lasercom
0.4	Secondary communication (RF)
0.2	Payload (magnetometer with board and boom)
6.0	**Total**

4.7 Data communications

Two relevant types of links have been discussed so far in this thesis: (1) the crosslink between CubeSats at 0.72 AU, and (2) the crosslink between a CubeSat at 0.72 AU and RelayCube. For both link budgets, the highest possible M is 256 and this M will be used for the data communications calculations. At this point, it is proposed that communication in the links shall be done every 30 minutes. This is due to the trade-off between two things: (1) the requirement to transmit payload data from the critical 36° sector to the Earth within two hours, and (2) the round-trip time in the links.

The transmission delay time in crosslinks at 0.72 AU is about 3.7 minutes. In the crosslink from a CubeSat at 0.72 AU to RelayCube, the delay at maximum is about 4.9 minutes. Furthermore, some of the communication time is allocated for transmitting and receiving. That is, the CubeSats cannot transmit and receive at the same time. The duration for transmitting data must also be taken into account. Measurements and lasercom can be done at the same time [90].

4.7.1 Data rates of crosslinks

The determining of how long it takes to transmit data from one CubeSat to another depends on the data rate. Data transmission times are discussed in subsection 4.7.3. The data rate R_b can be expressed from equation (4) as

$$R_\mathrm{b} = \frac{R_\mathrm{ECC} \log_2(M)}{T_\mathrm{w}} \tag{12}$$

As T_w is kept constant, the product of R_ECC and $\log_2(M)$ determines the data rate. Values for error correction coding rates R_ECC can be found in Figure 20, which shows R_ECC values as a function of n_s/M with n_b values of 10, 1, 0.1, 0.01, and 0. The difference between 0.01 and 0 is small for $n_\mathrm{s} = 3.43$ and $M \leq 512$. R_ECC is

increased when M decreases, and the highest R_{b} is achieved with $M = 256$, which is the maximum for both link budgets. In these cases, R_{ECC} is about 0.42 for both link types and M of 256 is proposed to be used in both link types. This results in $R_{\mathrm{b}} = 33.60$ kbits/s. When the SPE angle becomes smaller, n_{b} level rises. In this case, R_{ECC} can be increased. When a CubeSat is close to the sunlit sector (index 4 of Table 11), the ideal R_{ECC} is around 0.7 according to Figure 20, and, thus, R_{b} increases. However, further work and simulations are needed in order to determine how R_{b} changes under increased background noise.

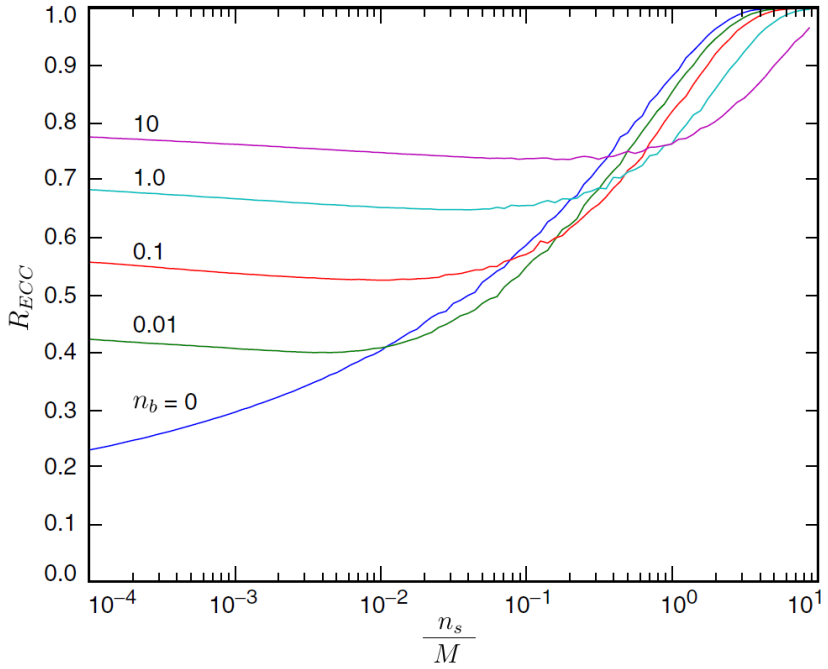

Figure 20: Error correcting coding rates (R_{ECC}s) as a function of n_{s}/M for n_{b} values of 10, 1, 0.1, 0.01, and 0. Adapted from [81].

In the case of losing a CubeSat at 0.72 AU, M can be at most 4 in the crosslink at 0.72 AU (index 8 of Table 9). Then the value for R_{ECC} is around 0.82. In this scenario, the data rate is reduced to $R_{\mathrm{b}} = 16.4$ kbits/s. In the same situation, the data transmission to RelayCube, M can be 32 at most (index 7 of Table 11). This results in R_{ECC} and R_{b} of 0.56 and 28.0 kbits/s, respectively.

4.7.2 Data protocol

A data protocol defines how a transmitter and a receiver communicate with each other. In the crosslinks, there is a timing schedule for each CubeSat so that it knows when to direct itself towards another CubeSat, and when communication should start. The receiving CubeSat receives a certain pulse sequence, which indicates incoming data. Once the data has been received, the receiver transmits a message back to the transmitting CubeSat of whether the data transmission was successful or not. The message may also contain commands from the ground stations. It is assumed that if

the transmission was unsuccessful, the same data would be sent again in the next transmitting period only if the data was critical. Payload data can be sent again anyway as it has a small size with respect to the H/K data.

Data transmission consists of frames. A single frame comprises of a header, a data packet and an end mark. The header includes the size of the frame in bits as well as an identifier which indicates from which CubeSat the data packet is. The data packet consists of payload and H/K data, and the end mark indicates the end of the frame. The frame can also contain information about which M size and what error correction code parameters are to be used. The majority of the frame data size is in the data packet and, thus, data calculations are based merely on these packets.

4.7.3 Communications schedule

Determining the scheduling in the crosslinks is a key part in the design of the lasercom concept. Each CubeSat must communicate at a certain time or at least in a certain period in order to relay data from all CubeSats to the Earth reliably. Figure 21 illustrates communication links in one of the critical events of the mission when one of the CubeSats (CS_2) is inside the 10° sunlit sector and cannot communicate with RelayCube. Instead, CS_3 at the edge of the 72° sector communicates with RelayCube. The direction of data flow is shown with the red arrows. In link L_{R3}, Venus is 9° from the line-of-sight and, thus, is not considered as a source of background noise.

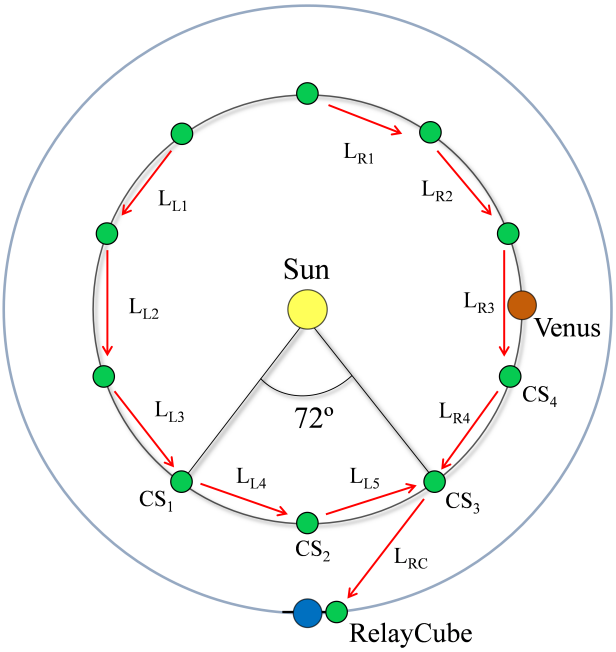

Figure 21: A representation of one of the most critical parts of the mission: the relaying of data to the Earth within the required time. L_{Li} represents a crosslink on the left side and L_{Ri} on the right, CS_i is a CubeSat at 0.72 AU. CS_3 transmits data from all CubeSats to RelayCube.

Figure 22 presents one option of communication in the crosslinks. In the figure, the communication schedule of link L_{L4} is shown as an example. In this example, CS_1 has data from the other three left above CubeSats (see Figure 21). First, CS_1 sends a laser pulse sequence (in red) indicating data transmission (in blue). Once the data has been transmitted, it will take about 4 minutes (see the arrow) to reach CS_2.

It was assumed it takes about two minutes (in violet) for the CubeSats to achieve the required pointing accuracy, though the time can be much shorter. CS_2 receives the pulse sequence, which can help in the synchronization of the laser pulses. Once CS_2 has received the data, it will send a message back to CS_1 about the status of the data transmission (in green). The message can be "successful transmission", for instance. The pulse-sequence and the status-of-data-transmission lines can be shorter, but they are lengthened here to make them more visible. Instead, the other lines are shown as realistic lengths with respect to time.

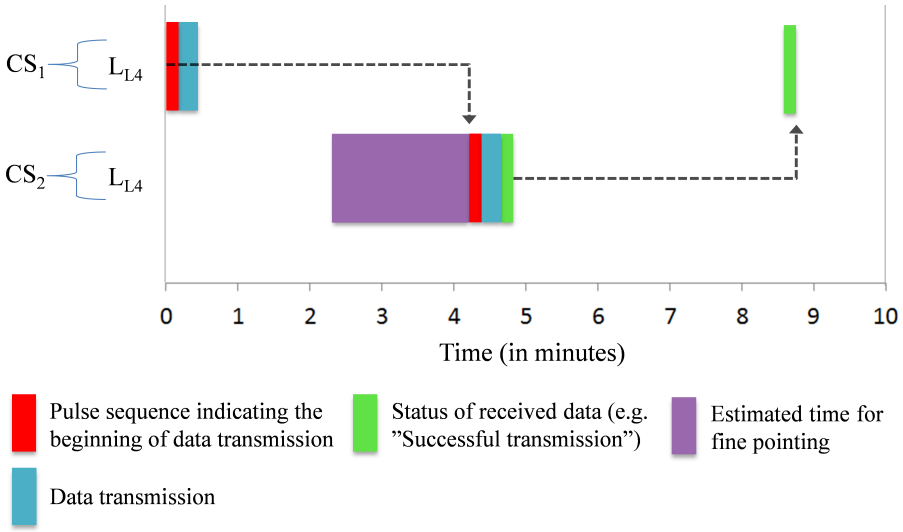

Figure 22: A communication schedule for link L_{L4} from Figure 21 in which CS_1 transmits data to CS_2. Firstly, CS_1 sends a pulse sequence which indicates the beginning of the data transmission to the receiver. Next, data is transmitted, and it will take about 4 minutes before the data reaches CS_2. CS_2 prepares to receive and fine pointing must be achieved before the pulse sequence arrives at CS_2. Once CS_2 has received data, it will send a message of the status of the data transmission back to CS_1.

The communication schedule of the CubeSats in the 72° sector and RelayCube is depicted in Figure 23. It is assumed that CS_1 has received data from the other three CubeSats as in Figure 21. The communication process of the first link, i.e. L_{L4}, is the same as in Figure 22. This is the starting point for Figure 23 in which the 30-minute graph is cyclic. Even though the most important data is from CS_2, as it is close to the Earth–Sun line, the figure demonstrates that the concept is able to manage the synchronization in communication by showing the data flow from CS_1 all the way to RelayCube. It is also assumed that CS_1 has achieved the required pointing accuracy in the direction of the receiver (CS_2).

Once CS_2 has received the data, it will send back a message of the status of the data transmission as well as commands, if necessary. Next, it goes to a transmitter mode at the end of the 30-minute period and sends data to CS_3. When CS_3 transmits the total data of 1.46 Mbits from all CubeSats to RelayCube, data transmission takes about 43 s. This is the longest data transmission time of all crosslinks, since the amount of data is the largest in this crosslink.

Communications is designed so that the CubeSats in the L_{Li} crosslinks transmit at the same time, and when they have transmitted data they will receive data from the CubeSat on the other side[7]. For example, when CS_2 has transmitted data to CS_3 it will receive data from CS_1. This is possible, since the transmission delay is much longer than the data transmission time. However, CS_3 cannot transmit and receive at the same time, so there is a data transmission time shift between L_{Li} and L_{Ri} crosslinks. The shift is designed to be around 7 minutes, but it can also be something else. In the case of Figure 21, the communication delay from the critical 36° sector to the ground station represents the longest delay, since in this case the data from CS_2 must be sent via CS_3 due to the 10° sunlit sector (see Figure 18.).

4.7.4 Communication delay to the Earth and ground stations

After presenting the communication schedule, the timeliness performance is shown in Figure 24. The data transmission delay from 0.72 AU is depicted from one of the most critical events where CS_2 is situated at the Earth–Sun line in Figure 21. The delays were deduced from Figure 23. Figure 24 shows a time period which begins when CS_2 has just sent the last data packet and measured the latest measurement. Thus, it takes 30 minutes to send new data. CS_3 receives the latest measurement in 34 minutes. Eventually, RelayCube receives this measurement after 54 minutes. Furthermore, about one minute is allocated for data processing.

To be able to determine how long it takes to send the measurement to the ground station, one has to know the orbit of RelayCube and the number of ground stations. Therefore, these questions are solved in the following. As was presented earlier, RelayCube could be launched to a Sun-synchronous dusk-dawn orbit with an orbit altitude of 730 km. Then, this orbit would almost equal to that of the TUGSAT-1 satellite which is also in the similar dusk-dawn orbit [91]. TUGSAT-1, with an orbital altitude of 790 km (orbital period of about 100 minutes), can communicate with its ground station eight times within 24 hours, i.e., every three hours [55]. If there were four ground stations uniformly distributed all over the world, RelayCube would be able to communicate with one of the ground stations every 45 minutes. It should be noted that the ideal orbit altitude of 730 km was presented earlier in section 4.2.1, and therefore, the altitude of 790 km leads to a longer eclipse period at some point. However, the altitude of 730 km has a shorter orbital period, which results in

[7]After transmitting the data, a HelioRing CubeSat turns approximately 144 degrees to receive data from another CubeSat. This turn can be done by reaction wheels of the ADACS. Since the CubeSat eventually turns back along, more or less the same trajectory for transmitting, there is no need to the detumble the wheels. However, there may be the need for small rotations done with the wheels in order to achieve sufficient coarse pointing accuracy. This might, in long term, lead to the need to detumble the wheels by, e.g., cold-gas systems (see subsection 4.3.3 for further information).

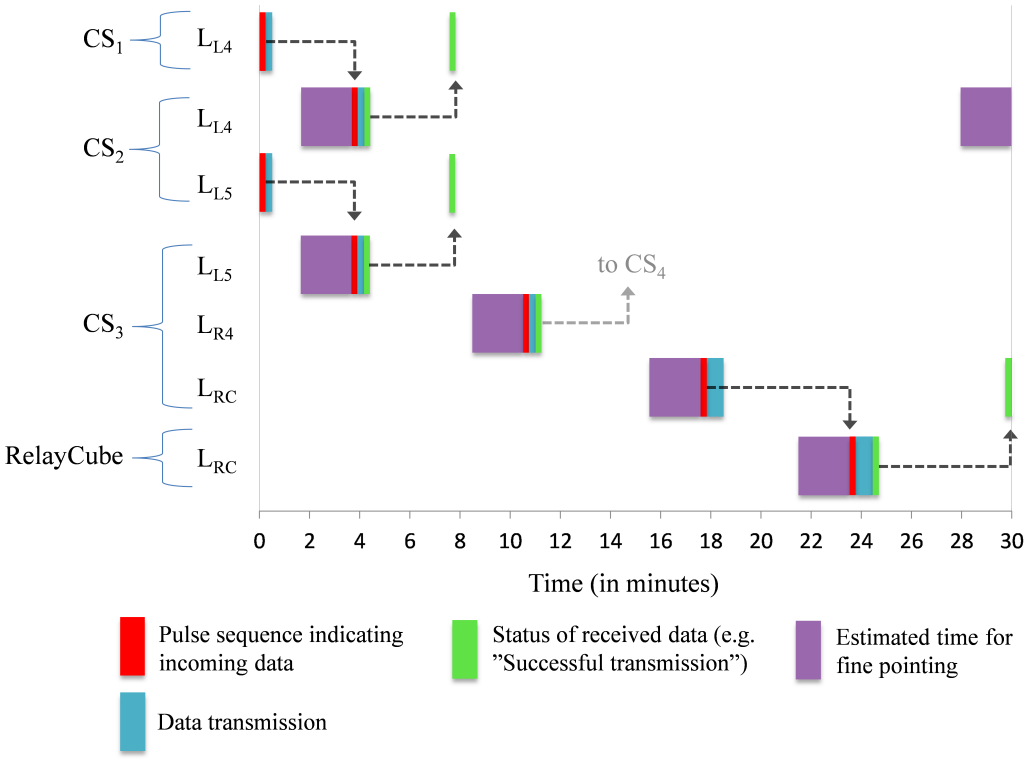

Figure 23: The communication schedule for Figure 21. In the L_{Ri} crosslinks, there should be a different starting point for transmitting data with respect to L_{Li}, since CS_3 cannot receive from two CubeSats at the same time. Therefore, there is about a 7-minute transmitting time shift in the L_{Ri} crosslinks, but the shift can also be something else.

a shorter communication interval with the ground station. The altitude difference is not large, but the difference in communication interval can be studied by simulations in future work.

The total amount of data from all CubeSats (including RelayCube) is about 1.60 Mbits for one 30-minute cycle. RelayCube transmits this data to one of the ground stations. RelayCube is available to downlink data for about ten minutes during a single overpass of a ground station (time estimated according to another CubeSat mission at a similar altitude) [92]. Therefore, to be able to transmit all data to the ground station, the data rate should exceed 2.70 kbits/s. At this point, it is reasonable to take a look at another CubeSat mission in order to determine what sort of systems this data rate demands. ESTCube-1 was an Estonian CubeSat that orbited the Earth at an altitude of 704 km [93]. It was capable of downlinking data with a data rate of 9.60 kbits/s at 437.505 MHz[8]. For this, the ground station required an antenna gain of 16 dB.

This kind of an antenna option is available commercially, such as in CubeSat-Shop.com [94]. The option also offers full ground station equipment (e.g. transceiver, software and computer for control) and would have fulfilled the requirements for

[8]Communications details of the ESTCube-1 CubeSat: http://www.estcube.eu/en/radio-details.

the ESTCube-1 ground station. The cost of the ground station kit is 32,500 euros. If the same ground station was used in the HelioRing mission, all data would be downlinked in less than three minutes. The data rate is more than three times higher than required and would enable the reliable downlinking of all data to the Earth. The number of ground stations would be four and, thus, the cost for ground stations would be around 130,000 euros. This is substantially less than in the RF communication concept (see page 29).

As the most important payload data from the closest CubeSats at 0.72 AU is downlinked first, it only takes some seconds to transmit this data to the ground station. Therefore, data from the CubeSats at 0.72 AU is available at the ground station within 99 minutes from the latest measurement. This is shorter than the required maximum delay of 120 minutes. Even though RelayCube was in an eclipse when it should communicate, there is still time to fulfil the 120-minute requirement. This is because the eclipses last 18 minutes or less, as explained in subsection 4.2.1.

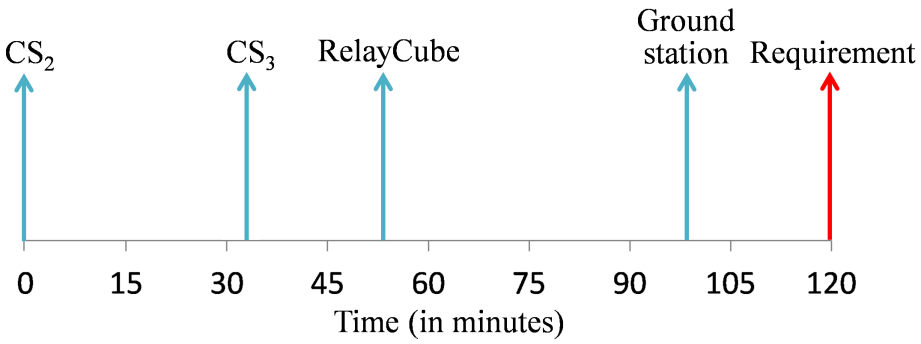

Figure 24: The data transmission delay from the critical point (sunlit sector) of CS_2 to the ground station. The transmission cycle begins when CS_2 has sent the latest data to CS_3, and it takes 30 minutes for the next data transmission. Eventually, this data is received by RelayCube after 54 minutes. One of the ground stations receives the data after 99 minutes at the latest. This time is shorter than the maximum allowed time delay of 120 minutes.

Data from the farthermost CubeSats, for example, from the transmitting CubeSat in link L_{L1}, is available at a ground station within less than four hours. Even if CS_2 transmitted data unsuccessfully to CS_3, and the transmission was successful only in the next period, data from CS_2 would still be on Earth in time. Thus, the synchronization and scheduling presented fulfil the 120-minute requirement for the mission. Therefore, the laser communication concept shows a great performance from the standpoint of timeliness.

4.8 Communication and thermal management

During data transmission, the average transmit power is 22 W. Since the electro-optic efficiency of the proposed transmitter is 0.19, the system demands a power of about 116 W in order to obtain the high-peak transmit power required. That means that

about 94 W of 116 W is converted into heat. This is a high value, especially compared with the MarCO CubeSats, transmit power of which is 4 W with a higher electrical efficiency. But in comparison with other lasercom systems, it is not exceptional. The AeroCube-OCSD CubeSat (see page 34) has a transmit power of 10 W for lasercom with an electro-optical efficiency of 0.20. This means 40 W is transformed into heat. The CubeSat is designed to transmit data for three minutes at most. Therefore, the amount of energy transformed into heat is 7200 joules. [22]

The longest data transmission in the HelioRing mission lasts 43 s (see page 57) per transmission. Thus, the amount of the total converted heat energy is about 4040 joules. This amount is roughly half of that of the AeroCube-OCSD CubeSat. Furhermore, a HelioRing CubeSat that would have a 6U form factor is about four times larger than the AeroCube-OCSD CubeSat. This is beneficial for radiating converted heat energy out of the spacecraft. Thus, it is anticipated that there is no challenge with thermal management. However, thermal management for the CubeSats will need a careful design.

4.9 Evaluation of the performance of the concept

The performance of the laser communication concept is evaluated in this section in order to discuss the advantages, disadvantages, and challenges of the concept as well as to indicate the importance of the concept for future research. The most important measures of performance of the communication concept are timeliness, feasibility, reliability, maintainability, and cost-effectiveness. These measures are analysed and compared to the RF communication concept in the following list. At the end of this section, the advantages and disadvantages of both concepts are briefly summarized.

- **Timeliness** measures whether the concept fulfils the requirement of communication time delay of 120 minutes from the nearest 36° heliospheric longitude at 0.72 AU to the ground station. The lasercom concept fulfils the requirement throughout the mission lifetime, and the payload data is received at the ground station in time. Even if one CubeSat was lost due to malfunction, the requirement would still be fulfilled. Data from the farthermost CubeSats is available in the ground station within four hours, which here is considered near real-time, since this data is not that critical. However, it is important scientifically and for reasons of spacecraft control.

  The RF communication concept would fulfil the same requirement for most of the time, since there is a clear line-of-sight in the downlinks from 0.72 AU to one of the ground stations. However, when a CubeSat orbits too close to the Sun seen from the Earth, data cannot be downlinked for approximately two days (see Appendix B). Also, this communication outage occurs about six times per year, and thus, one is unable to forewarn of possible CMEs for 3.2% of the mission lifetime (see Appendix B). This feature does not take place in the lasercom concept. This is also one of the major disadvantages of the RF concept, since space weather forecasting should be continuous. However, 3 %

of the mission lifetime is not too considerable and there would be a significant leap forward anyway in forecasting.

- **Feasibility** stands for how possible it is to implement the concept with existing technology. In principle, all systems and methods in the lasercom concept are possible to design and accomplish, but many of them have not been demonstrated yet on a CubeSat mission. This introduces some uncertainty to the feasibility, since CubeSats have stringent requirements of available volume. The concept is, however, estimated to be feasible, since all critical lasercom technologies were compared to other CubeSat missions[9], or a demonstrated design exists but it has not yet been flown on a CubeSat mission.

  The most challenging CubeSat subsystems which need to be designed for this concept are the attitude determination and control system (ADACS) and laser transmitter. The ADACS demands a high pointing accuracy and the same or better accuracy has not been demonstrated by any CubeSat to date. However, there are other CubeSat missions, which demand a pointing accuracy in the same order of magnitude, and, thus, they can be a huge benefit when used as a baseline for the ADACS development project. Most of the other deep-space lasercom missions demand an order of magnitude better pointing accuracy than this concept (see page 38). In this regard, the ADACS system is estimated to be feasible and the required pointing accuracy can probably be achieved.

  The most demanding lasercom subsystem is the transceiver. As was discussed in subsection 4.3.2, there is a designed model of a transceiver to be used in deep-space lasercom CubeSats. However, its transmitter and detector need to be replaced. Also, the diameter of the optical antenna should be larger. The most challenging system of the transceiver is the transmitter. There is a developed transmitter (achieving a sufficient peak power), but it should be designed to be a part of the transceiver presented. Also, the transmitter should be modified to fit to the required volume. As was estimated in the same subsection, it is feasible to design the transmitter for the concept. However, the transceiver including all presented relevant systems needs careful design and testing (including particle radiation testing).

  There are many other systems that need to be developed for the concept. These would be, e.g., the optical antenna and optics, the detector for the receiver, and the secondary RF communication system. Some models of these systems have been designed and built already and they provide good baselines, since extensive research on them exists. Compared with the challenges involved with the ADACS and the transmitter, it seems more feasible to implement systems for the lasercom concept from those models. They would, however, need extensive testing for HelioRing.

  It should be noted that deep-space lasercom to the Earth or deep-space crosslink lasercom have not been demonstrated to date. This introduces a challenge for

[9]There are either preliminary designs of these CubeSat missions or CubeSats that are planned to be launched in the near future.

designing of a reliable lasercom concept for the mission lifetime.

There are deep-space RF systems developed for CubeSats that could also be used in the HelioRing mission. Therefore, the RF communication concept is feasible for the space segment of the mission. However, in the ground segment, the construction of at least three large ground station antennas would need significant effort and funding. From the standpoint of the system, the ground segment is estimated to be feasible, but its general feasibility is difficult to estimate at the moment.

- **Reliability** refers here to an estimated probability of maintaining the performance of the communication concept. If, in the lasercom concept, a data transmission to the Earth was unsuccessful once, for some reason, the data transmission could still be in time in the next communication period. Overall reliability depends on the reliability of data transmission from the farthermost CubeSats to RelayCube as a chain, and therefore, a single crosslink must be very reliable. But this needs careful simulations and testing. If, for some reason, one CubeSat is lost at 0.72 AU, the concept can still be functional. The concept demands a high reliability from RelayCube as if it lost, communication in the concept would no longer work. Then the secondary RF communication should be the main communication mean. Therefore, the reliability of RelayCube might be one of the major challenges of the concept. On the other hand, there could be two RelayCubes in the same orbit. Thus, if one of them was lost, the concept is still fully functional. In general, the lasercom concept is tentatively estimated to be reliable, from the standpoint of communication.

  The RF communication concept is more reliable than the lasercom concept, as RF systems for deep-space CubeSat missions are more advanced, and developed flight models exist. In addition, communication depends only on each CubeSat, which communicates with the ground station, and not on the other CubeSats as in the lasercom concept.

- **Maintainability** means here how well some characteristics of the CubeSats and communication can be changed, and how well some defects and their causes can be corrected. These characteristics can be, e.g., the communication schedule or the H/K and payload data to be transmitted.

  In the lasercom concept, in order to command the farthermost CubeSats at 0.72 AU from the Earth, it will take about four hours to deliver commands, and to the 72° sector tens of minutes. If a defect caused a malfunction in laser communication, the secondary RF communication systems can be used in an urgent situation. However, it might take some time before communication is possible with the DSN. This time needs to be determined in future work. In general, the concept is therefore estimated to be well maintainable. The RF concept allows even better maintainability, since the ground stations would have direct and reliable contact with the CubeSats and it would take less time to communicate with them.

- **Cost-effectiveness** means how much the concept would cost compared to the cost of the whole mission. CubeSat missions are inherently low-cost missions due to their low launch mass and subsystems that can be purchased commercially or otherwise require less effort for design or testing.

  As discussed earlier, the costs of deep-space CubeSat missions are estimated to be around 30 million euros [42]. However, lasercom systems for the concept need several systems to be designed, and they need also careful testing, which will introduce an increase in the total mission cost. In addition, the concept needs one more CubeSat compared to the requirement of ten CubeSats at 0.72 AU. The relative cost increase is not, however, considered significant, since the number of the CubeSats is increased only from 10 to 11. One of the major advantages of the concept is its relatively low cost in the ground segment. The cost of the ground stations is about 130,000 euros, which is considered low compared to the cost of the whole mission. After all, the concept is considered very cost-effective.

  The cost of the RF concept in the space segment is estimated to be less than that of the lasercom concept, since there are existing RF system designs that could be used in the HelioRing mission. This keeps the space segment cost low, since there is less work in the development of communication systems for the CubeSats. However, there are massive costs for the ground segment (see page 29). The construction and operation of the ground stations would cost tens of millions of euros or more in total, which makes the cost for the whole mission substantially large. Therefore, the RF concept is not a cost-effective solution.

In summary, the lasercom concept has the advantages of timeliness and cost-effectiveness. It achieves the communication requirements all of the time. The major challenge of the concept is feasibility, i.e., developing it so that it is functional and reliable throughout the mission lifetime. The concept would require a high reliability of RelayCube as this additional satellite must be functional throughout the mission lifetime.

The major advantages of the RF concept are feasibility and reliability. The major disadvantages are timeliness and cost-effectiveness. That is, this concept cannot permit forewarning of CMEs for 3.2 % of the mission lifetime. However, for most of the time, forewarning is possible. Lastly, the cost of the ground segment increase the total mission cost significantly.

4.10 Summary of the concept design

This section gives a brief summary of the communication concept for the HelioRing mission in order to highlight the most important system and performance values. All research questions stated in subsection 3.8 were successfully answered in sections 3.9–4.9. Table 13 shows the type of orbit for the CubeSats, the transmit power, and the other parameters of the laser communication system. In addition, the data rate and modulation format are presented. All parameters shown are for the crosslinks unless the secondary RF system is mentioned.

Table 13: A summary of the laser communication concept, including the main performance values of the crosslinks

Parameter	**Value / Type**	**Notes**
Orbit for the HelioRing CubeSats	Heliocentric at 0.72 AU	
Orbit for RelayCube	Dusk-dawn Sun-synchronous, altitude about 730 km, orbit period around 100 minutes	
Carrier wavelength	1064 nm	
Average transmit power	22.00 W	
Peak transmit power	1.42 MW	
Diameter of antenna for a HelioRing CubeSat	8.3 cm	
Diameter of antenna for RelayCube	12.0 cm	
Required pointing accuracy for laser communication	3.33 - 5.00 μrad	
Modulation format	Pulse-Position modulation	
Data rate	33.60 kbits/s	
Generated data rate estimate	81 bits/s	1 bit/s for payload data and 80 bits/s for H/K data
Bit error rate with error correction coding	10^{-6} or lower	
Laser tracking type	Beaconless	Star tracker used for inter-CubeSat communication at 0.72 AU. Thermal images of the Earth and a star tracker used for communication with RelayCube.
Payload data transmission delay to the ground stations from the closest 36° heliospheric longitude at 0.72 AU to the Earth	99 minutes	
Payload data transmission delay to the ground stations from the farthermost CubeSats	About 4 hours	

Table 13: Continued

Required volume for main communication system	1.8 U	
Required volume for secondary communication system	0.4 U	
Ground station antenna	UHF Yagi antenna	
Number of ground stations	4	Uniformly distributed along orbit

4.10.1 Future work on the laser communication concept

This thesis was a preliminary study on the lasercom concept. However, several studies are needed after this work. The most relevant future investigations would be the following:

1. Development of the ADACS having a pointing accuracy of 3 to 5 μrad for the HelioRing CubeSats.
2. Development of the laser transceiver, including the transmitter introduced.
3. High-energy particle radiation testing of the transceiver.
4. The efficiencies of the transmitter and receiver.
5. Beaconless tracking: The thermal images of the Earth or a star-tracker-based approach for laser crosslink communication.
6. Simulations of ECC methods: What would be an ideal choice and how a low final BER can be achieved.
7. Investigation how the background noise of the Sun increases as a function of angle seen from the optical antenna of RelayCube.
8. The secondary communication system for the special cases: availability and cost estimations if using the DSN. The special cases can be, e.g., the travelling to the final orbit, the obtaining and updating the orbital parameters of the CubeSats, and a malfunction of some critical subsystem for laser communication.

5 Conclusions

In this thesis, a laser communication concept for the HelioRing mission was designed. The thesis is the first study of the mission and, thus, the thesis also defines the objectives and requirements of the mission. The primary goal of the mission is to provide magnetic field properties of Earth-directed coronal mass ejections (CMEs) by using a CubeSat fleet in a heliocentric orbit in order to increase the prediction lead time of geomagnetic storms on the Earth. Extending the lead time is crucial today as CMEs have the potential, e.g., to damage power grid systems on the Earth and satellites. However, forecasting these effects well in advance is impossible today. At the moment, only one satellite enables forecasting the effects beforehand by delivering in situ measurements from 1.5 million km sunward from the Earth (0.99 AU). Thus, the lead time is only about ten minutes for the fastest CMEs. The southward magnetic field component (negative B_z) of a CME is a critical parameter for determining whether the CME is geoeffective, and this component can only be measured in situ in space. Therefore, there is a great interest in the research society in increasing the lead time by placing a spacecraft more sunward that at 0.99 AU.

The HelioRing mission would revolutionize space weather forecasting due to its minimum prediction lead time of three hours. In the mission, ten CubeSats orbit the Sun at about 0.6–0.8 AU and measure the B_z component of a CME as well as the solar wind. The CubeSat form factor of 6U was estimated ideal for the mission. The use of CubeSats as spacecraft would reduce the cost of the mission significantly. However, this deep-space CubeSat mission faces several challenges, of which communication to the Earth is considered the most problematic. This is mainly due to the limited mass and volume of CubeSats and, thus, also for the antenna and transmitter. This results eventually in a limited antenna gain and transmit power. It was found that using RF communication in the mission would have two major disadvantages. Firstly, communication from the farthermost CubeSats to the Earth would require three large ground stations with a diameter of about 21 m for the dish antennas. This is mainly due to the large free-space loss. The construction and operation of such large stations would increase the total cost significantly. Secondly, for about 3 % of the mission lifetime space weather forecasting is impossible due to increased background noise from the Sun when a CubeSat resides near to the Sun-Earth line. There are six communication outage periods of about two days in a year.

The objectives of the thesis were the following with the main focus on the second one:

1. To define the objectives and requirements of the HelioRing mission.
2. To investigate how the CubeSat fleet would communicate with the Earth.
3. To evaluate the performance of the communication concept.

These objectives were achieved successfully. Firstly, the relevant objectives of the HelioRing mission were defined and they describe the goal of the mission. In addition, the requirements of the mission were derived, in order to achieve the objectives.

For the second objective of the thesis, it has not only been demonstrated in this thesis that communication is possible in the mission, but the two aforementioned communication problems of the possible RF concept have also been solved. The main principle of the designed communication concept is the use of laser for the inter-CubeSat communication. Each CubeSat communicates with its neighbouring CubeSat, and thereby data is delivered via the nearest CubeSat to the Earth. This CubeSat communicates with a CubeSat called RelayCube, which orbits the Earth in a Sun-synchronous dusk-dawn orbit, permitting almost continuous visibility for communication with the nearest CubeSat. RelayCube transmits the same data eventually to the ground stations by using RF instead of a laser wavelength. These stations can be very low-cost amateur radio systems. Another major advantage of the concept is that it permits continuous space weather forecasting on the Earth.

The laser communication concept would fulfil the requirements of the mission. However, it has some challenges that would, indeed, need further studies after this preliminary study. Firstly, the crosslink laser communication has never been demonstrated with the same or larger distance as in this concept. Secondly, the required pointing accuracy of 3.33–5.00 μrad for the CubeSats in HelioRing is a challenge, since the same order of accuracy for pointing has not been demonstrated by any CubeSat to date. However, there are promising CubeSat missions in the near future that aim to demonstrate the same order of magnitude of pointing accuracy as in this concept. Due to the significant advantages of the concept, these studies are seen worth investigating in the future. Even though the target orbit is around 0.6–0.8 AU and this thesis made calculations for 0.72 AU, the results show that it is probable to fulfil the mission requirements also in another orbital distance, e.g., at 0.8 AU.

The other results of the thesis demonstrate that inter-CubeSat communication is possible with distances of tens of millions of kilometers. Therefore, other missions using small deep-space spacecraft may benefit from the laser communication concept. They could also use a similar laser transmitter that is used for this concept. Its peak transmit power is the highest for space communication to the best knowledge of the author. The transmitter could possibly be used in another deep-space CubeSat mission, since it requires only little volume and mass. However, due to the high peak power, the average transmit power is also high, resulting in a limited data transmission time. Nevertheless, since CubeSat missions typically produce low amounts of data, the transmitter would be an excellent choice for a small deep-space spacecraft, e.g., a CubeSat mission, where the amount of scientific data is small.

For the third objective of the thesis, the performance of the laser communication concept was evaluated and was compared to the possible RF concept. The evaluation shows extensively the advantages as well as limitations of the laser and the RF communication concepts.

References

[1] A. K. Singh, D. Siingh, and R. P. Singh, "Space Weather: Physics, Effects and Predictability," *Surveys in Geophysics*, vol. 31, no. 6, pp 581–638, 2010.

[2] M. MacAlester and W. Murtagh, "Extreme Space Weather Impact: An Emergency Management Perspective," *Space Weather*, vol. 12, no. 8, pp. 530–537, 2014.

[3] V. Bothmer and I. Daglis. *Space Weather: Physics and Effects.* 1st ed. Springer-Verlag Berlin Heidelberg. 2007. 438 p.

[4] M. Chigomezyo, A. Pulkkinen, M. Mays, M. Kuznetsova, A. Galvin, K. Simunac, D. Baker, X. Li, Y. Zheng, and A. Glocer, "Simulation of the 23 July 2012 extreme space weather event: What if this extremely rare CME was Earth directed?" *Space Weather*, vol. 11, no. 12, pp. 671–679, 2013.

[5] G. M. Lindsay, C. T. Russell, and J. G. Luhmann, "Predictability of Dst index based upon solar wind conditions monitored inside 1 AU," *Journal of Geophysical Research: Space Physics*, vol. 104, no. A5, pp. 10335–10344, 1999.

[6] N. Gopalswamy, A. Lara, P. K. Manoharan and R. A. Howard, "An empirical model to predict the 1-AU arrival of interplanetary shocks," *Advances in Space Research*, vol. 36, no. 12, pp. 2289–2294, 2005.

[7] A. Pulkkinen, M. Hesse, S. Habib, L. Zel, B. Damsky, F. Policelli, D. Fugate, W. Jacobs, and E. Creamer, "Solar shield: forecasting and mitigating space weather effects on high-voltage power transmission systems," *Natural Hazards*, vol. 53, pp. 333–345, 2009.

[8] J. Eastwood, D. Kataria, C. McInnes, N. Barnes, and P. Mulligan, "Sunjammer," *Weather*, vol. 70, no. 1, pp. 27–30, 2015.

[9] B. Ritter, A. Meskers, O. Miles, M. Rußwurm, S. Scully, A. Roldán, O. Hartkorn, P. Jüstel, V. Réville, S. Lupu, and A. Ruffenach, "A Space weather information service based upon remote and in-situ measurements of coronal mass ejections heading for Earth: A concept mission consisting of six spacecraft in a heliocentric orbit at 0.72 AU," *Journal of Space Weather and Space Climate*, vol 5, no. A3, 2015.

[10] C. T. Russell, B. J. Anderson, W. Baumjohann, K. R. Bromund, D. Dearborn, D. Fischer, G. Le, H. K. Leinweber, D. Leneman, W. Magnes, J. D. Means, M. B. Moldwin, R. Nakamura, D. Pierce, K. M. Rowe, J. A. Slavin, R. J. Strangeway, R. Torbert, C. Hagen, I. Jernej, A. Valavanoglou, and I. Richter, "The Magnetospheric Multiscale Magnetometers," *Space Science Reviews*, vol. 199, no. 1, pp. 189–256, 2014.

[11] H. Scott. "CubeSats, Return on Investment, Deep Space, and Physics," *New Space*, vol 2, no. 1, 2014.

[12] R. M. Taylor, "Space communications," *IEEE Spectrum*, vol. 29, no. 2, pp. 30–33, 1992.

[13] R. W. Kingsbury, D. O. Caplan, and K. L. Cahoy, "Compact optical transmitters for CubeSat free-space optical communications," *Proceedings SPIE 9354, Free-Space Laser Communication and Atmospheric Propagation XXVII*, 93540S, 2015.

[14] W. A. Shiroma, L. K. Martin, J. M. Akagi, J. T. Akagi, B. L. Wolfe, B. A. Fewell, and A. T. Ohta, "CubeSats: A Bright Future for Nanosatellites," *Central European Journal of Engineering*, vol. 1, no. 1, pp. 9–15, 2011.

[15] K. Woellert, P. Ehrenfreund, A. J. Ricco, and H. Hertzfeld, "Cubesats: Cost-effective science and technology platforms for emerging and developing nations," *Advances in Space Research*, vol. 47, no. 4, pp. 663–684, 2011.

[16] N. Chahat, J. Sauder, M. Thomson, R. Hodges, and Y. Rahmat-Samii, "CubeSat deployable Ka-band reflector antenna for Deep Space missions," *2015 IEEE International Symposium on Antennas and Propagation & USNC/URSI National Radio Science Meeting*, Vancouver, BC, pp. 2185–2186, 2015.

[17] R. E. Hodges, D. J. Hoppe, M. J. Radway, and N. E. Chahat, "Novel deployable reflectarray antennas for CubeSat communications," *2015 IEEE MTT-S International Microwave Symposium (IMS)*, Phoenix, AZ, pp. 1–4, 2015.

[18] P. C. Liewer, A. T. Klesh, M. W. Lo, N. Murphy, R. L. Staehle, V. Angelopoulos, B. D. Anderson, M. Arya, S. Pellegrino, J. W. Cutler, E. G. Lightsey, and A. Vourlidas, "A Fractionated Space Weather Base at L5 using CubeSats and Solar Sails," *Advances in Solar Sailing*, Springer Praxis Books, pp. 269–288, 2014.

[19] A. Klesh and J. Krajewski. "MarCO: CubeSats to Mars in 2016," *29th Annual AIAA/USU Conference on Small Satellites, Technical Session III: Next on the Pad*, 2015. Available: `http://digitalcommons.usu.edu/smallsat/2015/all2015/16/` (accessed May. 10, 2016).

[20] M. Johnston, "Deep Space Network Scheduling Using Multi-Objective Optimization with Uncertainty," *SpaceOps 2008 Conference*, HeidelBerg, Germany, 2008. Available: `arc.aiaa.org/doi/pdf/10.2514/6.2008-3580` (accessed Apr. 25, 2016).

[21] H. Hemmati, A. Biswas, and I. B. Djordjevic, "Deep-Space Optical Communications: Future Perspectives and Applications," *Proceedings of the IEEE*, vol. 99, no. 11, pp. 2020–2039, 2011.

[22] S. W. Janson, R. P. Welle, T. S. Rose, D. W. Rowen, D. A. Hinkley, B. S. Hardy, S. D. La Lumondiere, G. A. Maul, and N. I. Werner. "The

NASA Optical Communication and Sensors Demonstration Program: Preflight Up-date," *29th Annual AIAA/USU Conference on Small Satellites, Technical Session III: Next on the Pad*, 2015. Available: `http://digitalcommons.usu.edu/smallsat/2015/all2015/14/` (accessed Dec. 15, 2015).

[23] D. N. Baker, X. Li, A. Pulkkinen, C. M. Ngwira, M. L. Mays, A. B. Galvin, K. D. C. Simunac, "A major solar eruptive event in July 2012: Defining extreme space weather scenarios," *Space Weather*, vol. 11, no. 10, pp. 585–591, 2013.

[24] D. F. Webb, "Coronal Mass Ejections and Space Weather," *Proceedings of the International Astronomical Union*, vol. 2004, no. IAUS223, pp. 499–508, 2004.

[25] R. Skoug, J. Gosling, J. Steinberg, D. McComas, C. Smith, N. Ness, Q. Hu, and L. Burlaga, "Extremely high speed solar wind: October 29–30, 2003," *Journal of Geophysical Research: Space Physics*, vol. 109, no. A9, 2004.

[26] T. Nieves-Chinchilla, R. Colaninno, A. Vourlidas, A. Szabo, R. P. Lepping, S. A. Boardsen, B. J. Anderson, and H. Korth, "Remote and in situ observations of an unusual Earth-directed coronal mass ejection from multiple viewpoints," *Journal of Geophysical Research: Space Physics*, vol. 117. no. A6, 2012.

[27] T. Rosenvinge and E. Christian. "Fifteen years of science and space weather studies," *Earth & Space Science News*, vol. 93, no. 40, pp. 385–386, 2012.

[28] S. Neeck, "The NASA Earth Science Flight Program: an update," *Proceedings SPIE 9639, Sensors, Systems, and Next-Generation Satellites XIX*, 963907, 2015.

[29] Y. Tsuda, O. Mori, R. Funase, H. Sawada, T. Yamamoto, T. Saiki, T. Endo, K. Yonekura, H. Hoshino, and J. Kawaguchi, "Achievement of IKAROS – Japanese deep space solar sail demonstration mission," *Acta Astronautica*, vol. 82, no. 2, pp. 183–188, 2013.

[30] J. Bouwmeester and J. Guo, "Survey of worldwide pico- and nanosatellite missions, distributions and subsystem technology," *Acta Astronautica*, vol. 67, no. 7—8, pp. 854–862, 2010.

[31] K. Liou, C. Wu, M. Dryer, S. Wu, N. Rich, S. Plunkett, L. Simpson, C. D. Fry, and K. Schenk, "Global simulation of extremely fast coronal mass ejection on 23 July 2012," *Journal of Atmospheric and Solar-Terrestrial Physics*, vol. 121, Part A, pp. 32–41, 2014.

[32] J. G. Luhmann, D. W. Curtis, P. Schroeder, J. McCauley, R. P. Lin, D. E. Larson, S. D. Bale, J .A. Sauvaud, C. Aoustin, R. A. Mewaldt, A. C. Cummings, E. C. Stone, A. J. Davis, W. R. Cook, B. Kecman, M. E. Wiedenbeck, T. Rosenvinge, M. H. Acuna, L. S. Reichenthal, S. Shuman, K. A. Wortman, D. V. Reames, R. Mueller-Mellin, H. Kunow, G. M. Mason, P. Walpole, A. Korth, T. R. Sanderson, C. T. Russell, and J. T. Gosling

"STEREO IMPACT Investigation Goals, Measurements, and Data Products Overview," *Space Science Reviews*, vol. 136, no. 1, pp. 117–184, 2007.

[33] California Polytechnic State University. CubeSat Design Specification, Revision 13. 2014. Available: `http://www.cubesat.org/` (accessed May 13, 2016).

[34] R. Hevner, W. Holemans, J. Puig-Suari, and R. Twiggs, "An Advanced Standard for CubeSats," *25th Proceedings of the AIAA/USU Conference on Small Satellites, Technical Session VII: Opportunities, Trends and Initiatives*, 2011. Available: `http://digitalcommons.usu.edu/smallsat/2011/all2011/15/` (accessed Jan. 17, 2016).

[35] G. Richardson, K. Schmitt, M. Covert, and C. Rogers, "Small Satellite Trends 2009-2013," *29th Proceedings of the AIAA/USU Conference on Small Satellites, Technical Session II: From 0 to 7.5 km/s*, 2015. Available: `http://digitalcommons.usu.edu/smallsat/2015/all2015/48/` (accessed May. 12, 2016).

[36] The polish 1U PW-sat CubeSat. Further details in `http://pw-sat.pl/en/pw-sat1/`. Accessed Apr. 10, 2016.

[37] M. Tsay, J. Frongillo, K. Hohman, B. K. Malphrus, "LunarCube: A Deep Space 6U CubeSat with Mission Enabling Ion Propulsion Technology," *29th Proceedings of the AIAA/USU Conference on Small Satellites, Technical Session XI: Advanced Technologies III*, 2015. Available: `http://digitalcommons.usu.edu/smallsat/2015/all2015/71/` (accessed May. 3, 2016).

[38] M. A. Viscio, N. Viola, S. Corpino, F. Stesina, S. Fineschi, F. Fumenti, and C. Circi, "Interplanetary CubeSats system for space weather evaluations and technology demonstration," *Acta Astronautica*, vol. 104, no. 2, pp. 516–525, 2014.

[39] A. Rajguru, N. Jerred, S. D. Howe, and A. Faler. "Laser Space Communication Concept for deep-space interplanetary missions using CubeSats," *45th AIAA Plasmadynamics and Lasers Conference*, AIAA Aviation, AIAA 2014-2234, 2014. Available: `http://arc.aiaa.org/doi/abs/10.2514/6.2014-2234` (accessed Feb. 24, 2016).

[40] J. Cirtain and J. Pelfrey, "Exploration Missions to Host Small Payloads," *28th Annual AIAA/USU Conference on Small Satellites, Technical Session IV: From Earth to Orbit*, 2014. Available: `http://ntrs.nasa.gov/search.jsp?R=20140012886` (accessed Apr. 4, 2016).

[41] A. T. Klesh and J. C. Castillo-Rogez, "Nano-satellite secondary spacecraft on deep space missions," *Global Space Exploration Conference*, Washington, DC, United States, 2012. Available: `http://trs-new.jpl.nasa.gov/dspace/handle/2014/44962` (accessed May. 13, 2016).

[42] R. L. Staehle, D. Blaney, H. Hemmati, D. Jones, A. Klesh, P. Liewer, J. Lazio, M. W. Lo, P. Mouroulis, N. Murphy, P. J. Pingree, T. Wilson, B. Anderson, C. C. Chow II, B. Betts, L. Friedman, J. Puig-Suari, A. Williams, and T. Svitek. "Interplanetary CubeSats: Opening the Solar System to a Broad Community at Lower Cost," *Journal of Small Satellites*, vol. 2, no. 1, pp. 161–186, 2013.

[43] J. Hudson, K. Lemmer, and A. Hine. "Integration of Micro Electric Propulsion System for CubeSat Orbital Maneuvers," *AIAA SPACE 2015 Conference and Exposition, SPACE Conferences and Exposition*, AIAA 2015–4669, 2015. Available: `http://arc.aiaa.org/doi/abs/10.2514/6.2015-4669` (accessed May. 13, 2016).

[44] W. P. Wright and P. Ferrer, "Electric micropropulsion systems," *Progress in Aerospace Sciences*, vol. 74, pp. 48–61, 2015.

[45] L. Johnson, A. Sobey, and K. Sykes, "Solar Sail Propulsion for Interplanetary Cubesats," *AIAA Propulsion and Energy 2015 Conference*, Orlando, FL, United States, 2015. Available: `http://ntrs.nasa.gov/search.jsp?R=20150016568` (accessed May 13, 2016).

[46] B. Seifert, A. Reissner, N. Buldrini, D. Krejci, F. Plesescu, and T. Hörbe, "Integrated Electric Propulsion Systems for Small Satellites," *Space Propulsion Conference*, Cologne, Germany, 2014. Available: `https://www.researchgate.net/publication/262933227_Integrated_Electric_Propulsion_Systems_for_Small_Satellites` (accessed May 13, 2016).

[47] M. H. Acuña, "Space-based magnetometers," *Review of Scientific Instruments*, vol. 73, no. 11, pp. 3717–3736, 2002.

[48] M. Archer, T. Horbury, P. Brown, J. Eastwood, T. Oddy, B. Whiteside, and J. Sample, "The MAGIC of CINEMA: first in-flight science results from a miniaturised anisotropic magnetoresistive magnetometer," *Annales Geophysicae*, vol. 33, pp. 725–735, 2015.

[49] J. Eastwood, P. Brown, T. Oddy, B. Whiteside, P. Fox, N. Adeli,T. Beek, C. Carr, N. Barnes and M. Macdonald, "Magnetic Field Measurements from a Solar Sail Platform with Space Weather Applications," *Advances in Solar Sailing*, pp. 185–200, 2014.

[50] W. Magnes, M. Oberst, A. Valavanoglou, H. Hauer, C. Hagen, I. Jernej, H. Neubauer, W. Baumjohann, D. Pierce, and J. Means, "Highly integrated front-end electronics for spaceborne fluxgate sensors," *Measurement Science and Technology*, vol. 19, no. 11, 2008.

[51] M. Johnson, T. Bonalsky, D. Chornay, C. Clagett, A. Cudmore, A. Ericsson, S. Hesh, S. Jones, L. Kepko, J. Rodriguez, E. Sittler, S. Starin, L. Santos,

S. Sheikh, P. Uribe, and E. Zesta, "Dellingr- A Path to Compelling Science with CubeSats," *European Planetary Science Congress 2015*, Nantes, France, 2015. Available: `http://adsabs.harvard.edu/abs/2015EPSC...10..720J` (accessed May 13, 2016).

[52] V. Maiwald, A. Weiß and F. Jansen, "Combining solar science and asteroid science with the space weather observation network (SWON)," *Acta Astronautica*, vol. 81, no. 2, pp. 411–418, 2012.

[53] D. Fischer. The Space Research Institute of Austrian Academy of Sciences, Schmiedlstraße 6, 8042 Graz, Austria. Personal communication, 16th Nov. 2015.

[54] P. Fortescue, G. Swinerd, and J. Stark. *Spacecraft systems engineering.* 4th ed. Chichester : Wiley, 2011. 691 p.

[55] P. Romano. Graz University of Technology, Institute of Communication Networks and Satellite Communications, Inffeldgasse 12A, 8010 Graz, Austria. Personal communication, 4th Dec. 2015.

[56] S. Santandrea, K. Gantois, K. Strauch, F. Teston, E. Tilmans, C. Baijot, D. Gerrits, A. Groof, G. Schwehm, and J. Zender, "PROBA2: Mission and Spacecraft Overview," *Solar Physics*, vol. 286, no. 1, pp. 5–19, 2013.

[57] K. E. Wilson, J. R. Lesh, K. Araki, and Y. Arimoto, "Overview of the Ground-to-Orbit Lasercom Demonstration (GOLD)," *Proceedings SPIE 2990, Free-Space Laser Communication Technologies IX*, 23, 1997.

[58] Z. Sodnik, B. Furch, and H. Lutz, "Optical Intersatellite Communication," *IEEE Journal of Selected Topics in Quantum Electronics*, vol. 16, no. 5, pp. 1051–1057, 2010.

[59] B. G. Boone, J. R. Bruzzi, W. P. Millard, K. B. Fielhauer, B. E. Kluga, C. W. Drabenstadt, and R. S. Bokulic, "Optical Communications Development for Spacecraft Applications," *Johns Hopkins Apl Technical Digest*, vol. 25, no. 4, pp. 306–315, 2004. Available: http://www.jhuapl.edu/techdigest/TD/td2504/Boone.pdf (accessed Sep. 11, 2015).

[60] S. R. Macgregor, *Low-Noise Systems in the Deep Space Network.* DESCANSO Book Series. Jet Propulsion Laboratory, California Institute of Technology. 2008. Available: `http://descanso.jpl.nasa.gov/monograph/series10/Reid_DESCANSO_sml-110804.pdf` (accessed Jan. 27, 2016).

[61] J. R. Lesh, W. K. Marshall, and J. Katz, "A Simple Method for Designing or Analyzing an Optical Communication Link," *The Telecommunications and Data Acquisition Progress Report 42–85, January–March 1986*, Jet Propulsion Laboratory, Pasadena, California, pp. 25–31, 1986. Available: `ipnpr.jpl.nasa.gov/progress_report/42-85/85C.PDF` (accessed Mar. 25, 2016).

[62] A. Biswas and S. Piazzolla. "Deep-Space Optical Communications Downlink Budget from Mars System Parameters," *The Interplanetary Network Progress Report*, vol. 42–154, pp. 1-38, 2003. Available: `http://adsabs.harvard.edu/abs/2003IPNPR.154L...1B` (accessed May. 13, 2016).

[63] H. Hemmati. *Deep Space Optical Communications*. 1 st. ed. Wiley-Interscience. 2006. 736 p.

[64] B. D. Metscher, "An evaluation of the communication system for the TAU mission study," *The Telecommunications and Data Acquisition Report*; pp. 108–117, 1987. Available: `http://homepage.univie.ac.at/brian.metscher/Metscher87_TAUcomm.PDF` (accessed Mar. 4, 2016).

[65] B. Moision, J. Wu, S. Shambayati, "An optical communications link design tool for long-term mission planning for deep-space missions," *Aerospace Conference, 2012 IEEE*, pp. 1–12, 2012.

[66] M. W. Wright and G. C. Valley. "Yb-Doped Fiber Amplifier for Deep-Space Optical Communications," *Journal of Lightwave Technology*, vol. 23, no. 3, 2005.

[67] F. Di Teodoro, P. Belden, P. Ionov, N. Werner, and G. Fathi, "Development of pulsed fiber lasers for long-range remote sensing," *Optical engineering*, vol. 53, no. 3, 2014.

[68] F. Di Teodoro, J. Morais, T. S. McComb, M. K. Hemmat, E. C. Cheung, M. Weber, and R. Moyer, "SBS-managed high-peak-power nanosecond-pulse fiber-based master oscillator power amplifier," *Optics Letters*, vol. 38, no. 13, pp. 2162–2164, 2013.

[69] F. Di Teodoro. Raytheon, Space and Airborne Systems, 10 Moulton St, Cambridge, MA 02138, USA. Personal communication, 16th Nov. 2015.

[70] H. Hemmati, "Laser-Communications with Lunar CubeSat," 2nd International Workshop on Lunar-Cubes, 2013. Available: `http://lunar-cubes.com/docs/Hamid_Hemmati_13_04_11.pdf` (accessed May. 13, 2016).

[71] J. Li, S. Greenland, G. Clark, M. Post, A. Vick, D. Pearson, D. Lee, and D. MacLeod. "Practical Strategies to Stabilize a Nanosatellite Platform with a Space Camera and Integrated Mechanical Parts," *65th International Astronautical Congress*, Toronto, Canada, 2014. Available: `www.maia.ub.es/~gerard/AstroNet-II/Papers/LiGreenlandEtal.pdf` (accessed Oct. 14, 2015).

[72] C. M. Pong, M. W. Smith, M. W. Knutson, S. Lim, D. W. Miller, S. Seager, J. S. Villaseñor, and S. D. Murphy. "One-Arcsecond Line-of-Sight Pointing Control on ExoplanetSat, A Three-Unit CubeSat," *Advancements in the Astronautical Sciences 141*, 2011.

[73] A. Biswas, V. Vilnrotter, W. H. Farr, D. Fort, and E. Sigman, "Pulse position modulated (PPM) ground receiver design for optical communications from deep space," *Proceedings SPIE 4635, Free-Space Laser Communication Technologies XIV*, 224, 2002.

[74] W. Farr, M. Regehr, M. Wright, D. Sheldon, A. Sahasrabudhe, J. Gin, and D. Nguyen, "Overview and Design of the DOT Flight Laser Transceiver," *The Interplanetary Network Progress Report*, vol. 42–185, pp. 1–31, 2011. Available: `ipnpr.jpl.nasa.gov/progress_report/42-185/185D.pdf` (accessed Apr. 5, 2016).

[75] W. K. Marshall, B. D. Burk, "Received Optical Power Calculations for Optical Communications Link Performance Analysis," *The Telecommunications and Data Acquisition Report, Jet Propulsion Laboratory*, pp. 32–40, 1986. Available: `http://ipnpr.jpl.nasa.gov/progress_report/42-87/87D.PDF` (accessed Oct. 20, 2015).

[76] S. Verghese, J. Donnelly, E. Duerr, K. McIntosh, D. Chapman, C. Vineis, G. Smith, J. Funk, K. Jensen, P. Hopman, D. Shaver, B. Aull, J. Aversa, J. Frechette, J. Glettler, Z.-L. Liau, J. Mahan, L. J. Mahoney, K. Molvar, F. O'Donnell, D. Oakley, E. Ouellette, M. Renzi, and B. Tyrrell, "Arrays of InP-based avalanche photodiodes for photon counting," *IEEE Journal of Selected Topics in Quantum Electronics*, vol. 13, no. 4, pp. 870–886, 2007.

[77] J. Katz, "Planets as Background Noise Sources in Free Space Optical Communications," *The Telecommunications and Data Acquisition Progress Report 42-85, January-March 1986*, Jet Propulsion Laboratory, Pasadena, California, pp. 13–24, 1986. Available: `ipnpr.jpl.nasa.gov/progress_report/42-85/85B.PDF` (accessed Oct. 22, 2015).

[78] L. Robert, J. Leach, and L. Shubin. "Earth albedo and emitted radiation," National Aeronautics and Space Administration, SP-8067, 1971. Available: `http://ntrs.nasa.gov/archive/nasa/casi.ntrs.nasa.gov/19710023628.pdf` (accessed Oct. 22, 2015).

[79] R. C. Ramsey. "Spectral Irradiance from Stars and Planets, above the Atmosphere, from 0.1 to 100.0 Microns," *Applied Optics*, vol. 1, no. 4, 1962.

[80] H. Hemmati. *Near-Earth laser communications.* CRC Press Taylor & Francis Group. 2009. 418 p.

[81] B. Moision and J. Hamkins, "Deep-Space Optical Communications Downlink Budget: Modulation and Coding," *IPN Progress Report 42-154*, 2003. Available: `http://adsabs.harvard.edu/abs/2003IPNPR.154K...1M` (accessed Nov. 2, 2015).

[82] Deep Space Services Catalog. Jet Propulsion Laboratory California Institute of Technology. 2015. Available: `https://deepspace.jpl.nasa.gov/files/dsn/820-100-F1.pdf` (accessed Feb. 12, 2016).

[83] L. A. Cangahuala, "Interplanetary navigation overview," *Proceedings of the 2000 IEEE/EIA International in Frequency Control Symposium and Exhibition*, Kansas city, USA, pp. 618–621, 2000.

[84] N. James, R. Abello, M. Lanucara, M. Mercolino, and R. Maddè, "Implementation of an ESA delta-DOR capability," *Acta Astronautica*, vol. 64, no. 11–12, pp. 1041–1049, 2009.

[85] C. Duncan, A. Smith, and F. Aguirre, "Iris Transponder – Communications and Navigation for Deep Space," *28th Annual AIAA/USU Conference on Small Satellites, Technical Session IX: Advanced Technologies-Communication*, 2014. Available: `http://digitalcommons.usu.edu/smallsat/2014/AdvTechComm/3/` (accessed Nov. 19, 2016).

[86] R. E. Hodges, D. J. Hoppe, M. J. Radway, and N. E. Chahat, "Novel Deployable Reflectarray Antennas for CubeSat Communications," *2015 IEEE MTT-S International in Microwave Symposium (IMS)*, 2015.

[87] C. Korendyke, D. Chua, R. Howard, S. Plunkett, D. Socker, A. Thernisien, P. Liewer, D. Redding, J. Cutler, J. Forbes, A. Vourlidas, "MiniCOR: A Miniature Coronagraph for Interplanetary CubeSat," *29th Annual AIAA/USU Conference on Small Satellites, Technical Session XII: Science/Mission Payloads*, 2015. Available: `http://digitalcommons.usu.edu/smallsat/2015/all2015/82/` (accessed Nov. 25, 2016).

[88] Y. Chen, J. Charles, H. Hemmati, and A. Biswas, "Infrared Earth tracking for deep-space optical communications: feasibility study based on laboratory emulator," *Proceedings SPIE 6457, Free-Space Laser Communication Technologies XIX and Atmospheric Propagation of Electromagnetic Waves*, 64570A, 2007.

[89] S. Lee, G. G. Ortiz, and J. W. Alexander, "Star Tracker-Based Acquisition, Tracking, and Pointing Technology for Deep-Space Optical Communications," *Interplanetary Network Progress Report 42-161*, Jet Propulsion Laboratory, Pasadena, California, 2005. Available: `ipnpr.jpl.nasa.gov/progress_report/42-161/161L.pdf` (accessed May. 12, 2016).

[90] W. Magnes. Vice director. The Space Research Institute of Austrian Academy of Sciences, Schmiedlstraße 6, 8042 Graz, Austria. Personal communication, 12th Nov. 2015.

[91] O. Koudelka, M. Unterberger, and P. Romano, "Nanosatellites - the BRITE and OPS-SAT missions," *e&i Elektrotechnik und Informationstechnik*, vol. 131, no. 6, pp. 178–187, 2014.

[92] G. Hunyadi, D. M. Klumpar, S. Jepsen, B. Larsen, and M. Obland, "A commercial off the shelf (COTS) packet communications subsystem for the Montana EaRth-Orbiting Pico-Explorer (MEROPE) CubeSat," *Aerospace Conference Proceedings, 2002 IEEE*, vol. 1, pp. 1-473 – 1-478, 2002.

[93] A. Slavinskisa, E. Kulua, J. Virua, R. Valnerb, H. Ehrpaisb, T. Uiboupinb, M. Jarve, E. Soolob, J. Envalla, T. Scheffler d, I. Sunter, H. Kuustea, U. Kvella, J. Kaldeb, K. Laizansa, E. Ilbisb, T. Eenmae, R. Vendta, K. Voormansika, I. Anskoa, V. Allika, S. Latt, and M. Noorma, "Attitude determination and control for centrifugal tether deployment on the ESTCube-1 nanosatellite," *Proceedings of the Estonian Academy of Sciences*, vol. 63, no. 2S. pp. 242–249, 2014.

[94] CubeSatShop.com. Full Ground Station Kit for VHF/UHF. Available: `www.cubesatshop.com/index.php?page=shop.product_details&flypage=flypage.tpl&product_id=24&category_id=3&option=com_virtuemart&Itemid=72` (accessed Dec. 30, 2015).

[95] W. A. Imbriale. *Large Antennas of the Deep Space Network*. Jet Propulsion Laboratory, California Institute of Technology, 2002. 298 p. Available: `http://thehowlandcompany.com/pdf/large-antennas-of-the-deep-space-network.pdf` (accessed Apr. 14, 2016).

[96] S. Shambayati, "Ka-Band Telemetry Operations Concept: A Statistical Approach," *Proceedings of the IEEE*, vol. 95, no. 11, pp. 2171–2179, 2007.

[97] European Space Operations Centre. ESA Tracking Stations (ESTRACK) Facilities Manual (EFM). DOPS-ESTR-OPS-MAN-1001-OPS-ONN, 2008.

[98] General Dynamics SATCOM Technologies, Model 21.0m Cassegrain Antenna datasheet, `http://www.gdsatcom.com/Antennas/Data_Sheets/655-0069B_21m.pdf` (accessed Apr. 5, 2016).

Appendices

A RF link budget calculation for the RF communication concept

This appendix shows the RF link budget calculation for the RF communication scenario. In this scenario, all CubeSats would communicate directly with one of the ground stations. The link budget is calculated from the farthermost CubeSat to the ground station. Therefore, only the downlink budget is calculated, since in a typical space mission, a ground station is able to transmit with a higher transmit power than a spacecraft. Thus, this method is sufficient to demonstrate the kinds of systems that are needed for the farthermost CubeSat to communicate with the ground stations.

The following downlink bands are available for deep-space communication [95, p. 6]:

- S-band at 2.290–2.300 GHz
- X-band at 8.400–8.450 GHz
- Ka-band at 31.800–32.300 GHz

It is well-known that with higher frequency in communication comes the possibility of higher performance in the link. This typically leads to a higher data rate [60, p. 13]. The influence of the Earth's atmosphere is negligible at S- and X-bands [96]. However, this influence can be very high at Ka-band sometimes, especially during rain, and thus this attenuation can decrease the link performance significantly [96]. Therefore, the Ka-band is not considered a favourable band for RF communication in HelioRing as space weather forecasting should be reliable regardless of the atmospheric weather conditions. Thus, this appendix focuses only on the downlink budget at X-band at 8.450 GHz.

The RF systems of the MarCO CubeSat [17, 19] are used as a baseline in the space segment. The aim is to calculate how large a diameter is required for the ground station antenna. The link budget equation presents the signal-to-noise-power-density ratio C/N_0, which is given by [54, p. 420–421]

$$C/N_0 = P_\mathrm{t} G_\mathrm{t} L_\mathrm{s} L_\mathrm{A} L_\mathrm{L} (G_\mathrm{r}/T_\mathrm{sys})(1/k_\mathrm{B}) \tag{A1}$$

where

P_t	is the transmit power
G_t	is the transmitter gain
L_s	is the free-space loss
L_A	is the atmospheric loss
L_L	is the total loss due to the attenuation by the transmission lines
G_r	is the receiver gain

T_{sys} is the system noise temperature, and
k_{B} is the Boltzmann constant ($\approx 1.3806 \times 10^{-23}$ J/K)

The ratio $(G_{\text{r}}/T_{\text{sys}})$ is typically regarded as a figure of merit of the receiving system. The free-space loss L_{s} is

$$L_s = \left(\frac{f}{4\pi c R_{\text{RF}}}\right)^2 \tag{A2}$$

where

f is the carrier frequency, and
R_{RF} is the range between a CubeSat and a ground station in the RF concept.

C/N_0 is related to the bit energy to noise power density E_{b}/N_0 as follows:

$$E_{\text{b}}/N_0 = C/R_{\text{b}}N_0 \tag{A3}$$

Table A1 shows the parameter values for the link budget. It is assumed that transmission lines in the space and ground segments produce a total loss of 2 dB. For E_{b}/N_0, a threshold of 0.4 dB was chosen as it is the minimum value that can be used by the DSN [82]. This threshold enables one to obtain with error correction coding a BER of about 10^{-5}, which is generally sufficient for a deep-space mission. Therefore it is a good estimate for the HelioRing ground segment as a lower value is challenging to obtain. It should be noted that pointing losses were not taken into account in the calculations and they would decrease the performance even more.

It can be seen in Table A1 that even with a low data rate of 85 bits/s, the $G_{\text{r}}/T_{\text{sys}}$ needs to be 42.3 dB/K. For this value, one commericial option can be found in [98]. The antenna presented has the $G_{\text{r}}/T_{\text{sys}}$ of 42.3 dB/K and a diameter of 21 m. Moreover, the ESA deep-space antenna Estrack reference [97] indicates the same values for the required diameter. It should be pointed out that the data rate of 85 bits/s is too a low data rate as there are nine other CubeSats generating data, and thus, a higher data rate is required. After all, this appendix showed that an antenna having a diameter of larger than 21 m is required for the data rate of hundreds bits/s.

Table A1: Estimated link budget values for the RF concept.

Parameter	**Value**	**Value in dB**
P_t	4.0 W	6.0 dBW
G_t		28
$G_\mathrm{r}/T_\mathrm{sys}$		42.3 dB/K
f	8.450 GHz	
L_s		-279.2
R_RF	257.3×10^6 km	
L_A		-1.0
L_L		-2.0
E_b/N_0		0.4
R_b	85 bits/s	
System link margin		3

B Communication outage calculation for the RF communication concept

In this appendix, the average duration of communication outages in the possible RF concept is calculated. The communication outage here means that the CubeSat closest to the Earth cannot communicate with a ground station due to increased background noise from the Sun. Consequently, a communication outage is also a break in space weather forecasting.

A reasonable starting point for the calculation is to determine how long one CubeSat stays in the so-called sunlit sector. If a CubeSat resides inside this sector, communication (with a reasonable data rate) is estimated to be impossible. After this calculation, it is determined that how many times this situation occurs in a year. Then, the average duration of communication outages can be obtained.

The antenna example used for the RF link budget calculation in Appendix A has the T_{sys} of approximately 60 K [98]. The measurements at X-band with the DSN's 34-m antenna show that the noise temperature increases significantly (a few tens of kelvins) with angles smaller than 1.5° from the Sun [60]. This decreases the $G_{\mathrm{r}}/T_{\mathrm{sys}}$ and eventually also reduces the data rate to such a low level that communication is estimated to be impossible when a CubeSat is inside a 3.0° sunlit sector. This is depicted in Figure B1 where one of the HelioRing CubeSats will orbit inside the 3° sector due to its faster orbital period than that of the Earth. The 3° sector is projected to the length of L_{N} ($\approx 2.17 \times 10^6$ km) at 0.72 AU which corresponds approximately to the real orbital distance as the straight line. In this case, the L_{N} is seen from the Sun as an angular separation of 1.15°.

Since the CubeSats are at the same orbital distance as Venus, the orbital periods are the same. Therefore, the orbital periods of the HelioRing CubeSats and Earth are 224.70 and 365.25 days, respectively. Thus, the angular frequencies, ω_{CS} and ω_{E} for the CubeSats and Earth are approximately 1.854×10^{-5} degrees/s and 1.141×10^{-5} degrees/s. Therefore, the time t when the CubeSat has just passed the sector can be determined from the following equation:

$$\omega_{\mathrm{CS}} t = \omega_{\mathrm{E}} t + 1.15^\circ \tag{B1}$$

Therefore, the communication outage duration is about $t = 1.87$ days. In a year, the Earth orbits naturally 360° and the CubeSats $\omega_{\mathrm{CS}}\times$ 365.25 days $\times$ 24 hours $\times$ 60 minutes $\times$ 60 s = 585.2 degrees. This is 225.2 degrees more than the Earth. Thus, the average number of CubeSats that pass the Earth-Sun line in a year is 225.2/360 $\times$ 10 CubeSats = 6.25 CubeSats. Finally, the average communication outage duration in the RF concept is about 6.25 $\times$ 1.86 days = 11.67 days. This is about 3.2 % of a year, and makes the average communication outage duration for the RF concept.

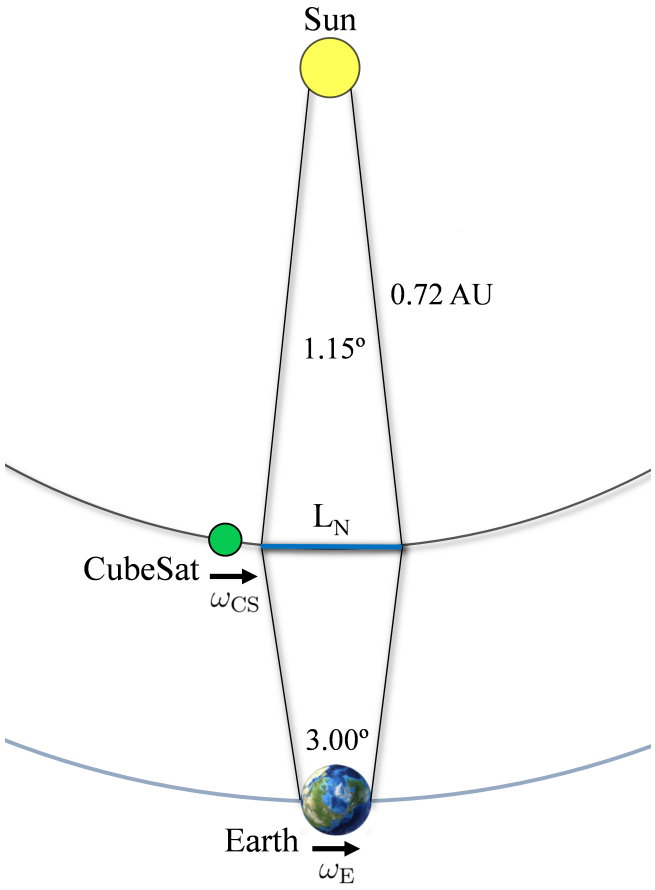

Figure B1: An illustration of an upcoming communication outage in the RF concept. When the CubeSat orbits inside the 3° sector seen from the Earth communication is estimated to be impossible.